UNIVERSITY OF CALIFORNIA
Santa Barbara

Spatial and Temporal Variability in Southern Ocean Sea Ice Coverage

A Thesis to be submitted in partial
satisfaction of the requirements for the degree of

Master of Arts

in

Geography

by

Sharon E. Stammerjohn

Committee in charge:
Professor Raymond Smith, Chairman
Professor Joel Michaelson
Professor David Siegel
Professor Libe Washburn

December 1993

The Thesis of Sharon E. Stammerjohn
is approved by:

Joel Michaelsen

Libe Washburn

Raymond C Smith

Committee Chairperson

December 10, 1993

ACKNOWLEDGEMENTS

I wish to express deep gratitude to my advisor, Dr. Ray Smith, who generously supported and encouraged me throughout the master's program. His enthusiasm for scientific endeavors is boundless and thoroughly contagious. I would also like to acknowledge my other committee members who freely availed themselves to my many questions and offered helpful suggestions in return. Many thanks are due to Steve Miley and Jim Davidson who patiently provided technical support of the computing resources at CRSEO. I would also like to thank Kirk Waters who deserves recognition for his unlimited good nature and willingness to answer almost any question. Acknowledgement is made to Jeff Hicke who provided programming assistance during the early stages of Interactive Data Language (IDL) image processing. The National Snow and Ice Data Center (Boulder, Colorado) made available the sea ice data and were always responsive to any inquiries concerning their data products. I would like to especially thank Claire Hanson and Michelle Holm for their many efforts and support at NSIDC. Finally, I am deeply indebted to Tim Newberger for many stimulating discussions concerning this research and for his helpful editorial comments. This research was supported by National Science Foundation grant DPP90-11927.

ABSTRACT

Spatial and Temporal Variability in Southern Ocean Sea Ice Coverage

by

Sharon E. Stammerjohn

Spatial and temporal variability in Southern Ocean sea ice coverage is analysed from October, 1978 to December, 1991. Sea ice coverage is calculated from passive microwave satellite data, using Scanning Multi-Channel Microwave Radiometer (SMMR) and Special Sensor Microwave/Imager (SSM/I) data. Spatial variability in sea ice coverage was based on the following eight regions: Southern Ocean, Weddell, Indian, West Pacific, Ross, Amundsen and Bellingshausen regions, as well as a subregion of the Bellingshausen, the Long Term Ecological Research (LTER) study area located west of the Antarctic Peninsula. The six adjacent Southern Ocean regions all show unique interannual variability which is confirmed by cross spectral analysis of monthly anomalies, and no two regions have the same anomalous years of extreme maximum or minimum ice coverage. Regional interannual variability appears to be a yearly re-distribution of near constant ice coverage for the whole Southern Ocean, and in extreme high or low ice years there are asymmetries in Southern Ocean ice coverage. Spectral analysis of monthly anomalies confirmed that most of the variance in regional ice coverages is due to interannual variability. Several patterns in interannual and annual variability are observed in the 13.25-year time series of Southern Ocean ice coverage, and possible climatic forcings contributing to these patterns are discussed. A thorough characterization of LTER ice coverage in comparison to the other regional ice coverages is provided, and possible ice-ocean-air and ice-ecosystem dynamics in the LTER region are explored.

Contents

List of Tables vii

List of Figures viii

1 Introduction 1
- 1.1 Southern Ocean Sea Ice Coverage 1
- 1.2 Research Objectives 6

2 Background 9
- 2.1 Sea Ice Data 9
- 2.2 Passive Microwave Remote Sensing of Sea Ice 13
  - 2.2.1 Theory 13
  - 2.2.2 Algorithm 17
  - 2.2.3 Error Assessment 22

3 Methods 27
- 3.1 Data Preparation 27
  - 3.1.1 Temporal Averaging 28
  - 3.1.2 Regional Ice Coverages 28
- 3.2 Time Series Analysis 31
  - 3.2.1 Autospectral Analysis 32
  - 3.2.2 Autoregressive Modeling 33
  - 3.2.3 Cross-spectral Analysis 34

4 Results 37
- 4.1 Monthly Seasonal Variability 37
- 4.2 Annual Cycles 41

4.3 Monthly Non-Seasonal Variability 49
4.3.1 Anomalies 49
4.3.2 Periodicities 52
4.4 Higher Frequency Variability 55
4.5 Inter-Regional Comparisons 55

5 Discussion **63**
5.1 Interannual Spatial Patterns 63
5.2 Seasonal Spatial Patterns 68
5.3 LTER Temporal and Spatial Patterns 70
5.4 LTER Ice-Ecosystem Dynamics 73
5.5 Future Directions 79

6 Conclusions **81**

A Acronyms **85**

B NASA Team Algorithm **87**

C LTER Sampling Grid **91**

D LTER Ice Indices **95**

Bibliography **99**

List of Tables

2.1 Summary of Southern Ocean satellite sensors 10
2.2 SMMR and SSM/I sensor characteristics 11
2.3 SMMR radiometric channels 12
2.4 SSM/I radiometric channels 12
2.5 A summary of passive microwave sea ice algorithms 17
2.6 Validation of NASA Team algorithm derived ice concentrations . . . 25

3.1 SMMR and SSM/I missing dates 29

4.1 Local maximum ice coverages for the Amundsen and Bellingshausen time series 40
4.2 Characteristics of the 13-year interannual variability in LTER ice coverage. 41
4.3 Mean monthly growth and decay rates of annual ice coverage 44

B.1 SMMR and SSM/I algorithm tie points for the Southern Ocean . . . 90

D.1 Maximum ice coverage within the 75% ice concentration contour . . 96
D.2 Maximum ice coverage within the 50% ice concentration contour . . 97
D.3 Minimum ice coverage within the 15% ice concentration contour . . 98

List of Figures

2.1 Atmospheric transmittance in the microwave frequency domain . . . 14

2.2 Brightness temperatures of sea ice and open water as measured by SMMR for three regions in the Arctic 16

2.3 Sources of radiation detected by satellite microwave radiometers . . 18

3.1 Southern Ocean regional map 30

4.1 Monthly ice coverage for the Southern Ocean, Weddell, Indian, West Pacific, Ross and Bellingshausen/Amundsen regions 38

4.2 Monthly ice coverage for Bellingshausen/Amundsen, Amundsen, Bellingshausen and LTER regions. 39

4.3 Mean annual cycles for 8 selected regions 42

4.4 Contour plot of LTER annual cycles for years 1979-1991 46

4.5 LTER monthly mean percent ice cover from January to June 47

4.6 LTER monthly mean percent ice cover from July to December . . . 48

4.7 Standard deviates of monthly anomalies for 8 selected regions. . . . 50

4.8 Autocorrelations of monthly anomalies for 8 selected regions. . . . 53

4.9 Autospectra for 8 selected regions. 54

4.10 Southern Ocean and Bellingshausen autospectra generated from 2-day time series of each season. 56

4.11 LTER autospectra generated from 2-day time series of each season. . 57

4.12 Squared Coherence between six Southern Ocean regions 58

4.13 Squared Coherence between the LTER subregion and six subregions near LTER 60

4.14 Standard deviates of monthly anomalies for 15° longitudinal pie sections 61

5.1 Estimated LTER production associated with the annual *retreat* of the pack ice from 1979 to 1991 75

C.1 Universal Transverse Mercator projection of the LTER study area . . 93

Chapter 1

Introduction

1.1 Southern Ocean Sea Ice Coverage

Spatial and temporal variability in Southern Ocean sea ice coverage has been well documented since the launch of the first polar orbiting passive microwave remote sensor in 1973. Passive microwave remote sensing of sea ice provided the first year-round data set on sea ice coverage which revealed the extreme seasonality of Southern Ocean sea ice coverage. Southern Ocean sea ice in mid-winter covers an area of about 1.5×10^{7} km^2 which can be distributed over a sea surface area of 2.0×10^7 km^2, reaching a mean latitude of 60° S [1, 2, 3]. About 85% of the winter sea ice melts every spring, and by mid-summer an area of about 2.3×10^6 km^2 of sea ice remains which may extend over an area of 4×10^6 km^2 and is distributed mostly in the western Weddell Sea, in the Amundsen and Bellingshausen Seas and in the eastern Ross Sea regions [3]. Sea ice coverage is circumpolar but not evenly distributed around the continent, and the distribution changes year to year, revealing high interannual variability in sea ice coverage, particulary on regional spatial scales.

The vastness of the Southern Ocean and its inaccessibility makes remote sensing an ideal tool for observing both the short and long term changes in sea ice coverage. Several books and articles have appeared in recent years addressing satellite remote sensing of sea ice in polar regions, providing reviews of past, present and future satellite systems, as well as summarizing theory, methods and applications [4, 5, 6, 7, 8, 9, 10, 11]. This increased attention on polar regions is in part due to the idea that evidence of global warming will be detected first in polar regions [12]. For example, a decreasing trend in annual extent of Southern Ocean pack ice may indicate an increasing trend in global temperatures resulting from the increase in greenhouse-gas concentrations. However, no trends are discernible in the Southern Ocean sea ice cover from 1978 to 1987 [13, 14], despite observed increases in air temperatures in south polar regions [15, 16]. Nonetheless, it is clear that variations in sea ice coverage are closely coupled to variations in both oceanic and atmospheric fields. The relevent spatial and temporal scales of these interactions range spatially from meters to thousands of kilometers and temporally from diurnal to decadel [17].

In order to address why regions show distinctly different interannual and annual variability in ice coverage, the processes controlling ice growth and decay as well as ice advection into and out of regions need to be defined. The actual physical mechanisms controlling ice growth and decay and ice advection are complicated by interconnections and feedbacks and are not completely understood. However, numerous dynamic-thermodynamic ice models which predict ice drift, ice thickness and ice concentration with moderate success use observed winds, air temperatures, oceanic heat fluxes and surface radiation as forcing parameters [18, 19]. Hibler and Ackley (1983) [19] concluded from a numerical simulation of the Weddell pack ice that ice advance is mostly driven by thermodynamics, whereas ice retreat depends on lead generation and ice advection. The generation of leads during the ice retreat period allows for increased solar radiation to be absorbed by surface waters which in turn heats the surrounding sea ice. Antarctic sea ice is typically snow covered so that surface radiation is reflected by the high albedo of the snow covered sea ice. Low albedo open leads are therefore critical in transferring heat into the pack ice which accelerates ice retreat. However, Gordon (1981) [20] concluded in a study of the seasonality of Southern Ocean sea ice that the atmospheric-to-ocean heat flux, including the heat flux associated with the numerous leads in Antarctic pack ice, was insufficient to account for the rapid ice retreat in spring. Gordon suggested that the additional heat required to melt the pack ice at the observed rates for the Southern Ocean came from upwelling of warmer deep water caused by regional Ekman divergence of the surface layer and by cross-pycnocline mixing. Gordon also suggested in an earlier study (1975) [21] that ice advance is not purely driven by thermodynamics but by wind-driven Ekman transport as well. A cyclonic wind field induces divergent Ekman transport of sea ice which opens leads in the interior of the pack ice. In winter ice continues to form in these open leads at the same time ice is advected northward. In this way, ice advance is both due to thermodynamics in open leads and to Ekman drift.

In addition to coupled ice-ocean modelling efforts, there have been numerous studies attempting to find relationships between ice extent and atmospheric circulation patterns [22, 1, 23, 24, 25, 26, 27]. Streten and Pike (1980) [27] stressed that both oceanic current and atmospheric circulation patterns are intrinsically coupled to the Antarctic continental coastline configuration and thereby promote very different *regional* patterns. In general, climate (air temperature, pressure, wind speed, cyclogenesis and storm tracks) over the Antarctic continent is relatively stable, whereas over the perennial sea ice zone, the climate is highly variable on both annual and interannual temporal and spatial scales [24]. The atmospheric circulation over the Southern Ocean and Antarctic continent is dominated by two features: 1) a persistent high pressure cell located over the east Antarctic continent, and 2) a ring of low pressure cells located between 60-75° S which delimits the *circumpolar trough.* The circumpolar trough is defined by three semi-permanent lows, one each located over the Weddell and Ross Seas and one off the east Antarctic coast, as well as by less permanent lows which show high annual and interannual variability both in number and longitudinal position [1, 24, 25]. The circumpolar trough intensifies in winter and weakens in summer, and its mean position oscillates from a more equatorward position in July (60-70° S) to a more poleward position in January (65-75° S) [1, 25]. In addition, Carleton (1981) [25] determined from an analysis of mean monthly (1973-1977) distributions of cyclonic vortices located poleward of 20° S that the maximum frequency of cyclones located most *equatorward* (40-49° S) is in July while the maximum frequency of cyclones located most *poleward* (60-75° S) is in September [25]. The most southerly cyclones located over the pack ice are mature/dissipating cloud vortices which may have originated just north of the ice edge. As cyclones mature they drift southeastward over the pack ice, influencing both regional ice coverages and relationships between adjacent regions by ice advection [24, 25]. Several studies have observed that on a seasonal or interannual basis more northerly (or southerly) ice extents are often located west of (or east of) regions showing an increased frequency of low pressure centers. This would suggest that cyclonic (clockwise) winds act to increase ice extents to the west of the pressure center by direct ice transport and/or by *in situ* freezing from high latitude cold air advection [22, 23, 25, 26, 27]. Likewise, the cyclonic winds would decrease ice extent east of the pressure center by compaction of the ice edge and/or by *in situ* melting from low latitude warm air advection. Ice edge advection eastward along zonal flow has also been observed when low pressure centers were located well poleward of the ice edge [23, 25]. More southerly ice extents also have been observed in regions of high pressure ridges which are usually associated with warm air advection from lower latitudes [23, 27]. The above relationships seem to hold true on seasonal to interannual temporal scales, but on daily to weekly temporal scales Carleton (1989) [22] found that the relationships between ice extents and polar low development is not always evident. To summarize the above studies, longitudinal variations in the frequencies of high latitude polar lows in winter may contribute to regional variabilities in ice coverage by one or more of the following processes:

- promotion of *in situ* freezing from advection of higher latitude cold air west of low pressure centers
- northwestward advection of ice by wind-driven circulation west of low pressure

centers

- promotion of *in situ* melting from advection of lower latitude warm air east of low pressure centers

- southeastward compaction of ice extent by wind-driven circulation east of low pressure centers

- eastward advection of ice edge by wind-driven circulation north of low pressure centers

- inhibition of ice growth in regions of high pressure ridges

Other studies have looked for relationships between air temperatures and ice extent [28, 15, 16, 29, 26]. Cavalieri and Parkinson (1981) [26] found that the mean position of the ice edge for years 1973-75 lagged zonally-averaged temperatures for those same years by 1 to 1.5 months, while Lemke *et al.* (1980) [30] found sea ice maximums to lag solar radiation minimums by 1.5 to 3 months, dependent on latitude. Weatherly *et al.* (1991) [28] found that lag correlations between 15-year seasonal anomalies for sea ice and air temperatures were strongest when ice lagged the summer temperatures and when ice lead the winter temperatures, suggesting that summer temperatures predispose the near-surface waters to above or below normal ice coverage in the following fall and winter. They also found that correlations were strongest (and negative) for the Bellingshausen/Amundsen Sea region.

There have been numerous studies trying to relate El Niño Southern Oscillation (ENSO) events to Southern Ocean atmospheric circulation and sea ice variability [31, 32, 33, 34, 35, 36]. Karoly (1989) [31] found that upper tropospheric height anomalies may form a weak wavetrain pattern over Australia and the South Pacific Ocean to South America in Southern Hemisphere winters during early stages of ENSO events. During mature stages of ENSO events in Southern Hemisphere summers the circulation anomalies are more stable and zonally symmetric. Karoly stressed that his results are based on a very short time period (1972-1983) and to fully elucidate the variability in circulation features, especially at high latitudes, a much longer period of data is required. Carleton (1989) [35] analyzed possible relationships between sea ice extent and several atmospheric indices, the Southern Oscillation Index (SOI), the Trans-Polar Index (TPI) and several local indices. SOI is calculated by subtracting sea level pressure at Tahiti from sea level pressure at Darwin (northern Australia) and the difference is then normalized to the standard deviations of the differences for the record length. TPI is calculated in a similar way and is the normalized pressure anomaly difference of Hobart (Tasmania) minus Stanley (Falkland Islands). Carleton concluded that generally sea ice extent may lag the SOI but lead the TPI in key months (although he found that for the data period 1973-82, Ross sea ice lead SOI). However, Carleton also concluded that confirmation of these weak relationships between sea ice extent and low-frequency atmospheric variations will have to wait for longer data records.

1.2 Research Objectives

The Antarctic Marine Long Term Ecological Research (LTER) project funded by the National Science Foundation's Office of Polar Programs focuses on temporal and spatial variability in Antarctic marine ecosystems. A key hypothesis of this LTER project proposes that interannual and annual variability in sea ice coverage is the major physical determinant in spatial and temporal changes in Antarctic marine communities. General objectives of the LTER project are to:

1. document interannual variability in ice coverage, life-history parameters of primary producers and populations of key species from different trophic levels in the Antarctic marine food web.

2. understand and quantify the processes that contribute to natural variation in these representative populations.

3. construct models that link ecosystem processes to physical environmental variables and simulate the spatial/temporal relationships between representative populations.

4. employ such models to predict/validate ice-ecosystem dynamics.

Field research for the Antarctic Marine LTER project began in November, 1991 and is proposed to continue through 2000, providing the long term temporal record needed to understand the variability and interconnections between sea ice coverage and marine communities. The Antarctic Marine LTER focuses on a study area west of the Antarctic Peninsula which extends 900 km along the length of the Peninsula and 200 km out from the Peninsula (see Appendix C for a more detailed description of the LTER study area). Thus, the spatial and temporal scales, upon which the Antarctic Marine LTER is conducted, is pertinent to studying air-sea-ice interactions as well as ice-ecosystem interactions.

The focus of this research is to provide an historical record of sea ice coverage for the LTER study area provided by the passive microwave remote sensing data sets. In order to better understand and/or distinguish variability in LTER sea ice coverage from variability in other Southern Ocean regions, the entire Southern Ocean will be regionalized for comparative purposes. The regionalization will be mostly based on those regions traditionally used in previous studies [37, 2, 1] so that results can be compared to those studies as well. This provides a thorough characterization of the interannual and annual variability in LTER sea ice coverage, as well as insight into the processes controlling sea ice variability in the LTER region and into the spatial and temporal scales most relevant to: air-sea-ice and ice-ecosystem interactions within the LTER region.

Background information on passive microwave remote sensing of sea ice will be addressed in the next chapter which includes a review of how sea ice concentrations are derived from passive microwave data and comments on the error involved in this derivation. Methods used in analyzing the spatial and temporal variability in

Southern Ocean sea ice coverage are presented in Chapter 3. The results are described in Chapter 4 which illustrates the spatial and temporal variability in Southern Ocean ice coverage, detailing LTER sea ice coverage where appropriate. Chapter 5 provides discussion of results, including discussion on interannual and annual spatial patterns and possible ice-ocean-air and ice-ecosystem dynamics in the LTER region. Chapter 6 provides a summary of the key points made in the discussion.

Chapter 2

Background

2.1 Sea Ice Data

The satellite sensors used to determine sea ice extent and concentrations are visible and infrared sensors as well as microwave sensors. Table 2.1 (page 10) highlights the most *common* sensors used for determining ice extent and concentrations for the Southern Ocean and is not meant to be a complete listing of all sensors viewing the Southern Ocean. Active microwave achieves the best resolution, but historically there has not been much coverage of the Southern Ocean. However, the number of synthetic aperture radars (SARs) in polar orbit is increasing, and it is hoped by the end of this decade, SAR data for the Antarctic will be routinely available. Moderate resolution is obtained from visible and infrared sensors, however both are limited by cloud cover and in the case of visible sensors, by polar darkness. Passive microwave, although having the poorest resolution, provides the most complete temporal record of the annual advance and retreat of sea ice, since clouds or polar darkness do not interfere with its remote sensing capabilities.

To study temporal and regional variability in Southern Ocean sea ice coverage, the historical record provided by the passive microwave sensors provides the most complete time series for temporal and spatial analyses. The National Snow

Table 2.1: Summary of Southern Ocean satellite sensors

Satellite	Sensor	Sponsor	Type	Resolution	Date
TIROS-N & NOAA[a]	AVHRR	NOAA	Vis and NIR/IR/TIR	1 km	1978-
DMSP	OLS	USAF	Vis/TIR	0.56-2.8 km	1976-
Nimbus 5/6	ESMR	NASA	Passive Microwave	30 km	1973-77
Nimbus 7	SMMR	NASA	Passive Microwave	30 km	1978-87
DMSP	SSM/I	USAF	Passive Microwave	25 km	1987-
ERS-1	SAR	ESA	Active Microwave	25 m	1991-

---

[a] See Appendix A for List of Acronyms

and Ice Data Center (NSIDC) distributes data from Electrically Scanning Microwave Radiometer (ESMR), Scanning Multi-Channel Microwave Radiometer (SMMR) and Special Sensor Microwave/Imager (SSM/I). The ESMR data is provided on 9-track tape and the SMMR and SSM/I data are provided on cdrom. The cdroms contain both brightness temperatures as well as two sets of calculated ice concentrations, one using the NASA Team algorithm [38, 39] and one using the Comiso algorithm [40, 41]. Both SMMR and SSM/I ice concentrations are gridded in a polar stereographic projection at a resolution of 25 x 25 km. The ice concentration grids are displayed as raster images and include coverage south of 50° S latitude. The cdroms also contain a landmask and latitude and longitude pairs for geolocating pixels. A user guide is included with the cdroms, providing documentation on data processing, cdrom content and grid format [42]. This study utilizes NSIDC's SMMR and SSM/I datasets only, because ESMR data have not yet been converted to the SMMR and SSM/I format. However, NSIDC plans in the near future to regrid and reformat

Table 2.2: SMMR and SSM/I sensor characteristics

Sensor	Operational Dates	Altitude (km)	Incident Angle	Scan Geometry
SMMR	10/24/78-8/25/87	~ 950	50°	Conical cross-track
SSM/I	6/19/87-present[b]	~ 833	53.1°	Conical cross-track

---

[b] Archived data starts 7/8/87; sensor turned off from 12/3/87 to 1/12/88

Table 2.2 cont.: SMMR and SSM/I sensor characteristics

Sensor	Swath Width (km)	Scan Period	Dynamic Range (K)	Absolute Accuracy (K)	Temporal Coverage	Maximum Latitude
SMMR	783	4.1 sec	10-330	2	every 2 days	84° N/S
SSM/I	1394	1.9 sec	375	1.5	twice daily	87° N/S

ESMR data to make it compatible with SMMR and SSM/I, as well as provide it on cdrom.

The SMMR and SSM/I sensor characteristics and channels are described in Tables 2.2, 2.3 and 2.4. As shown in Tables 2.3 and 2.4 (page 12), the SMMR channels were slightly changed for the SSM/I sensor. The lower SMMR frequencies (channels 1 and 2) enabled detection of sea surface temperatures, a feature not available with SSM/I. The addition of the 85.5 GHz frequency on the SSM/I sensor was solely for polar applications and in part experimental. Preliminary results show that the 85 GHz data may help to identify newly formed sea ice and snow cover [43], characteristics not detectable by the other SMMR and SSM/I frequencies. SMMR channel 4 (21.0 GHz) and SSM/I channel 2 (22.235 GHz) are sensitive to the water vapor resonance line (see Section 2.2.1) and allows for correction of the other channels. Both the SMMR and SSM/I sensors have dual-polarized frequencies at 18-19 GHz and at 37.0

Table 2.3: SMMR radiometric channels

SMMR	Channel 1	Channel 2	Channel 3	Channel 4	Channel 5
Frequency (GHz)	6.63	10.69	18.0	21.0[c]	37.0
Polarisation	H,V	H,V	H,V	H,V	H,V
Radar Wavelength (cm)	4.52	2.81	1.67	1.43	0.81
Geometric Footprint (km)	136x89	87x58	54x35	44x29	28x18
Temperature Resolution (K)	0.9	0.9	1.2	1.5	1.5

---

[c] Channel 4 turned off 3/85

Table 2.4: SSM/I radiometric channels

SSM/I	Channel 1	Channel 2	Channel 3	Channel 4
Frequency (GHz)	19.35	22.235	37.0	85.5
Polarisation	H,V	V	H,V	H,V[d]
Radar Wavelength (cm)	1.55	1.35	0.81	0.35
Geometric Footprint (km)	70x45	60x40	38x30	16x14
Temperature Resolution (K)	0.8	0.8	0.6	1.1

---

[d] H Channel failed on 2/26/90

GHz. Sea ice algorithms use these two dual-polarized frequencies to calculate ice concentrations from SMMR and SSM/I brightness temperatures (see Section 2.2.2). Comparison studies have shown that ice concentrations calculated from SMMR and SSM/I datasets (using the NASA Team algorithm) during the two month overlap in data acquisition (July-August) differ by 0.2% ± 5% for the Southern Hemisphere [3]. These differences are well within the error associated with the ice concentration calculations (see Section 2.2.3).

2.2 Passive Microwave Remote Sensing of Sea Ice

2.2.1 Theory

Passive microwave radiometers operate at electromagnetic frequencies between 1 to 300 GigaHertz (GHz) (10^{-9} cycles per second) which correspond to wavelengths between 1.5 to 300 mm. Figure 2.1 (page 14) shows atmospheric transmittance in the microwave frequency domain. Frequencies typically used for sea ice detection are between 9 to 90 GHz. Within this range there are three atmospheric windows that permit detection of the natural microwave radiation emitted by the surface. These windows are bounded by absorption lines due to water vapor near 22.2 GHz and oxygen near 60 and 118.8 GHz. Most sea ice algorithms use frequencies below 40 GHz, where in polar latitudes the atmosphere is relatively transparent, except in the water-vapor absorption band at 22.2 GHz.

Passive microwave radiometers measure the natural microwave radiation emitted by the targetted surface which is expressed as the brightness temperature, T_B. Because real surfaces emit only a fraction of the radiation that would be emitted by a perfect emitter or black-body at the same physical temperature, the emitting properties of a real surface are described by its spectral emissivity, ε. According to the Raliegh-Jeans approximation of the Planck radiation law, emissivity (ε) is defined by the ratio of the microwave radiant flux (T_B) to that of a blackbody at the same

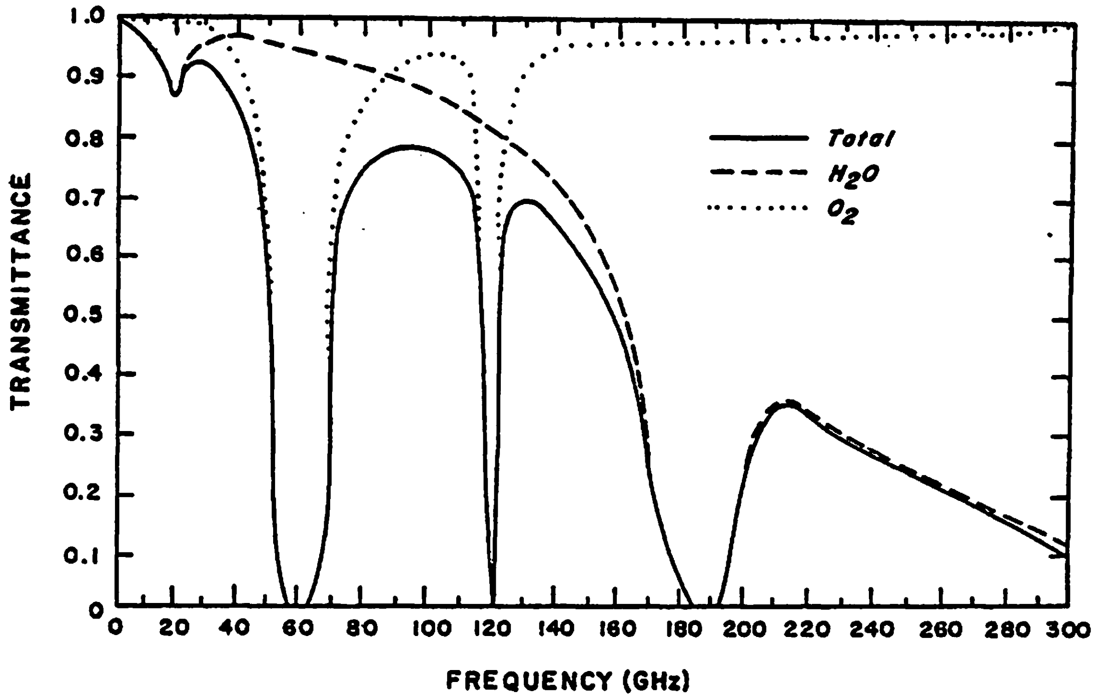

Figure 2.1: Atmospheric transmittance in the microwave frequency domain. From Liou (1980) [44].

physical temperature (T_S). Both ε and T_B are frequency or wavelength (λ) and polarization (p) dependent and can be expressed by the following relationship:

$$T_B[\lambda, \mathrm{p}] = \varepsilon[\lambda, \mathrm{p}]\, T_S \qquad (2.1)$$

Thus, factors which influence T_B include the physical temperature of the surface as well as the emissivity. The range of T_S over sea ice is about 240-270 K and varies uniformally with latitude [1, 3]. Emissivity varies with surface roughness and the dielectrical properties of the medium, which are in turn a function of temperature, salinity and density. Spatial variations in emissivity contribute more to the overall spatial variations in T_B than does T_S in polar regions [45]. The emissivity of calm seawater at 19 GHz is about 0.44, of first-year sea ice, 0.92 and of multiyear sea ice, 0.84 [45]. First-year sea ice (*FY*) has a higher emissivity than multiyear sea ice (*MY*) primarily due to the higher brine content. Surface layers in *MY* have typically been flushed of brine due to the surface melting/refreezing process occuring between spring and fall. These brine channels are replaced by air/gas pockets which act as volume scatterers, further decreasing emissivity. In general, emissivity of sea ice *decreases* with [46]:

- increasing density
- decreasing salinity
- decreasing temperature
- with empty brine channel scattering

Snow cover can complicate the measured T_B, because it can either increase or decrease the emissivity. If the snow is dry, non-saline and less than about 35 cm thick, then it is relatively transparent at microwave frequencies [9]. However, if the snow is thicker than about 35 cm, it can effectively insulate the sea ice, keeping the ice relatively warm compared to the surface. This increased emission at the snow/ice interface can either be absorbed or scattered by the overlying snow. Wet snow is a better absorber and emitter, increasing emissivity, whereas dry granular snow scatters the emittance at the snow/ice interface, decreasing emissivity.

Figure 2.2 (page 16) shows the spectral dependence of T_B for three common surface types in polar oceans, open water (OW), FY and MY. Figure 2.2 illustrates two characteristics upon which most sea ice algorithms are built. The first characteristic is the difference between the vertically and horizontally polarized radiances which is small for both FY and MY but large for OW. The second characteristic is that the discrimination between ice types increases with decreasing wavelength (increasing frequency) and is largest at 0.81 cm (37 GHz). Section 2.2.2 describes how these two characteristics are used to calculate sea ice concentrations.

The spectral differences between FY and MY in the Antarctic are not as strong as for these ice types in the Arctic (ie., Figure 2.2). Surface winds blowing

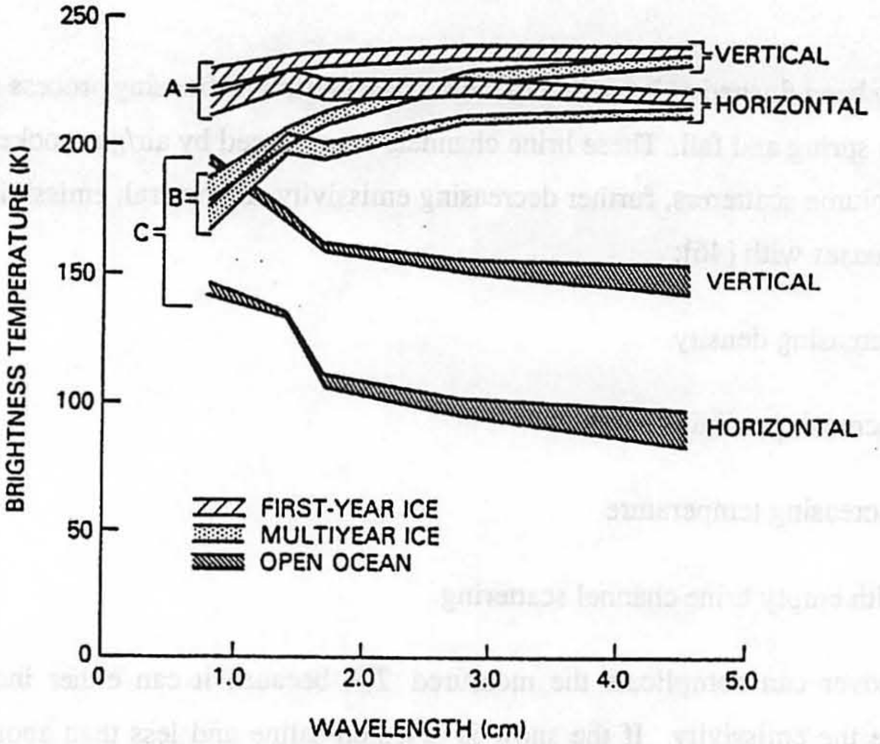

Figure 2.2: Brightness temperatures of sea ice and open water as measured by SMMR for three regions in the Arctic: (A) Baffin Bay which contained consolidated FY, (B) Canadian Arctic which contained mostly MY and (C) Norwegian Sea which contained OW. The SMMR wavelengths from 0.81 to 4.52 cm correspond to frequencies from 37 to 6.63 GHz. From Cavalieri *et al.* (1984) [39].

over the pack ice are on the average stronger in the Antarctic than in the Arctic which decreases relative humidity [47]. As a result, higher temperatures are required to melt sea ice surfaces. Therefore, spring melt ponds and seasonal brine flushing associated with Arctic MY is less common in the Antarctic [9, 47]. Also, Antarctic MY consist mostly of frazil ice which has granular ice crystals, inhibiting brine drainage, whereas Arctic MY consist mostly of congelation ice which has columnar ice crystals, promoting brine drainage [48, 49, 50]. Therefore, the radiometric signatures of Antarctic FY and MY are less distinct than Arctic FY and MY for frequencies less than 40 GHz [48]. Overall, Antarctic pack ice is more saline than Arctic pack ice, presumably due to more flooding or intrusion of seawater [51]. For example,

Table 2.5: A summary of passive microwave sea ice algorithms

Algorithm[e]	Method	Application
NASA Single Frequency	radiative transfer with mixing formalism, linear: 37 GHz	gridded ESMR
NASA Team	radiative transfer with mixing formalism, nonlinear: 18 V/H, 37 GHz; hemispheric/regional tie points	gridded SMMR and SSMI, hemispheric and regional
AES-YORK[f] and FNOC	radiative transfer with mixing formalism, linear: 18, 37 GHz for ice concentrations $> 70\%$, 37 GHz for ice concentrations $< 70\%$; iterative for atmospheric opacity	gridded SMMR and SSMI, hemispheric and regional
NORSEX	radiative transfer with mixing formalism, linear: 10 V, 37 V GHz; iterative for atmospheric opacity	gridded SMMR, regional
U-Mass	radiative transfer with mixing formalism, linear: 10 V/H, 19 V/H, 37 V/H GHz; iterative	orbital SMMR and SSM/I, northern hemisphere only
GSFC	radiative transfer with mixing formalism, linear: 10 V/H, 18 V/H, 37 V/H GHz; bootstrap	gridded SMMR and SSMI, hemispheric

---

[e] Table composed from Steffan *et al.* (1992) [45]

[f] See Appendix A for List of Acronyms

salinity content of Antarctic FY and MY is about 4.6 and 3.7 ppt, respectively [48], whereas the salinity content of Arctic FY and MY is 3.0 and 2.0 ppt, respectively [52].

2.2.2 Algorithm

Table 2.5 lists a selection of passive microwave sea ice algorithms and summarizes the methods and applications for which the algorithms were developed. All but the NASA single frequency algorithm were developed for SMMR and SSM/I data and uses the multifrequency, dual-polarized spectral characteristics of open water

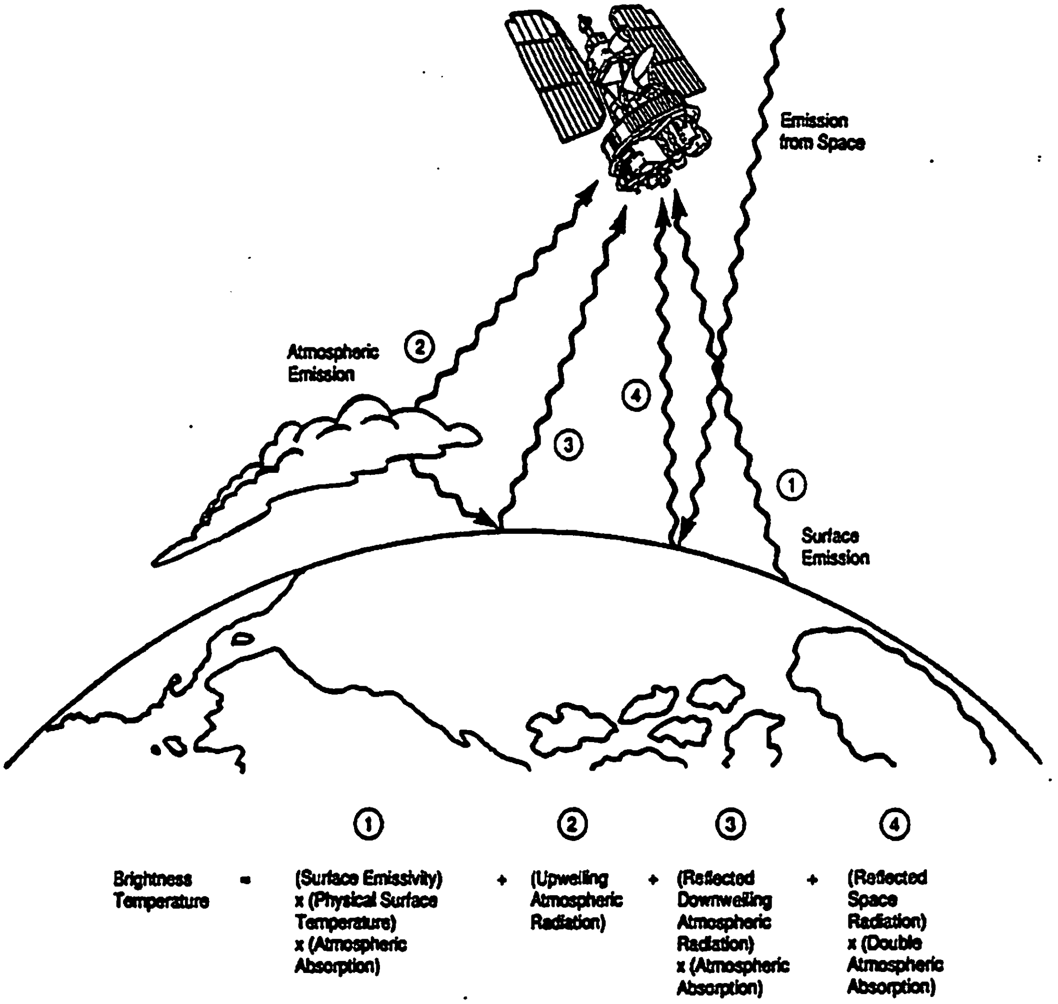

Figure 2.3: Sources of radiation detected by satellite microwave radiometers. From Swift and Cavalieri (1985) [53].

and sea ice (ie., Figure 2.2) to calculate sea ice concentrations. All the algorithms use the radiative transfer equation as the basis for converting satellite radiance data into sea ice parameters. Figure 2.3 shows schematically the sources of radiation detected by a satellite microwave radiometer and how these sources are expressed in the radiative transfer equation. The radiative transfer terms as illustrated in Figure 2.3 is expressed in the radiative transfer equation as:

$$T_B = \varepsilon T_S e^{-\tau} + T_{up} + (1-\varepsilon)T_{down}e^{-\tau} + (1-\varepsilon)T_{sp}e^{-2\tau} \qquad (2.2)$$

where

T_B is the brigthness temperature measured at the satellite,
ε is the surface emissivity,
T_S is the physical surface temperature,
$e^{-(2)\tau}$ is the (double) atmospheric absorption,
T_{up} is the upwelling atmospheric radiation,
$(1 - \varepsilon)T_{down}$ is the reflected downwelling atmospheric radiation,
$(1 - \varepsilon)T_{sp}$ is the reflected space radiation

T_B and ε are both wavelength and polarization dependent and τ is wavelength dependent (these subscripts in Equation 2.2 were left out for simplicity). For frequencies greater than 1 Ghz, reflected space radiation (the 4th term in Figure 2.3 and in Equation 2.2) is insignificant [54] and is therefore ignored in calculations of sea ice concentrations. The second and third terms are typically combined into an atmospheric correction term and is assumed to be linearly related to T_S and therefore to T_B to the first order.

The NASA Team algorithm (formally the SMMR Team algorithm) is most widely used by the research community. Numerous validation programs were carried out to estimate the NASA Team algorithm accuracy [55, 56, 57, 58] which will be discussed in Section 2.2.3. The NASA Team algorithm was first formalized by Cavilieri et al. (1984) [39] to derive sea ice parameters from SMMR data. The algorithm was later improved by Gloersen and Cavalieri (1986) [38] to reduce weather-related effects over open ocean areas and in the vicinity of marginal ice zones. The NASA Team algorithm assumes that there are three surface types within the footprint of the viewing sensor: OW, FY and MY. These three surface types are distinguished by two ratios, the polarization ratio (PR) and the spectral gradient ratio (GR):

$$PR = \frac{T_B[18V] - T_B[18H]}{T_B[18V] + T_B[18H]} \tag{2.3}$$

$$GR = \frac{T_B[37V] - T_B[18V]}{T_B[37V] + T_B[18V]} \tag{2.4}$$

It is noted that channels 18 H/V are replaced by channels 19.35 H/V in Equations 2.3 and 2.4 when calculating PR and GR from SSM/I data. The physical basis for these two ratios is based on the spectral characteristics of the three surface types illustrated in Figure 2.2. The advantage of using ratios of radiances is that the calculations are independent of surface temperatures (T_S cancels in Equation 2.1), eliminating the problem of estimating temporally and spatially varying surface temperatures.

Assuming that the three surface types sum to unity within a footprint, the radiative transfer equation can be written as:

$$T_B = T_{B,OW}(1 - C_{FY} - C_{MY}) + T_{B,FY}(C_{FY}) + T_{B,MY}(C_{MY}) \tag{2.5}$$

where

T_B is the brigthness temperature measured at the satellite,
$T_{B,OW}$, $T_{B,FY}$ and $T_{B,MY}$ are the algorithm tie points,
C_{FY} and C_{MY} are the fractional ice concentrations of FY and MY

Equation 2.5 can be substituted into Equations 2.3 and 2.4 and solved simultaneously for C_{FY} and C_{MY} (see Appendix B for derivation):

$$C_{FY} = \frac{a_0 + a_1 PR + a_2 GR + a_3(PR)(GR)}{D} \tag{2.6}$$

$$C_{MY} = \frac{b_0 + b_1 PR + b_2 GR + b_3(PR)(GR)}{D} \tag{2.7}$$

where

$$D = c_0 + c_1 PR + c_2 GR + c_3(PR)(GR) \tag{2.8}$$

The total ice concentration is the sum of FY and MY concentrations (Equation 2.6 plus 2.7). The numerical coefficients in Equations 2.6, 2.7 and 2.8 are functions of nine brightness temperatures referred to as algorithm tie points and are empirically determined for the three surface types. The ice concentrations used in this study were calculated using two different sets of *hemispheric* tie points, one set for the SMMR data and one set for the SSM/I data (see Appendix B). Hemispheric tie points assume that the T_B's determined for the three surface types are spatially and temporally consistent throughout the southern (or northern) region. However, studies have shown that T_B's vary both spatially and temporally for a given ice type which may justify using *local* tie points [57, 59]. The difficulty of using local tie points are the logistics involved in empirically determining them. Errors associated with using hemispheric versus local tie points will be discussed in Section 2.2.3.

The NASA Team algorithm ignores both the atmospheric correction term and the reflected space term in the radiative transfer equation (see Equation 2.2) in calculating sea ice concentrations with Equations 2.6 and 2.7. It was already noted that above 1 GHz, reflected space radiation is insignificant [54]. Because high latitudes are characterized by low humidity and high transmittance (with the exception of the 22.2 GHz band), atmospheric correction is minimal. However, at lower latitudes, for example in the region of the marginal ice zone at *maximum* ice extent, humidity levels and cloud liquid water contents increase, and atmospheric attentuation and emission become detectable [38, 60]. In addition, winds and precipitation from the passage of storms contributes significantly to increased microwave emissions (especially over open ocean) [38, 57], as well as alters ambient air temperatures and physical characteristics of ice and snow [61]. To reduce errors related to weather and atmospheric effects in the marginal ice zone, Gloersen and Cavalieri (1986) [38] improved the NASA Team algorithm with a "weater filter". Based on their analyses, if the *gradient* ratio (Equation 2.4) is constrained to ≤ 0.08, spurious ice concentrations due to weather-related effects (winds, water vapor and cloud liquid water) in the marginal ice zone will be reduced. The NSIDC ice concentration data were calculated using a GR threshold of 0.05. The lower GR threshold not only eliminates weather-related effects, but also eliminates ice concentrations below 15%, the ice concentration contour that most accurately defines the ice edge according to a 1991 validation study [56]. Additional errors created by ignoring the atmospheric correction term will be discussed in Section 2.2.3.

2.2.3 Error Assessment

The sources of error in the calculated ice concentrations lie in three limitations of the NASA Team algorithm which are the following:

1. The algorithm accounts for only three surface types.

2. The atmospheric correction in the radiative transfer equation is ignored.

3. The algorithm is dependent on empirically derived tie points.

The first limitation which assumes that there are only three surface types within the footprint of the sensor (ie., relatively calm open water, first year ice and/or multiyear ice) neglects identifying many other surface types that can exist such as wind-roughened open water, new ice, thin ice, melting ice or snow covered ice. Fortunately this study is not concerned with concentrations of various ice types, but with the total concentration of ice cover. Therefore it is not critical if multiyear ice is identified as first year ice which, as discussed previously, is often the case in the Southern Ocean. However, microwave signatures of new and thin ice can be close to that of open water [62, 63], whereas microwave signatures of storm roughened water can be close to that of first year ice [45]. Increases in wind speed cause increases in surface roughness, foam and atmospheric water vapor. These conditions can increase the temperature brightness of open water as much as 40 K which could give it the radiometric signature of first year ice. The misidentification of new ice and storm roughened open water will decrease the accuracy of the ice concentrations, particularly in marginal ice zones and in polyna regions. Melting ice also decreases the accuracy of spring and summer ice concentration estimates. Nonetheless, the estimation of *total* ice coverage for the Southern Ocean is highly accurate (< 2% error) [51], because the size of the marginal ice zone is small compared to the total ice coverage. This is not true for regional studies, where marginal ice zones are proportionately bigger compared to the total ice coverage of the region being studied. Because validation studies have not been located in regions with a dominant marginal ice zone, the error involved with most regional studies of ice coverage has not been quantified at this time.

The second limitation that the atmospheric correction term in the radiative transfer equation is negligible for polar regions is not valid for lower latitudes associated with maximum ice extents and for severe weather conditions in open ocean areas and in marginal ice zones. Heavy cloud cover is usually associated with open water areas. An increase in cloud liquid water decreases the accuracy of the 37 GHz channels which are more sensitive to clouds than are the 18 GHz channels. This increased sensitivity to cloud liquid water in the 37 GHz channels is avoided by using the weather filter mentioned in Section 2.2.2 which constrains the GR to below 0.05 and redefines the ice edge at the 15% ice concentration contour. In a comparison study between weather filters used by four different ice algorithms (including the NASA Team algorithm), it was shown that the 0.05 GR threshold was in fact successful in eliminating weather-related effects over open ocean areas [45]. However, using such a high threshold reduces the ice concentration resolution along the marginal ice zones and in polynya regions. Also, the weather filter does not address weather-related effects over ice. Maslanik (1992) [60] showed that although *total* ice concentration estimates are not much affected by weather-related effects, ice type classification and the detection of small trends in ice covered areas are affected.

The third limitation of the NASA Team algorithm is the use of algorithm tie points. The NASA Team ice concentrations used in this study were calculated using hemispheric tie points which are statistically derived from representative samples of pure surface types from Southern Ocean satellite data. Consequently, temporal and spatial variability in tie points is not considered. Steffan and Schweiger (1991) [57] discuss using locally and seasonally adjusted tie points to improve algorithm accuracy. Their results show that mean differences between SSM/I and Landsat ice concentrations for local Antarctic areas is 7.2% using local tie points and 11.7% using hemispheric tie points. Presumably, if these local tie points were seasonally adjusted as well, accuracy would have been further improved. Another recent study by Thomas (1993) [59] discusses using tie points derived from the overall means of temporally varying signatures taken from representative samples of pure surface types. This approach significantly improves precision estimates of multiyear ice fractions for the Arctic, but it is unknown how it would improve Southern Ocean ice concentration estimates.

Validation of the NASA Team algorithm for Southern Ocean sea ice concentrations is limited which precludes a quantitative measure of the precision and accuracy of the estimated ice concentrations. Most validation efforts have been focused in Arctic regions due to easier logistics involving difficult coordinations of multi-platform and multinational field efforts. Validation programs use a number of different data sets to validate the geophysical parameters estimated from sea ice algorithms. Such data sets may include visible and infrared satellite imagery, visual observations from aircraft and high resolution active and passive microwave data collected from aircraft. Airborne microwave measurements are particularly useful, because airborne measurements can be taken coincident with the satellite measurements. At best, validation studies should address both spatial and temporal variabilities in sea ice by including regions of consolidated ice (containing both multiyear and first-year sea ice), marginal ice zones and regions of re-occuring polynyas and conducting these studies during each season. The estimated accuracies resulting from Arctic-based validation studies provide some idea of algorithm performance but cannot be *directly* applied to estimates of Southern Ocean sea ice concentrations due to different predominant ice types and radiometric ice signatures between the two polar regions. Table 2.6 (page 25) lists the results of the three validation studies which were conducted in Southern Ocean regions and which compared SMMR or SSM/I derived ice concentrations using the NASA Team algorithm against other satellite derived ice concentration datasets. The mean and standard deviation of the difference between

Table 2.6: Validation of NASA Team algorithm derived ice concentrations

Region	**Month**	**Sensor**	**Mean difference, ± std, %**	**Validation data set**	**Reference**
Weddell Sea	October	SMMR	1.7 ± 7.4	SIR-B	Martin et al., (1987) [64]
Weddell Sea	November	SSM/I	-1.1 ± 3.1	Landsat MSS	Steffan and Schweiger (1991) [57]
Amundsen Sea	December	SSM/I	1.3 ± 3.6	Landsat MSS	Steffan and Schweiger (1991) [57]

SMMR or SSM/I ice concentrations and the validation dataset are shown for each study. The study by Martin et al. (1987) involved a region in the Weddell sea that had 40-100% ice coverage of consolidated ice. From a Student's t-test calculated in the study, the mean of 1.7% was not significantly different from zero ($p \leq 0.05$). The accuracy of the SIR-B sea ice concentrations was not given however, so the absolute accuracy of the NASA Team algorithm based on this validation study is unknown. In the second and third validation studies by Steffan and Schweiger (1991), both regions were dominated by > 70% consolidated ice coverage. The accuracy of the cloud-free Landsat MSS ice concentrations was estimated to be within 2-4%. Both the mean differences and standard deviations were slightly lower in the Steffan and Schweiger study than in the Martin et al. study. These results indicate that the estimation of *total* ice concentrations for regions with > 40% ice coverage can be determined with very little bias. Unfortunately, the accuracy of the NASA Team algorithm in predicting ice concentrations in marginal ice zones and in polynas or where ice concentrations are less than 40% is still unknown for Antarctic regions. Arctic validation studies found that mean differences between SSM/I ice concentrations and the validation dataset are as much as 9% in regions with large areas of new and young ice [57]. The mean difference could potentially be much higher for Antarctic marginal ice zones because these zones are generally more divergent than Arctic marginal ice zones [51].

Chapter 3

Methods

3.1 Data Preparation

The sea ice concentration data used in this study were provided by NSIDC on cdrom and include the SMMR and SSM/I data. Two sets of ice concentrations were available, one calculated by the NASA Team algorithm and the other by the GSFC algorithm. The ice concentrations calculated by the NASA Team algorithm are used in this study, because it has been most widely used by the scientific community and thus provides comparative studies for this research. In addition, numerous validation programs have been carried out to estimate algorithm accuracy, although most of these studies have been located in Arctic regions. Image processing of the SMMR and SSM/I cdrom data was done on DECstations (Digital Equipment Corporation) using IDL (Interactive Data Language) [65]. Initially the entire dataset (ie., the whole Southern Ocean) was processed into monthly averages. The monthly averages were then divided up into regions and percent concentrations were converted into regional sea ice coverages for temporal and spatial analyses. The data for three selected regions were then reprocessed into 2-day averages for higher frequency time series analysis.

3.1.1 Temporal Averaging

SMMR raw data were collected *on the average* every two days and SSM/I every day. Table 3.1 (page 29) lists all the missing dates for the SMMR and SSM/I datasets. When more than 50% of the days in a month were missing, as was the case for December 1987, then that month was linearly interpolated. Both August 1984 and January 1988 had 40% of the month missing (recalling that SMMR data is every two days and SSM/I data is daily), however, the monthly averages appeared reasonable with respect to the months before and after, indicating that linear interpolation was not needed. Since the months of July and August 1987 overlap between the SMMR and SSM/I datasets, the monthly averages for those two months are averages from both datasets. As mentioned in Section 2.1 ice concentration differences calculated from SMMR and SSM/I datasets using the NASA Team algorithm during the two month overlap are 0.2% ± 5% [3], which are well within errors associates with the NASA Team algorithm. The monthly data record is from October 1978 to December 1991.

In developing 2-day time series from the SMMR dataset, missing days were linearly interpolated and extra days were removed so that each year had 182 2-day values. For the SSM/I dataset which included daily records, missing values were first linearly interpolated, then 2-day averages were calculated, so that again each year had 182 2-day values. In joining the SMMR and SSM/I datasets for the 2-day time series, July 1987 SMMR data was joined with August 1987 SSM/I data. The data record for the 2-day time series is from October 24, 1978 to March 31, 1991. The rest of 1991 data was not received from NSIDC until late in this year and due to time constraints was not included in the 2-day processing.

3.1.2 Regional Ice Coverages

The Southern Ocean monthly time series was initially divided into five main regions, the Weddell, Indian, West Pacific, Ross and Bellingshausen/Amundsen re-

Table 3.1: SMMR and SSM/I missing dates

SMMR Missing Dates		
Year	**Month**	**Day(s)**
1982	June	15, 31
	August	6, 8, 16
1984	August	13, 15, 17,
		19, 21, 23
1986	March	30
	April	1
	December	9, 17

SSM/I Missing Dates		
Year	**Month**	**Day(s)**
1987	December	3-31
1988	January	1-12
	May	6-9
	June	18
	September	22
	December	24-26
1989	January	14
	June	7
	July	23-4
	August	23
1990	August	13, 25-6
	October	21-2, 26-8
	December	22-26
1991	December	19, 27

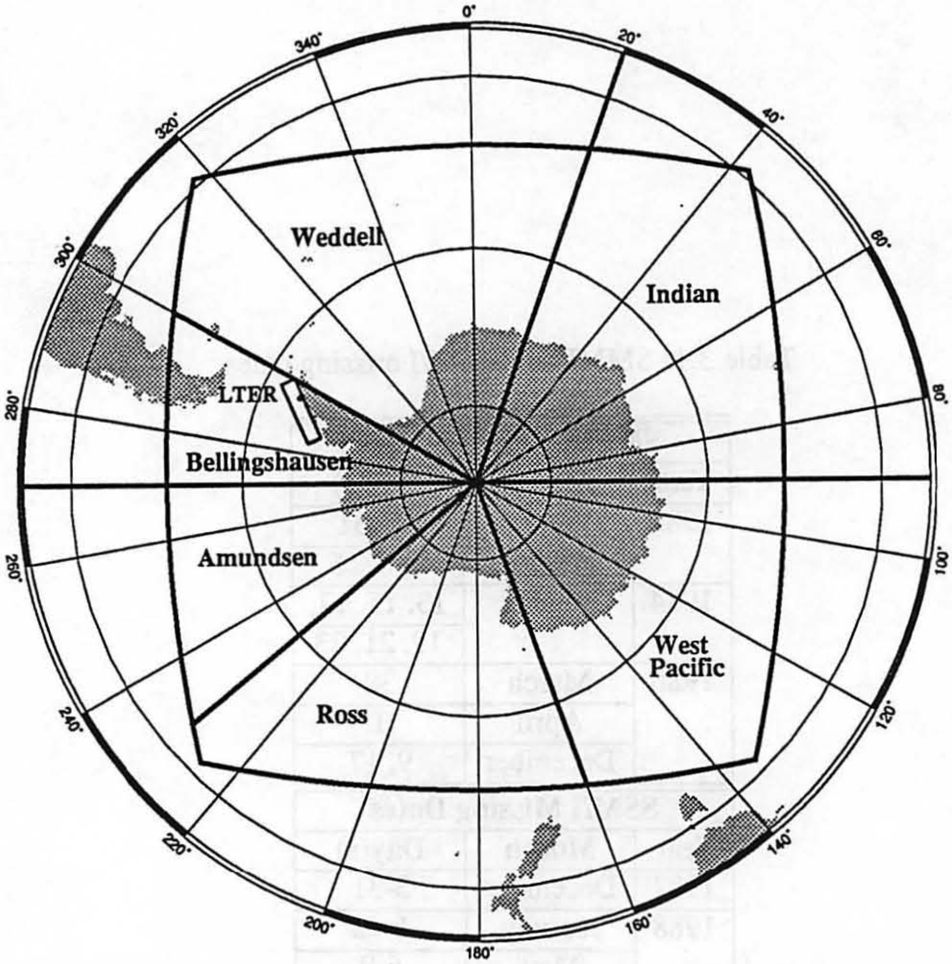

Figure 3.1: Southern Ocean regional map in a stereographic projection.

gions as shown in Figure 3.1. These are the typical regions used in other Southern Ocean regional studies [37, 2, 1]. The Bellingshausen/Amundsen region was subsequently divided into two separate regions, and because the monthly time series of Amundsen ice coverage and Bellingshausen ice coverage were distinctly dissimilar, further analyses included these two regions separately. The rectangle just west of the Antarctic Peninsula in Figure 3.1 represents the LTER study area (Appendix C gives a detailed description of the LTER study area). Longitudinal lines enclosing the LTER study area at 60°W and 77°W will represent the LTER subregion. Longitudinal pie sections of 10° east and west of the LTER subregion will be tested against the LTER subregion using cross spectral analysis to determine the longitudinal spatial extent of coherence. The box in Figure 3.1 represents the entire NSIDC southern polar grid for which data is supplied and therefore represents the region referred here as the Southern Ocean.

The regions used for the 2-day time series analyses were limited to the following three: the Southern Ocean, the Bellingshausen and the LTER study area. These three regions represent the range in regional spatial scales used in the monthly time series. The 2-day time series analyses will address whether higher frequency periodicities are detectable on smaller temporal scales.

The percent sea ice concentrations were converted into sea ice coverage for each pixel by multiplying the area of the pixel (ie., 625 km^2) by the percent sea ice concentration for that pixel. Regional sea ice coverages were calculated by summing the converted pixels for each region. It must be noted that sea ice coverage is distinct from another sea ice parameter often seen in the literature, sea ice extent. Sea ice extent is defined as the area of sea ice bounded by an ice concentration contour corresponding to a given threshold (usually 15%). Thus, sea ice extent may include open areas of water as well as varying percentages of sea ice cover, whereas sea ice coverage is the total area of actual sea ice. Throughout this study, sea ice coverage is exclusively used and may be referred to simply as ice coverage, where it is implied that only sea ice and not land ice is intended.

3.2 Time Series Analysis

In order to analyze the interannual variability in the regional time series, the seasonal fluctuations which dominate the time series need to be removed. If the time series show no significant trends, it is sufficient to subtract an appropriate mean from the respective values [66]. The Southern Ocean regional time series show no significant trends, therefore the monthly anomalies were calculated by subtracting the 13.25-year monthly means from the respective monthly values, and the 2-day anomalies were calculated by subtracting the 13.25-year 2-day means from the respective 2-day values. The regional monthly and 2-day anomalies were then transferred into Splus (Statistical Sciences, Inc.) [67] for spectral analysis and autoregressive modeling.

3.2.1 Autospectral Analysis

Spectra were calculated to better describe the variability in the time series and to determine whether there are any dominate periodicities. The periodogram of each time series was first calculated in the following way:

$$\hat{S}(f_k) = \frac{1}{n} \mid \sum_{t=1}^{n} \tilde{x}_t \, e^{(-i2\pi f_k t)} \mid^2 = \frac{n}{4} R_k^2, \quad k = 0, 1, \ldots, n/2 \qquad (3.1)$$

where

$\hat{S}(f_k)$ is the estimated spectral density or spectrum of the time series x_t,
$\tilde{x}_t = w_t(x_t - \hat{\gamma} - \hat{\beta}t)$ is the tapered, detrended and demeaned time series,
$f_k = k/\Delta n$ is the frequency,
Δ is the sampling interval,
n is the length of the series,
R_k^2 is the amplitude squared

Tapering was accomplished by applying a split cosine taper of ten percent to each end of the series to reduce leakage of power [66, 68]. The discrete Fourier transform sum in equation 3.1 was computed using a mixed radix fast Fourier transform algorithm [67]. Because the estimates in the periodogram do not become less variable as the length of the time series increases, the periodograms were smoothed with a sequence of running averages (modified Daniell smoothers) by grouping the ordinates in sets of a specified window length and finding their average value. A Daniell smoother has all values equal except for the two end values which are half the size of the others [67, 66]. A window of 7 was used to smooth all periodograms. When the smoothed periodograms or autospectra are plotted against frequency, the total area under the curve is equal to the variance of the time series [66].

The autospectra of the regional monthly anomalies were computed from the entire time series, from October 1978 to December 1991 and had a sampling interval of $\Delta = 1/12$ and a length of n=150 months, thus the frequencies are based on cycles per 12-month year. However, the 2-day time series were first separated into seasons before autospectra were computed to better resolve potential higher frequency periodicities. The seasons were divided in the following manner: spring (October - December, n=46), summer (January - March, n=45), fall (April - June, n=45) and winter (July - September, n=46). New time series were then created for each season which included the anomalies for that season from 10/78 to 3/91. Thus, the frequencies for the 2-day autospectra are based on cycles per season, where summer and fall have 90-day seasons and winter and spring have 92-day seasons (in accordance with the sample numbers for the season divisions - see above).

3.2.2 Autoregressive Modeling

The estimated autospectra were tested against autospectra generated by autoregressive models of the time series in order to confirm any significance peaks in the estimated autospectra and to further characterize the time series. The fitted autoregressive (AR) model is of the form: $x_t = \alpha_1 x_{(t-1)} + \ldots + \alpha_p x_{(t-p)} + \epsilon_t$ where p denotes the order of the AR model. If $\gamma(k)$ is the autocovariance function for the AR(p) process x_t, then the AR(p) coefficients, $\alpha_1, \alpha_2, \cdots, \alpha_p$, satisfy the Yule-Walker equations:

$$\sum_{k=1}^{p} \gamma(k-i)\,\alpha_k = \gamma(i), \quad i = 1, 2, \ldots, p \tag{3.2}$$

The AR(p) coefficients can be estimated by replacing $\gamma(k)$ in Equation 3.2 with the estimated autocovariance, $\hat{\gamma}(k)$, of the finite time series, $x_1, x_2, \ldots, x_n$. Equation 3.2 is then expanded out into p equations with p coefficients to be determined. Since the coefficient matrix has elements on each diagonal which are all the same, a recursive method, the Levinson-Durbin algorithm, estimates the k^{th}-order model from estimates of the $k-1$ model [69, 70, 67]. The order of the AR process can be selected using the Akaike's Information Criterion (AIC) which balances the reduction in error variance with the number of parameters in the AR(p) model. However, the intention here is not to fit the best AR model, but to assume that the time series behaves according to a low order AR model (ie., AR(1)), which is to say that the time series can be characterize as red noise. Confidence intervals were calculated for the estimated autospectrum and applied to the autospectrum generated from the AR(1) model. The estimated autospectra were then plotted with the 95% confidence intervals. If the estimated autospectrum falls within the confidence intervals, then the time series can be characterize as a low order AR process (red noise).

3.2.3 Cross-spectral Analysis

Cross-spectral analyses were performed in order to determine whether there are any significant coherences between regional ice coverages. Squared coherency is a function derived from the cross-spectrum and has the following expression:

$$K(f_j) = \frac{| S_{xy}(f_j) |^2}{S_x(f_j)S_y(f_j)} \tag{3.3}$$

where

$0 \leq K(f_j) \leq 1$,

$S_{xy}(f_j)$ is the cross spectral density function of the series x_t and y_t at frequency f_j,

$S_x(f_j)$ and $S_y(f_j)$ are the individual spectral density functions,

Squared coherency measures the linear correlation (or anticorrelation) between the two time series at each frequency and is analogous to the square of the usual correlation coefficient. The closer $K(f_j)$ is to one, the more closely related are the two processes at frequency f_j.

Squared coherences were first calculated for six major Southern Ocean regions (Weddell, Indian, West Pacific, Ross, Amundsen and Bellingshausen), where every two adjacent regions were tested. The subregions surrounding the LTER subregion were then tested against the LTER subregion to determine the spatial extent of coherence with LTER ice coverage. Where there was significant coherence, the phase spectrum was determined:

$$\phi_{xy}(f_j) = tan^{-1}\frac{-q(f_j)}{c(f_j)} \tag{3.4}$$

where

ϕ_{xy} is the phase angle of $S_{xy}(f_j)$
$-q(f_j)$ is the quadrature spectrum of the series x_t and y_t at frequency f_j
$c(f_j)$ is the co-spectrum of the series x_t and y_t at frequency f_j

The phase angle reveals whether the two time series are in or out of phase at the frequencies which show significant coherence.

Chapter 4

Results

4.1 Monthly Seasonal Variability

Time series of monthly ice coverages for 9 regions are shown in Figures 4.1 and 4.2 (pages 38 and 39). Figure 4.1 shows time series of monthly ice coverage for the Southern Ocean, Weddell, Indian, West Pacific, Ross and Bellingshausen/Amundsen regions. The time series are dominated by strong, regular seasonal variations with no discernible trends. The interannual variability in ice coverage, in particular maximum and to a lesser extent minimum ice coverage, is apparent for all regions. For the entire Southern Ocean the interannual variability is smoothed by the areal averaging and most years reach the 13.25-year mean maximum and minimum ice coverage. In contrast, the interannual variability for the five regions dividing up the Southern Ocean show several anomalous years in maximum ice coverage, as well as a few anomalous years in minimum ice coverage. No two regional time series have the same anomalous years of maximum and minimum ice coverages.

Figure 4.2 shows monthly ice coverage for the Bellingshausen/Amundsen region contrasted with monthly ice coverage for the Amundsen, Bellingshausen and LTER regions. The Bellingshausen/Amundsen and Amundsen time series are very similar, suggesting that the interannual variability in the Amundsen, more so than

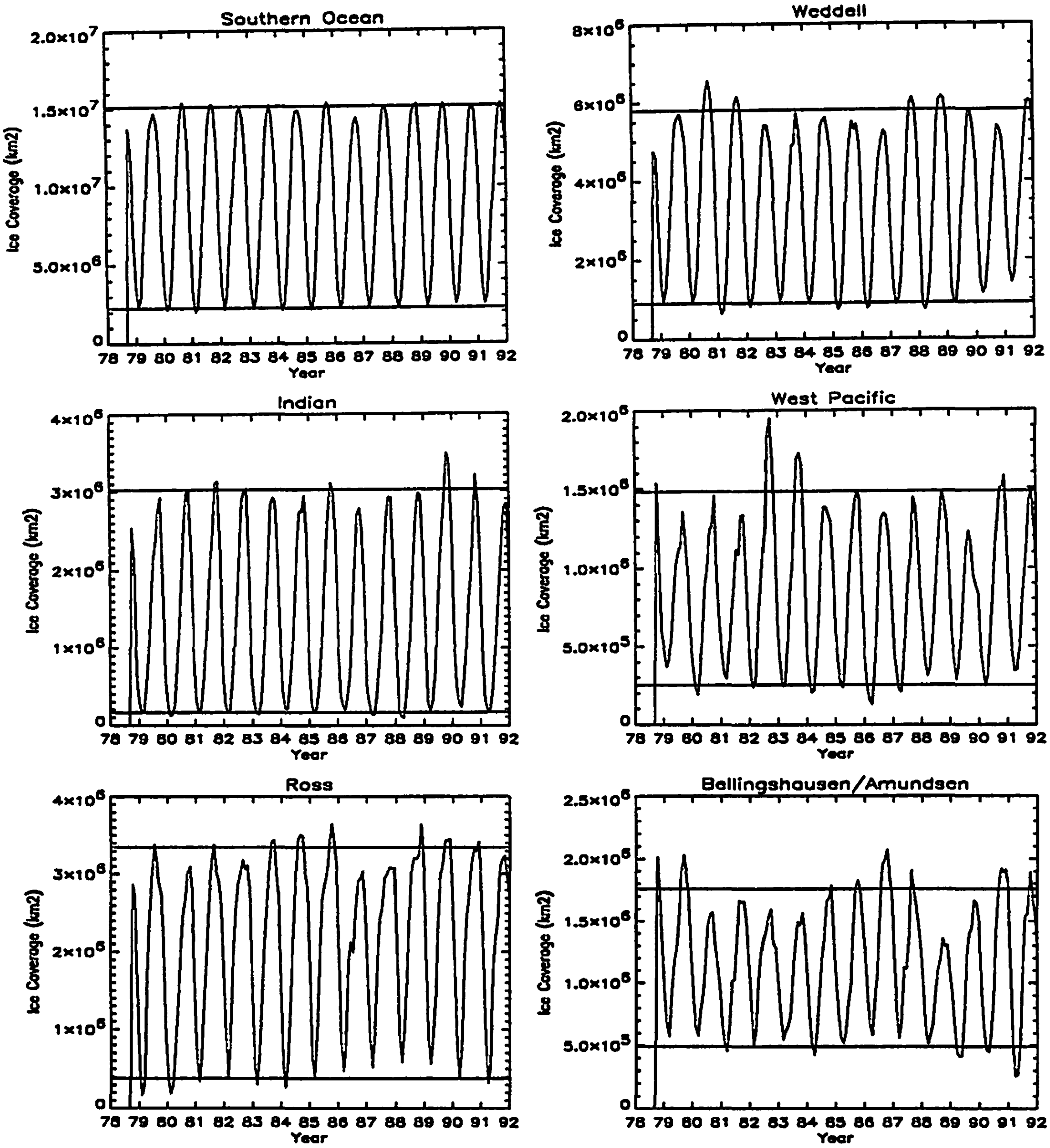

Figure 4.1: Monthly ice coverage for the Southern Ocean, Weddell, Indian, West Pacific, Ross and Bellingshausen/Amundsen regions. The time series begins October 1978 and ends December 1991. The horizontal lines are 13.25-year mean maximum and minimun ice coverage. Note that the y axes have different scales.

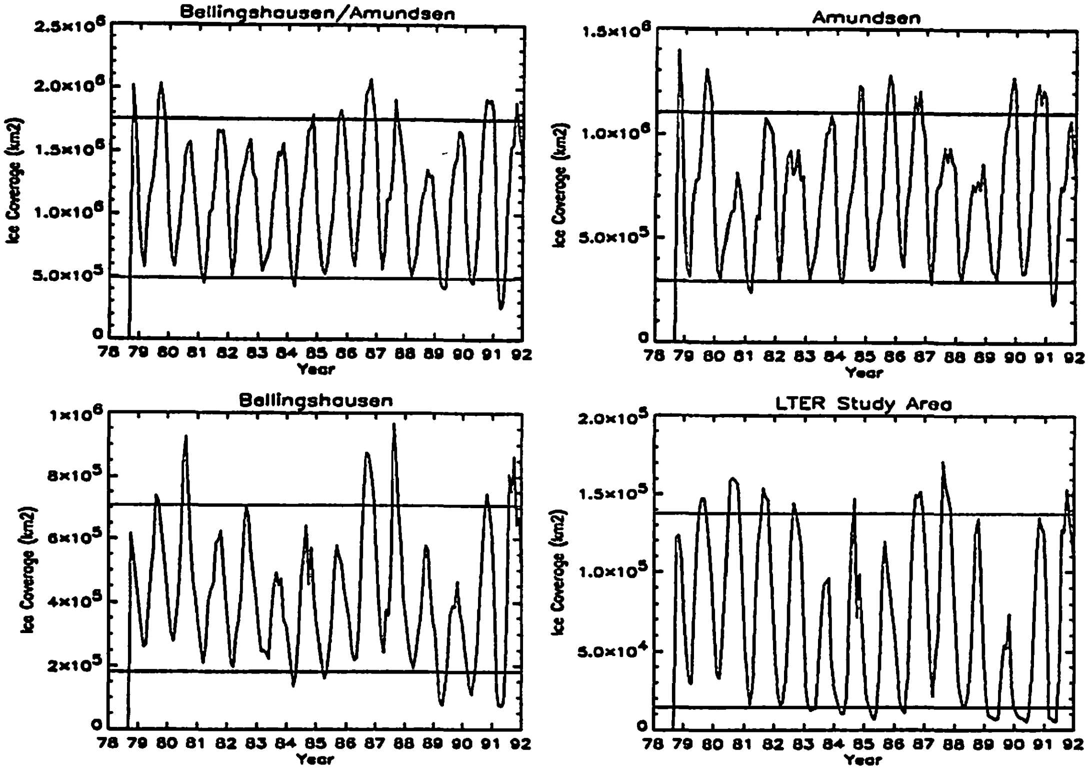

Figure 4.2: Monthly ice coverage for Bellingshausen/Amundsen, Amundsen, Bellingshausen and LTER regions. The time series begins October 1978 and ends December 1991. The horizontal lines are 13.25-year mean maximum and minimun ice coverage. Note that the y axes have different scales.

in the Bellingshausen, dominates the signal in the Bellingshausen/Amundsen region. This is not surprising since the Amundsen mean maximum ice coverage is 4 x 10^5 km^2 greater than the Bellingshausen mean maximum ice coverage. The Amundsen and Bellingshausen time series are distinctly different. If a line were to connect the points of maximum ice coverage in the 13.25-year time series for both the Amundsen and Bellingshausen regions, the inflection points would distinguish local maximum and minimum ice coverage years for each region respectively. A comparison of these inflection points or local maximums and minimums reveals that the Amundsen local maximums seem to lag the Bellingshausen local maximums by roughly one

Table 4.1: Local maximum ice coverages for the Amundsen and Bellingshausen time series. See text for definition of local maximums and minimums.

Amundsen Local Maximums (year)	**Bellingshausen Local Maximums (year)**	**Lag: Bellingshausen-Amundsen (year)**
1978	1980	2
1981	1982	1
1985	1987	2
1989	1991	2

to two years as shown in Table 4.1. Local minimums from both regions also do not coincide, but it is less clear whether one lags the other. Since the monthly ice coverages for the Amundsen and Bellingshausen regions are distinctly different, further analyses include these two regions separately instead of the single combined Bellingshausen/Amundsen region.

The LTER and Bellingshausen time series are very similar. Three out of four of the Bellingshausen local maximums agree with the LTER local maximums. The exception is the Bellingshausen local maximum occurring in 1982 which does not appear as a local maximum in the LTER time series. In contrast, the local minimums from the two regions are not in agreement, but this may be due in part to the error involved in observed low ice concentrations where coastal and weather-related effects may be elevating local minimums (see Section 2.2.3 for further detail on coastal and weather-related effects on sea ice concentrations). Although this error would be contributing to both regional local minimums, the LTER region has proportionately more coastal area than the Bellingshausen region. Table 4.2 characterizes the 13-year interannual variability in LTER ice coverage.

Table 4.2: Characteristics of the 13-year interannual variability in LTER ice coverage.

Above Mean Winter Ice Years	**Below Mean Winter Ice Years**	**Above Mean Summer Ice Years**	**Below Mean Summer Ice Years**
1979	1983	1979	1983
1980	1985	1980	1984
1981	1988	1981	1985
1982	1989	1982	1986
1984	1990	1987	1989
1986		1988	1990
1987			1991
1991			

4.2 Annual Cycles

Figure 4.3 (page 42) shows mean annual cycles for the 8 selected regions. The annual cycles show the expected increase and decrease in sea ice coverage sometime in austral Fall and Spring respectively, but there is considerable differences in the shapes of the 8 annual cycles. Two distinguishing characteristics are illustrated by the shapes of the annual cycles:

- The mean months of minimum and maximum ice coverage
- The mean duration of ice advance and retreat

For the Southern Ocean, Weddell, Indian and West Pacific regions, the mean month of minimum and maximum ice coverage is consistently February or February/March and September. This is not the case for the other four regions, the Ross, Amundsen, Bellingshausen and LTER regions, which show significant variability in mean months of minimum and maximum ice coverage. The mean annual cycle for the Ross region shows a distinct mean minimum in February, whereas the mean maximum is broadly between August to October. The Amundsen annual cycle is similar to the Ross except

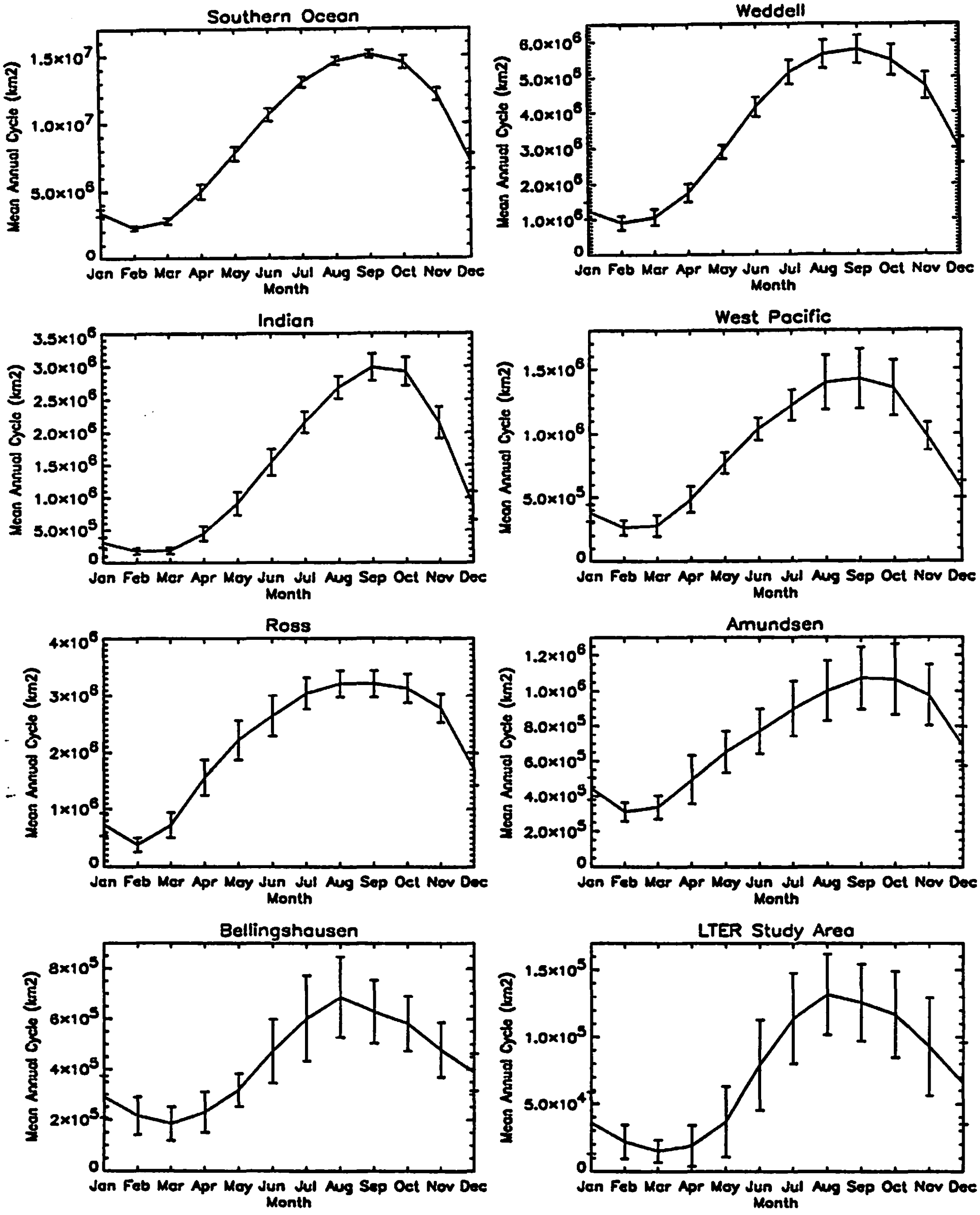

Figure 4.3: Mean annual cycles for the Southern Ocean, Weddell, Indian, West Pacific, Ross, Amundsen, Bellingshausen and LTER regions. The vertical bars represent one standard deviation above and below the 13.25-year mean. Note that the y axes have different scales.

the mean maximum is more defined in September-October. The mean minimum and maximum ice coverage for the Bellingshausen and LTER regions are most distinctly different from the other regional cycles. For both annual cycles the mean minimum and maximum are in March and August, respectively, one month later and one month earlier than the overall mean month of minimum and maximum ice coverage.

The mean duration of ice advance and retreat for most of the regions involves a long period of ice advance followed by a short period of ice retreat, a phenomenon which has been well documented in the literature since it differs from the symmetric annual cycle found in the Arctic [71, 1, 20]. In contrast, the Bellingshausen and LTER mean annual cycles tend towards a shorter period of ice advance and a longer period of ice retreat. It should be noted, however, that the Bellingshausen and LTER annual cycles (as well as the Amundsen annual cycle) show more year to year variability, therefore the shape of the *mean* annual cycles should be regarded cautiously. It is also clear in Figure 4.3 that year to year variability (the standard deviations above and below the mean) for the annual cycles is greatest during months of mid-winter to early spring ice coverage (June to November). An exception is the Southern Ocean annual cycle which shows the months April, May and December to have the highest interannual variability.

To better distinguish the regional differences in mean duration of ice advance and retreat, the mean monthly growth and decay rates were calculated by subtracting the previous mean monthly ice coverage from the mean monthly ice coverage in question. The difference was normalized by dividing by the 13.25-year mean *maximum* ice coverage for the region in question, then multiplied by 100 so that the rates are expressed as *percent* growth (or decay) of mean maximum ice coverage per month. Table 4.3 (page 44) shows the mean growth and decay rates for each of the 8 annual cycles shown in Figure 4.3. All regions, except the Bellingshausen and LTER, show positive rates from March to September, a period of 7 months during which ice is advancing. These same regions show negative rates from October to February, a period of 5 months during which ice is retreating. The Bellingshausen and LTER

Table 4.3: Mean monthly growth (+) and decay (-) rates (% per month)

Region	Jan	Feb	Mar	Apr	May	Jun
Southern Ocean	-25	-8	3	15	19	19
Weddell	-29	-6	3	12	20	22
Indian	-19	-4	<0.5	9	15	21
West Pacific	-12	-8	1	14	19	18
Ross	-29	-11	10	25	20	13
Amundsen	-22	-12	2	14	14	11
Bellingshausen	-14	-11	-4	6	12	22
LTER	-22	-10	-5	3	13	31

Table 4.3 cont: Mean monthly growth and decay rates

Region	Jul	Aug	Sep	Oct	Nov	Dec
Southern Ocean	16	10	3	-4	-16	-33
Weddell	17	9	2	-5	-13	-31
Indian	20	17	10	-2	-25	-42
West Pacific	12	12	2	-5	-25	-28
Ross	12	5	<0.5	-3	-10	-32
Amundsen	12	9	6	-1	-8	-26
Bellingshausen	18	12	-8	-7	-15	-13
LTER	25	13	-4	-6	-18	-20

annual cycles show the opposite trend in mean periods of ice advance and ice retreat: 5 months during which ice advances from April to August and 7 months during which ice retreats from September to March. The highest rates for the first six regions are in December, showing dramatic decreases in ice coverage, whereas the highest rates for the Bellingshausen and LTER regions are in June, showing moderate (relative to that region) increases in ice coverage.

To better resolve the year to year variability in the LTER mean annual cycle, a contour plot of each LTER annual cycle for the 13 complete years from 1979-1991 is illustrated in Figure 4.4 (page 46). The year to year variability in the LTER annual cycles shows that near minimum ice coverage (< 2.5 x 10^4 km^2) may persist for one (March 1987) to 4.5 months (January through half of May 1990) or in high minimum ice years, never reaching < 2.5 x 10^4 km^2 (1979 and 1980). Near maximum ice coverage (> 1.25 x 10^5 km^2) may persist for two (July through August 1984) to five months (June through November 1980) or in low ice years, never reaching 1.25 x 10^5 km^2 (1983, 1985 and 1989). Year 1980 stands out as the highest ice year for the 13-year record, reaching a maximum ice coverage greater than 1.5 x 10^5 km^2 for three consecutive months. Year 1987 is the only other year which reached a maximum ice coverage greater than 1.5 x 10^5 km^2. The rates of ice advance and retreat are also different for each year. All years except the two lowest ice years, 1983 and 1989, show the same trend observed in the mean annual cycle, a shorter period of ice advance versus a longer period of ice retreat. In the two lowest ice years, the period of advance is longer than the period of retreat. Year 1984 is particularly unusual in that it shows two periods of ice advance (the small enclosed contour centered on September, 1984 is a depression and should be labelled 7.5 x $10^{\overset{4}{\cancel{5}}}$ km^2). Years 1984, 1985, 1990 and 1991 show long periods of minimum ice coverage from January to approximately May followed by dramatic increases in ice coverage. Years 1983 and 1989, the two lowest ice years, also show long periods of minimum ice coverage, but the increase in ice coverage in fall is not as dramatic. The contour plot in Figure 4.4 shows in particular the oscillation between consecutive high ice years followed by

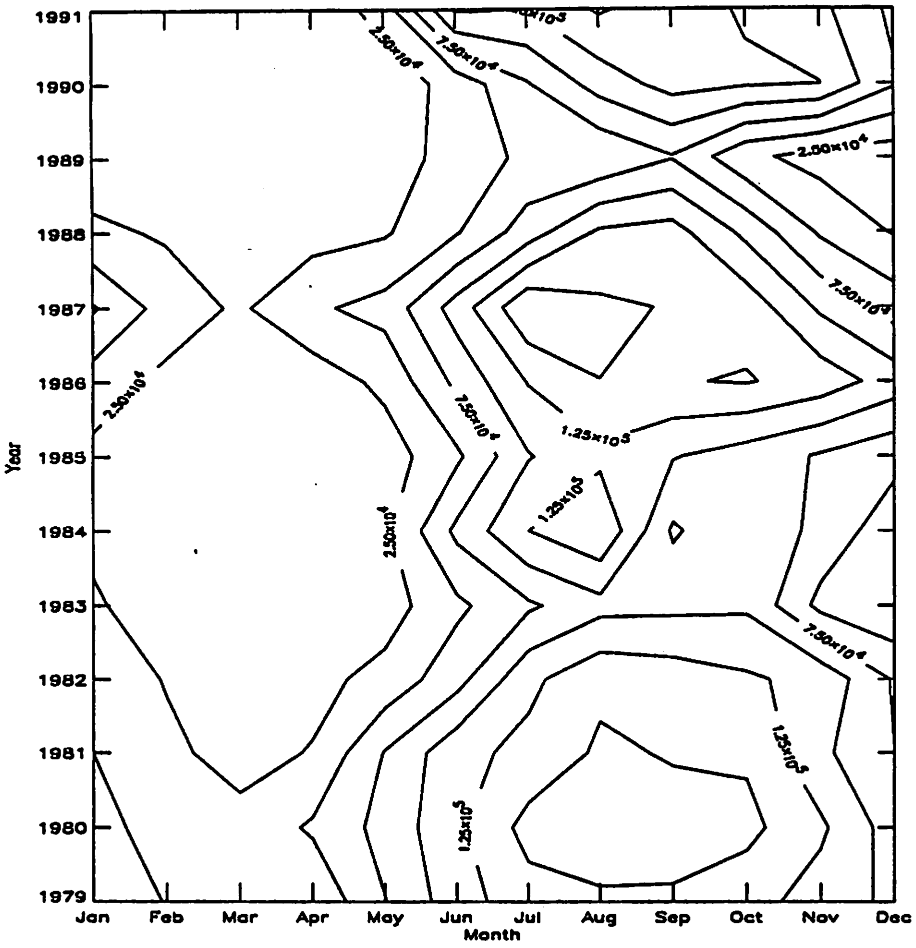

Figure 4.4: Contour plot of LTER annual cycles for years 1979-1991. Contours are labelled with ice coverages in km^2.

consecutive low ice years. For example, an approximate two to four year trend of high ice years (1979-1982 and 1986-1987) is followed by a two to three year trend of low ice years (1983-1985 and 1988-1989).

The distribution of ice throughout the LTER grid from year to year is consistent in that ice advances from the south northward and from the Peninsula northwestward. Figures 4.5 and 4.6 (pages 47 and 48) show the mean distributions of the LTER annual ice coverage. In July to October 1980, August 1981, July 1987 and August 1991 the entire LTER grid was covered with 50% ice coverage and greater

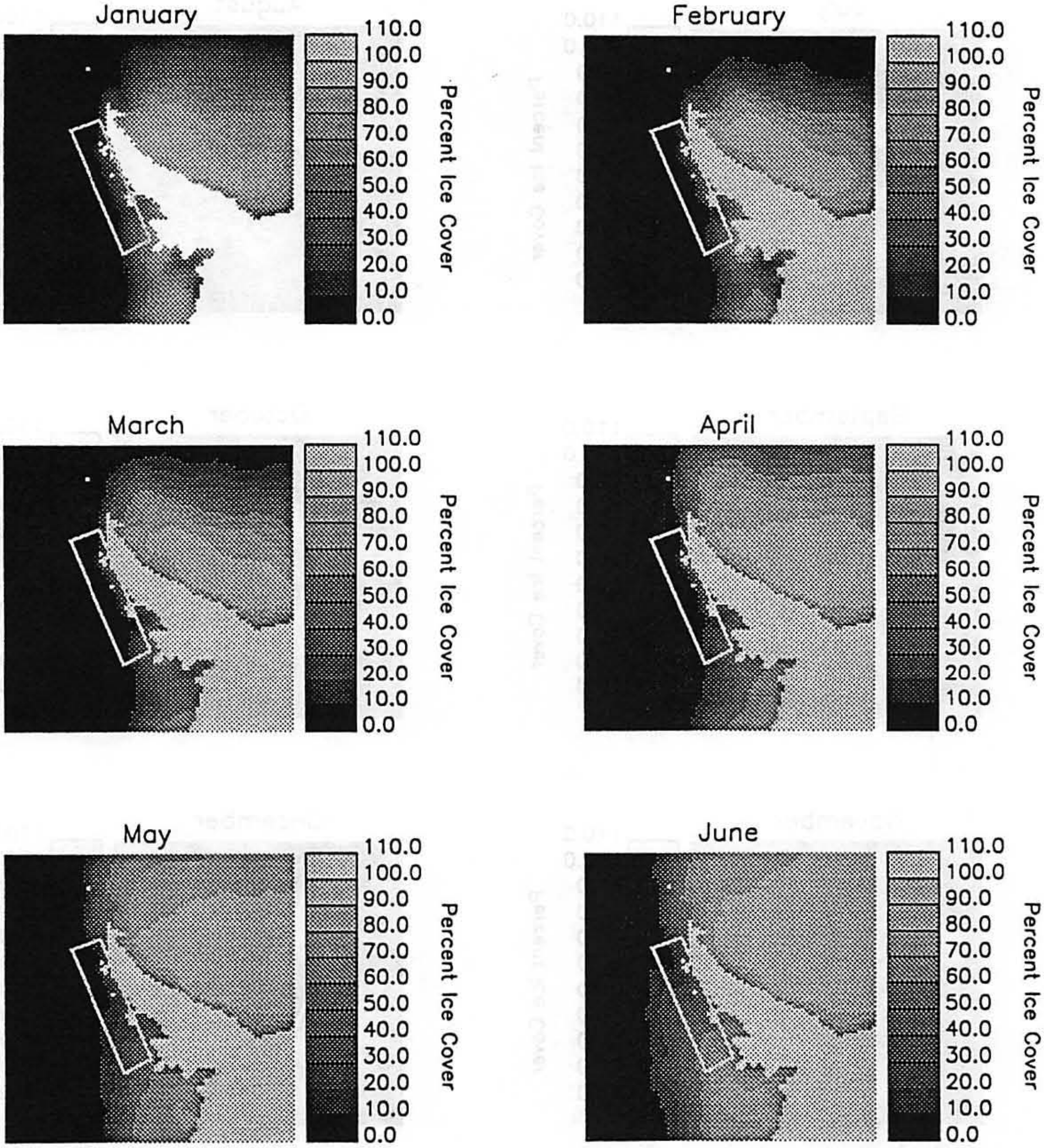

Figure 4.5: LTER monthly mean percent ice cover from January to June. The box indicates the LTER study area. Percent ice cover is from 0 to 100%, and the landmask and box outline are identified by the 100-110 shade.

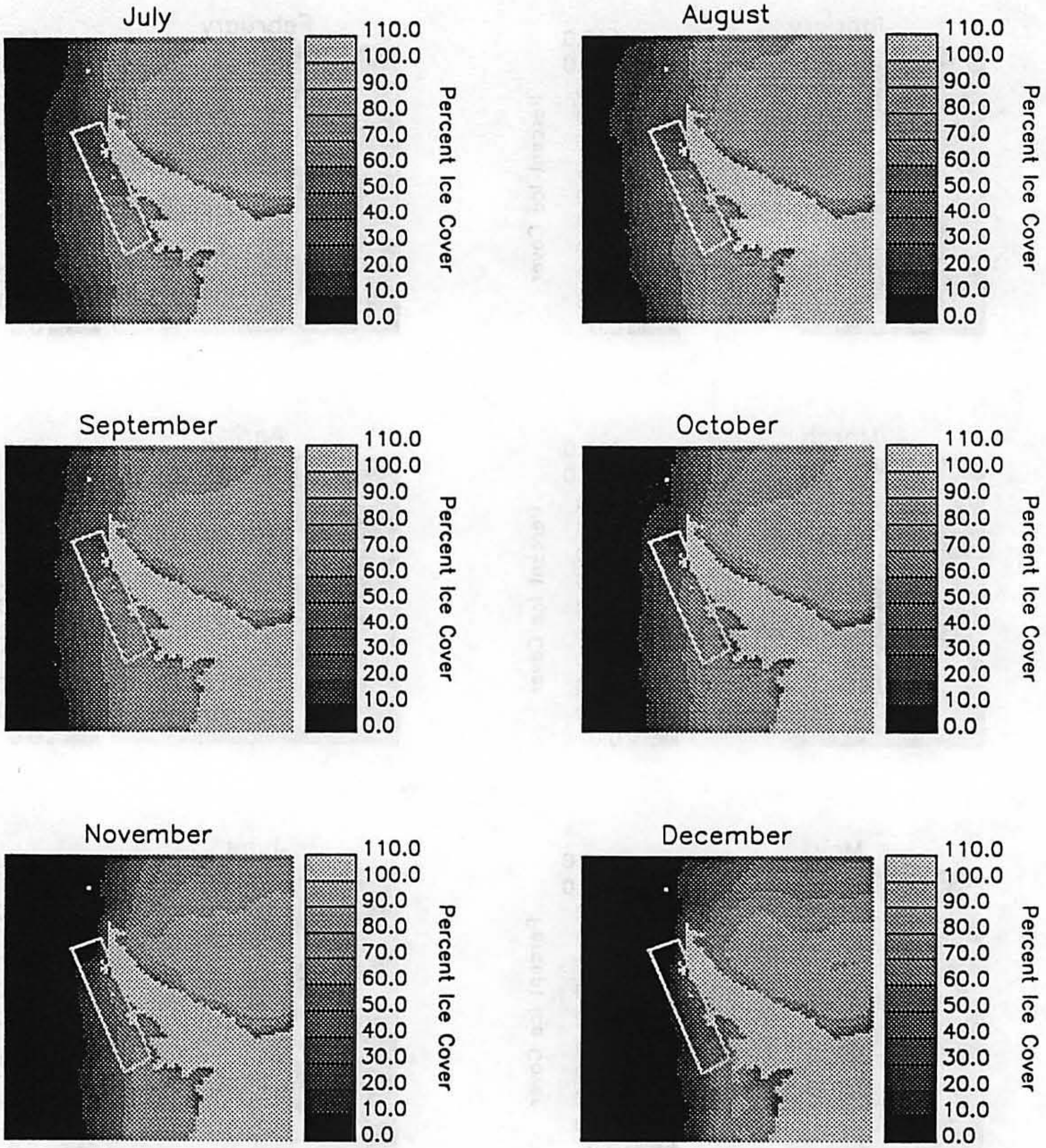

Figure 4.6: LTER monthly mean percent ice cover from July to December. The box indicates the LTER study area. Percent ice cover is from 0 to 100%, and the landmask and box outline are identified by the 100-110 shade.

(not apparent in Figure 4.6 because of the 13.25-year mean). Year 1980 was again particularly remarkable in that the high ice coverage (50% ice coverage and greater) lasted four months as opposed to one month in the other three years. In near normal ice years, the ice coverage advances to just south of Anvers Island and extends northwestward across the grid. This is illustrated for the month of August in Figure 4.6 (page 48). (Anvers Island in Figure 4.6 is depicted by the most northerly landmask that lies within the box.) From January to April there is little ice coverage in about 90% of the LTER study area, thus mean summers are long for the LTER region. The region north of Anvers Island and along the coast is often ice free during maximum ice coverage and in high ice years (eg., 1981, 1986, 1987, 1991) marks the location of a coastal polynya. In extreme low ice years (1983 and 1989), the maximum ice coverage extends diagonally from about 200 km south of Anvers Island towards the lower left corner of the grid (from 400.000 to 200.200 in LTER grid coordinates). Thus, the southeast region of the LTER grid experiences the most consistent ice coverage from year to year, whereas the northern third of the LTER grid experiences the most dramatic fluctuations in year to year ice coverage.

4.3 Monthly Non-Seasonal Variability

4.3.1 Anomalies

The monthly anomalies have the annual cycle removed and thus represent the non-seasonal variability in ice coverage. Figure 4.7 (page 50) shows the time series of the standard deviates (the normalized monthly anomalies) for the 8 selected regions. The monthly anomalies have been normalizied by subtracting the mean and dividing by the standard deviation. All regions show regular departures from the annual mean. Most regions oscillate consistently from above average to below average monthly values on time scales of a few months, but there are a few exceptions. For example, in the Indian region the departures remain well above the annual mean

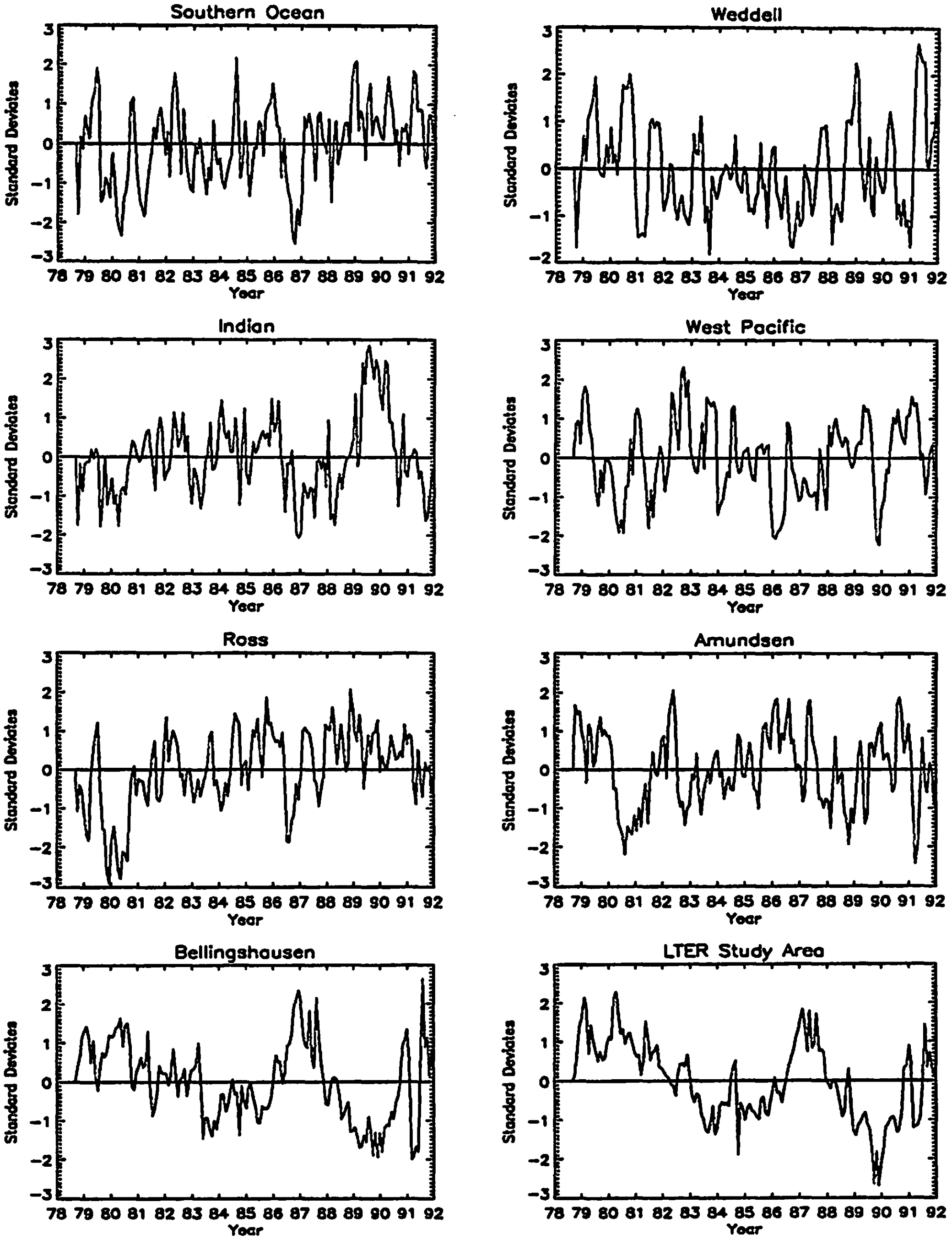

Figure 4.7: Standard deviates of the monthly anomalies for the Southern Ocean, Weddell, Indian, West Pacific, Ross, Amundsen, Bellingshausen and LTER regions.

during mid-1989 to mid-1990, and in the Ross region the departures remain well below the annual mean during mid-1979 to 1981. A similar below average period shows in the Amundsen region as well, only it occurs about a half year later. In contrast, the Bellingshausen and LTER regions oscillate from above average to below average monthly values on time scales of a few years. For example, the LTER region has above average ice coverage from 1979 to 1983 and again from 1986 to 1988, and below average ice coverage from 1983 to 1986 and again from 1988 to 1991. This is most likely due to the fact that these regions respond uniformally to the forces causing non-seasonal variability, so that these interannual patterns become more distinct. For the whole Southern Ocean, interannual trends in regional sea ice variability are averaged out. For example, in the Weddell region there are more months below the mean than above from about 1982 to about 1987, whereas this *trend* is the opposite in the Ross region, where during this same time frame, more months are above the mean than below. The end result is that for the Southern Ocean there is no evident interannual trend. However, the anomalously low years, 1980 and 1986, did not get averaged out for the Southern Ocean. Year 1980 was anomalously low for West Pacific, Ross and Amundsen regions, average for the Indian region and anomalously high for the Weddell, Bellingshausen and LTER regions. Year 1986 was anomalous for all regions with the interesting exception of the Bellingshausen and LTER regions, where 1986 was a particularly high ice year.

The Amundsen and Bellingshausen seasonal time series revealed that anomalously high ice years in the Bellingshausen region lagged anomalously high ice years in the Amundsen region by one to two years (see Table 4.1, page 40). This relationship was tested with the monthly anomalies. Cross-correlation analysis between the Amundsen and Bellingshausen monthly anomalies shows the highest correlation when the Bellingshausen anomalies lag the Amundsen anomalies by 11 months ($\rho = 0.56$). Correlation decreases substantially for months less than 10 ($\rho = 0.50$) and greater than 12 ($\rho = 0.53$), indicating an approximate yearly lag. The one to two year lag observed previously in Section 4.1 (see Table 4.1, page 40) was for local *maximum* ice coverages, whereas cross-correlation anaylsis shows that regardless of the magnitude of ice coverage, there is a significant cross-correlation when Bellingshausen ice coverage consistently lags the Amundsen ice coverage by 10-12 months.

Autocorrelations were calculated to confirm the short-term correlation observed in the monthly anomaly plots and are shown in Figure 4.8 (page 53). All regions show a decreasing autocorrelation with increasing monthly lags. For the Southern Ocean, Weddell, West Pacific, Ross and Amundsen regions, autocorrelations become insignificant within 2-4 monthly lags, indicating that an above (or below) average month is followed by 2 to 4 above (or below) average months. For the Indian, Bellingshausen and LTER regions, monthly lags are significantly autocorrelated up to 7, 10 and 12 months, respectively. The longer lag times in significant autocorrelations for these three regions, in particular for the LTER region, is due to the interannual trend observed in the monthly anomaly time series (Figure 4.7, page 50), where two to three consecutive years have above mean ice coverage, followed by two to three consecutive years of below mean ice coverage.

4.3.2 Periodicities

Autospectra calculated from the monthly anomalies are shown for the 8 selected regions in Figure 4.9 (page 54). Also plotted are the 95% confidence intervals which were calculated with the assumption that the time series are first order autoregressive processes (see Section 3.2.2). The autospectra show that most of the variance is in the low end of the frequency spectrum (ie., most of the variance is due to interannual variability). The autospectra also lie within the confidence intervals, verifying that the time series are low order autoregressive processes (red noise). Besides there being little high frequency variance, there is no indication that any regular periodicities occur between a 6 month to 2 year periodicity which would have indicated a semi-annual to biennial fluctuation in anomalous ice coverages. Unfortunately, the time series are not nearly long enough to determine at this time

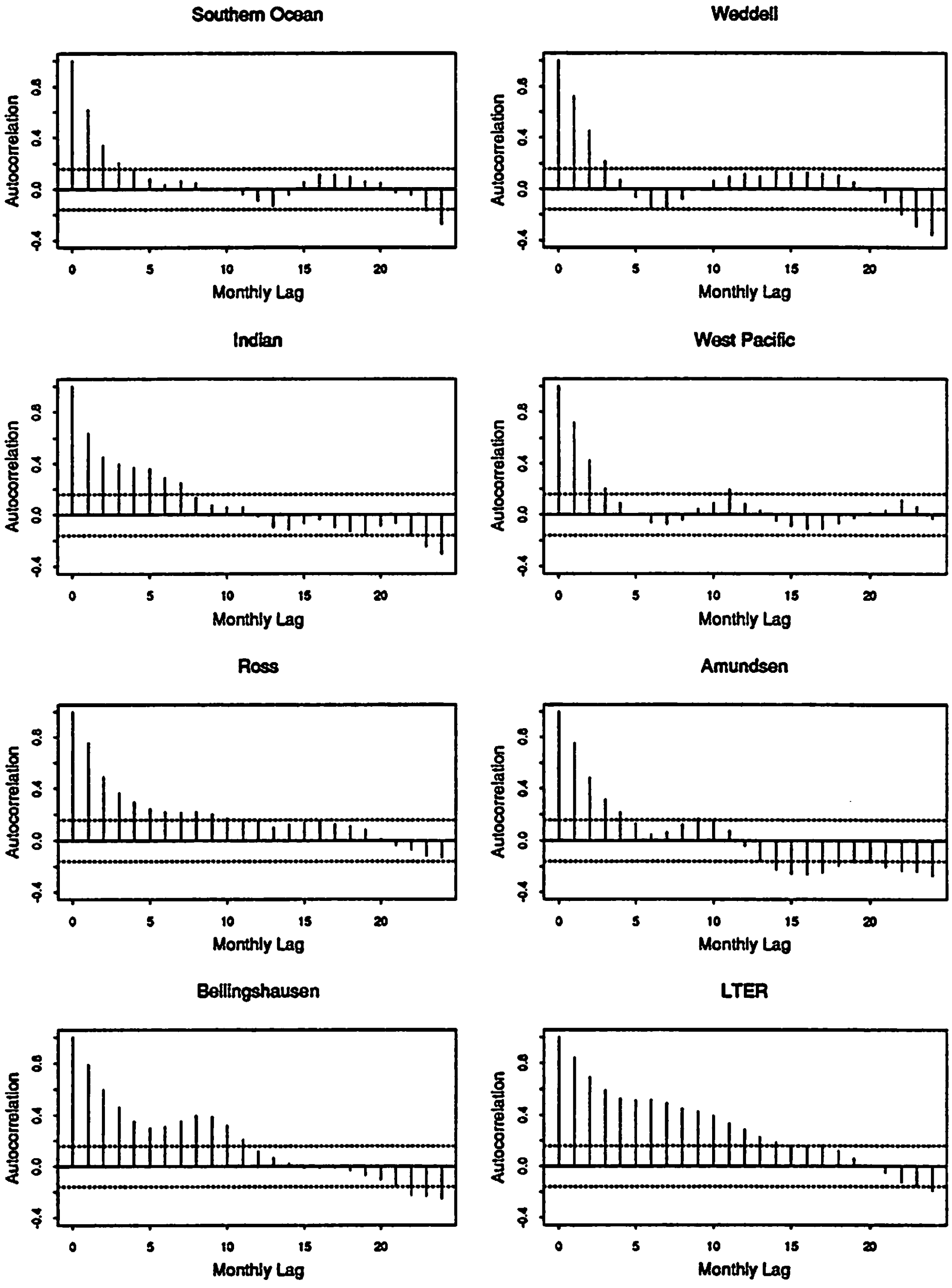

Figure 4.8: Autocorrelations of the monthly anomalies for the Southern Ocean, Weddell, Indian, West Pacific, Ross, Amundsen, Bellingshausen and LTER regions. The dotted lines are approximately the 95% confidence intervals based on the assumption that the autocorrelation is zero.

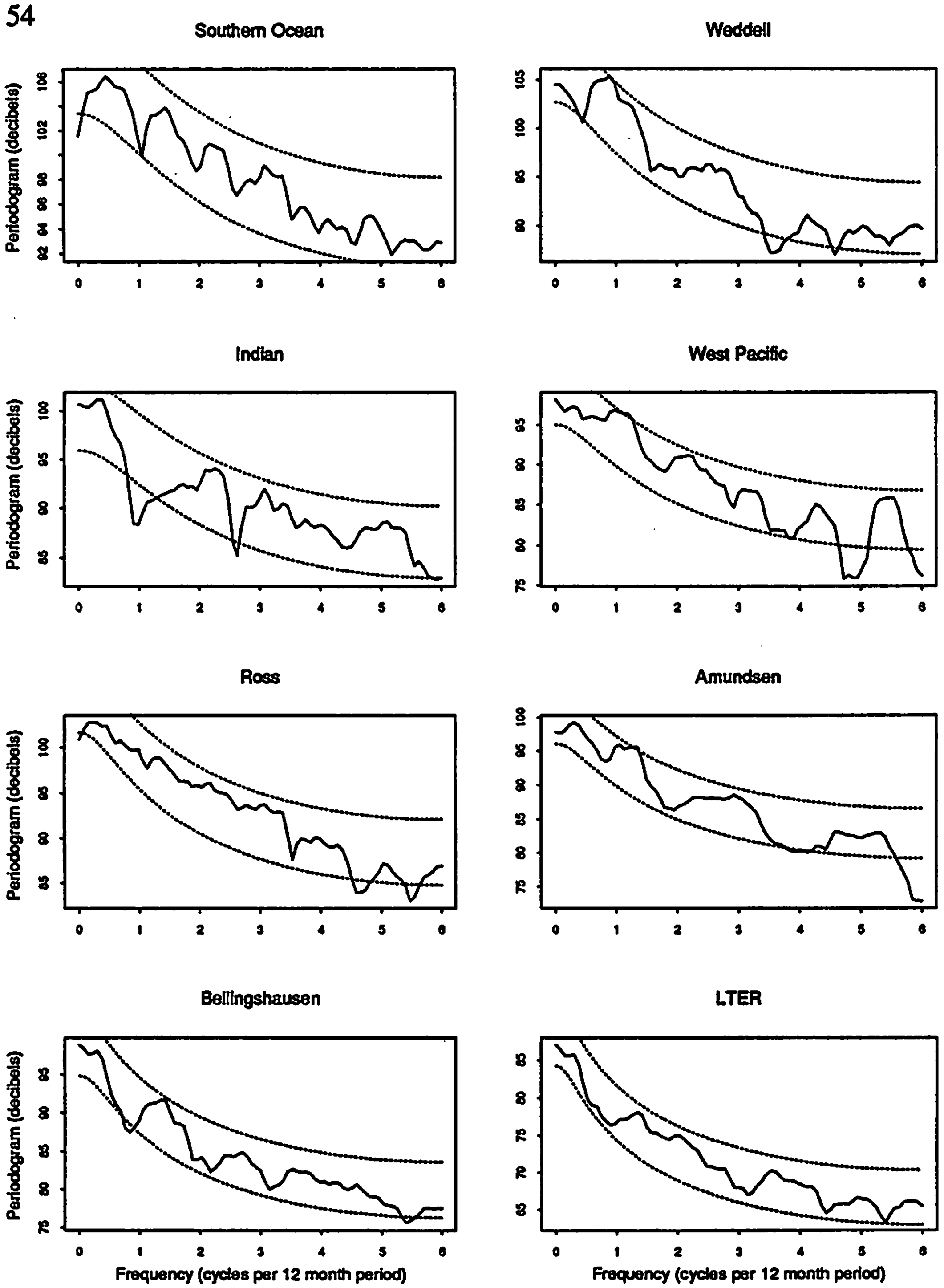

Figure 4.9: Autospectra for the Southern Ocean, Weddell, Indian, West Pacific, Ross, Amundsen, Bellingshausen and LTER regions. The dashed lines represent 95% confidence intervals for autospectra generated from first order autoregressive models.

what, if any, periodicities are occurring on time scales of years.

4.4 Higher Frequency Variability

Three regions were selected to explore higher frequency variance, the Southern Ocean, Bellingshausen and LTER regions. The time series were divided into four seasons to better resolve possible periodicities which may only occur at certain times of the year. The regional autospectra of the 2-day time series for each season are shown in Figures 4.10 and 4.11 (pages 56 and 57). The autospectra are plotted with the 95% confidence intervals which were calculated under the same assumption that the time series are first order autoregressive processes. There is one distinct peak in the Southern Ocean summer autospectrum in Figure 4.10 (at approximately 16 cycles per 90-day season) that lies outside the 95% confidence intervals. This deviation from the assumption that the time series is a first order autoregressive process implies that the variability in the time series is not red noise (ie., not pure persistence). This peak may reveal a significant periodicity at an approximate 5-6 day interval in the variability of Southern Ocean summer sea ice coverage. Similar peaks are revealed in the Bellingshausen winter autospectrum and in both the LTER summer and fall autospectra.

4.5 Inter-Regional Comparisons

Cross spectra between adjacent regions were calculated to test inter-regional coherence. Figure 4.12 (page 58) shows the squared coherence between six Southern Ocean regions (Weddell, Indian, West Pacific, Ross, Amundsen and Bellingshausen). There is little significant coherence between any of the adjacent regions except for some low frequency coherence between the Weddell and Indian and between the Amundsen and Bellingshausen monthly anomalies. The phase angle of the cross

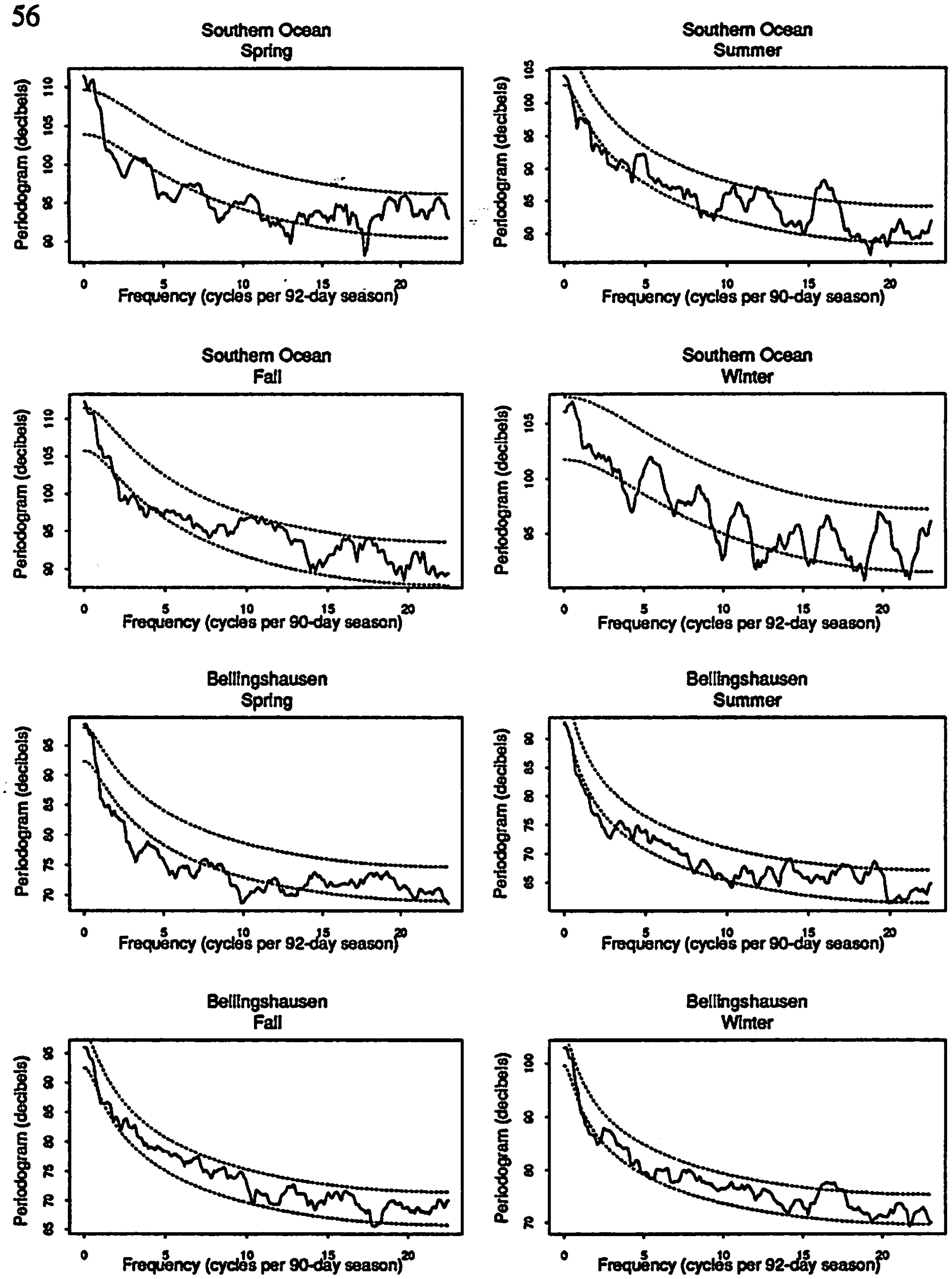

Figure 4.10: Southern Ocean and Bellingshausen autospectra generated from 2-day time series of each season. The dashed lines represent 95% confidence intervals for autospectra generated from first order autoregressive models.

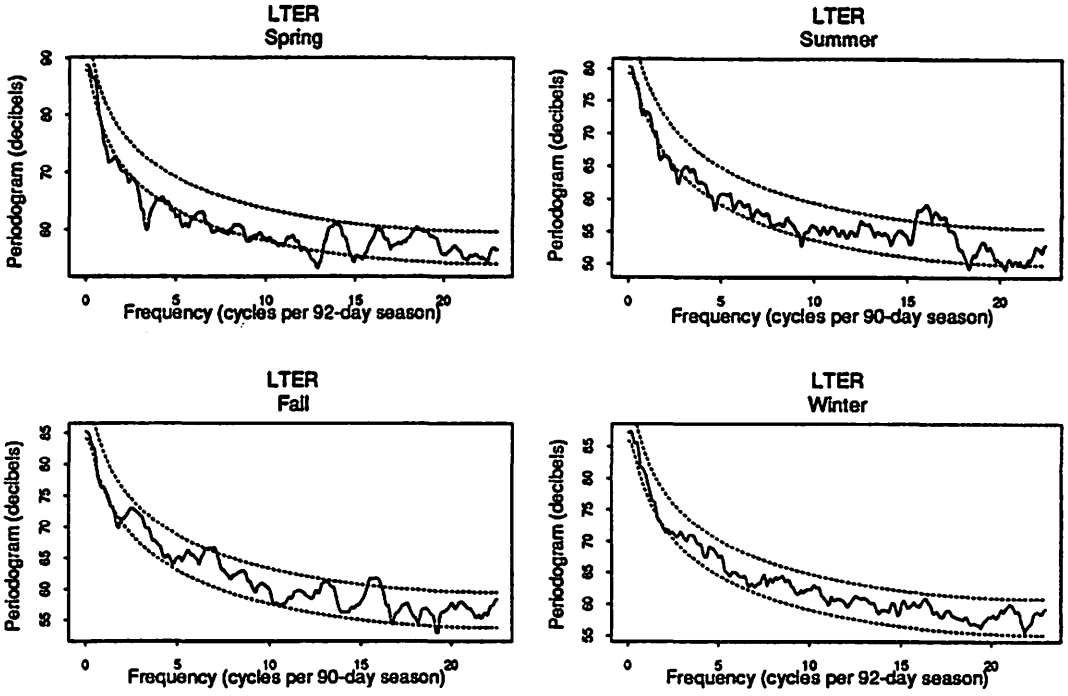

Figure 4.11: LTER autospectra generated from 2-day time series of each season. The dashed lines represent 95% confidence intervals for autospectra generated from first order autoregressive models.

spectrum indicates that the low frequency coherence between the Weddell and Indian monthly anomalies is 6-7 months out of phase, with the Weddell leading. Upon re-examination of the Weddell and Indian seasonal time series (Figure 4.1, page 38), it appears that below (or above) mean summer coverage in the Weddell region is followed approximately 6 months later by above (or below) mean winter coverage in the Indian region. This pattern holds for 10 of the 13 complete years. For the low frequency coherence between the Amundsen and Bellingshausen monthly anomalies, the phase angle indicates a 9-11 month difference, with the Amundsen leading, which supports the result from the cross-correlation analysis. However, the overall lack of significant coherences between any of the adjacent regions indicates that variability in ice coverage is unique for each region. Cross spectral analysis of the Southern Ocean versus the six regions is not shown, but as expected is most coherent with

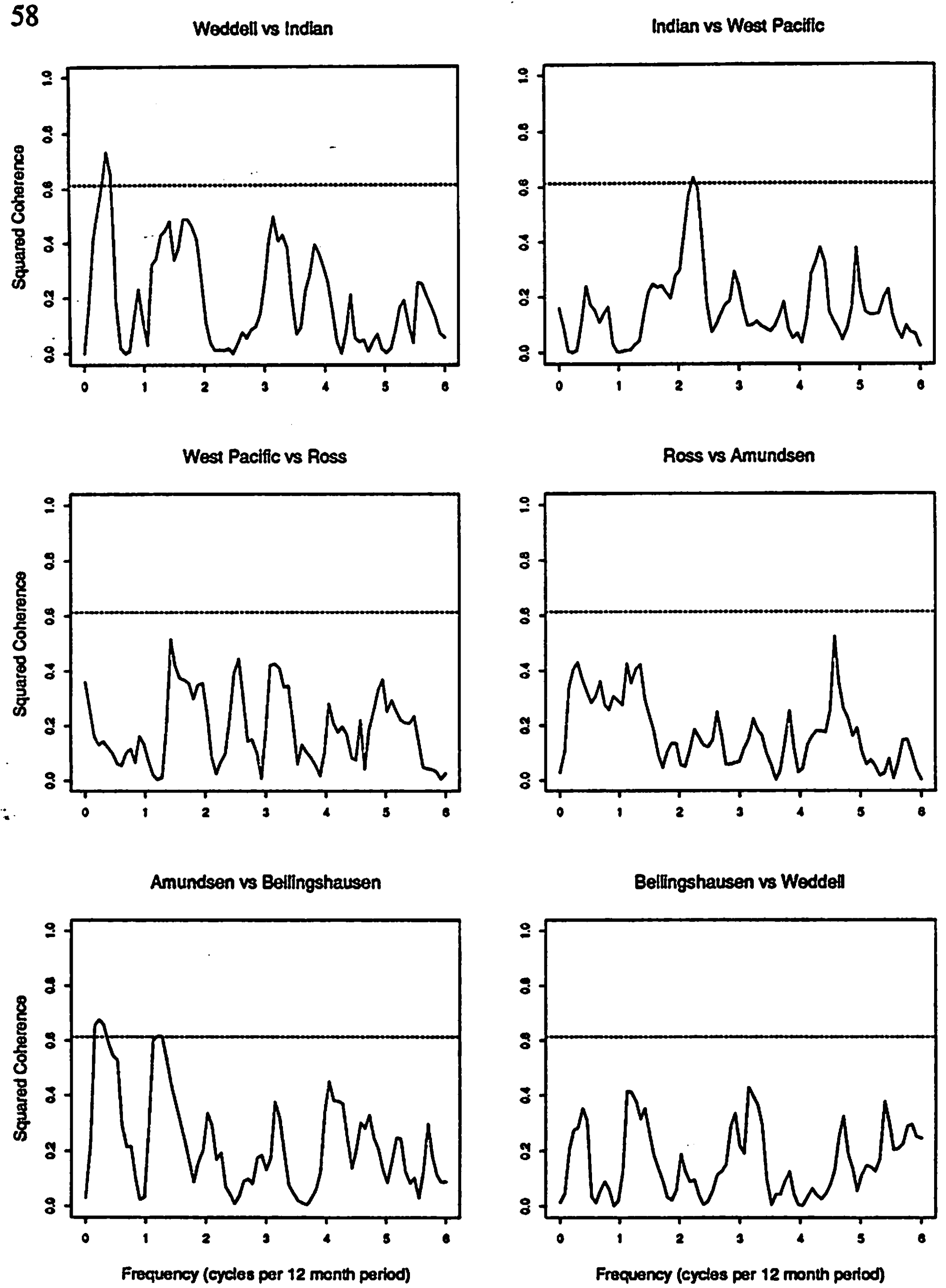

Figure 4.12: Squared Coherence between six Southern Ocean regions. The dotted line indicates the 0.01 significance level for the null hypothesis that the true coherence is zero.

the regions which proportionately contain the majority of the ice coverage (Weddell, Ross and Indian regions, in that order).

Cross spectral analysis of a subregion containing the LTER study area versus subregions to the east and west of the LTER subregion (see Figure 3.1 on page 30) was performed to determine the longitudinal spatial extent of coherence. Figure 4.13 (page 60) shows the squared coherence between LTER and six subregions. The top two plots are squared coherences against two subregions to the east of the LTER subregion (ie., east of the Antarctic Peninsula), which show little significant coherence. There is however significant coherence against the first two subregions to the west of the LTER subregion (the middle two plots) which together include a 20° longitudinal distance from the west boundary of the LTER subregion. The phase spectrum indicates that the two regions west of the LTER subregion are slightly out of phase and leading, indicating that the propagation of coherence is from west to east. Beyond a longitudinal distance of about 97°, there is no significant coherence (the bottom two plots). In general, the cross spectral analysis suggests that variability in ice coverage for the LTER study area is not characterized by variability east of the Antarctic Peninsula but may be characterized by variability west of the Antarctic Peninsula to about 97° W.

To determine whether there are other areas which show a temporal evolution of monthly anomalous ice coverages across longitudes, the whole Southern Ocean was re-divided into 15° longitudinal pie sections. Figure 4.14 (page 61) shows the plots of the normalized monthly anomalies for each of the 15° longitudinal pie sections. The plot in the upper left corner represents the pie section just east of the Antarctic Peninsula and is followed by pie sections moving clockwise around the continent, so that the plot in the lower right corner represents the pie section just west of the Antarctic Peninsula. There are several positive and negative broad anomaly 'peaks' (high positive or negative anomalies for 3 or more consecutive months) which appear in several of the adjacent pie sections in various regions around the continent. For example, there is a broad positive anomaly peak which appears in the 0-75° E pie

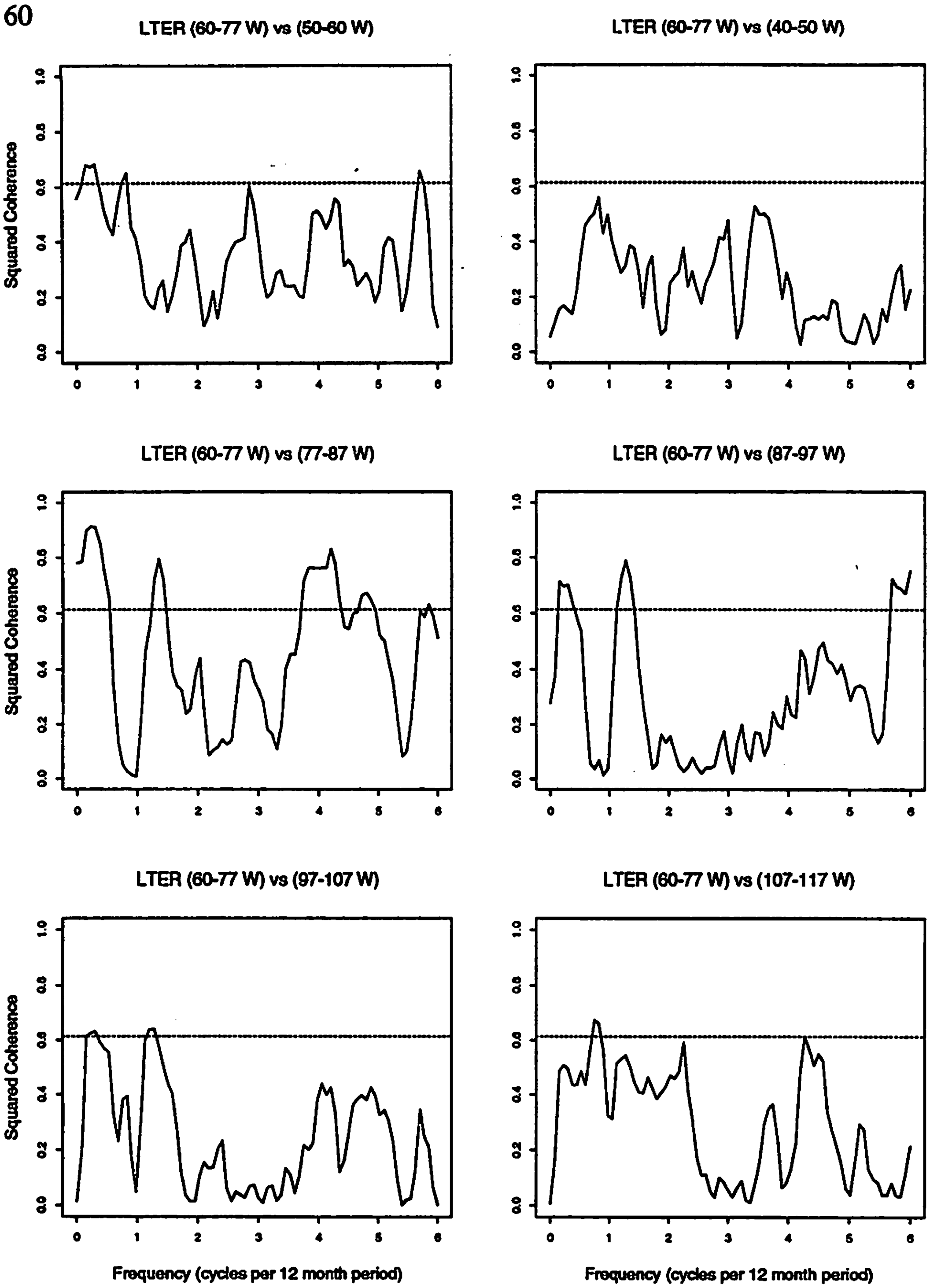

Figure 4.13: Squared Coherence between the LTER subregion and six subregions near LTER. The dotted line indicates the 0.01 significance level for the null hypothesis that the true coherence is zero.

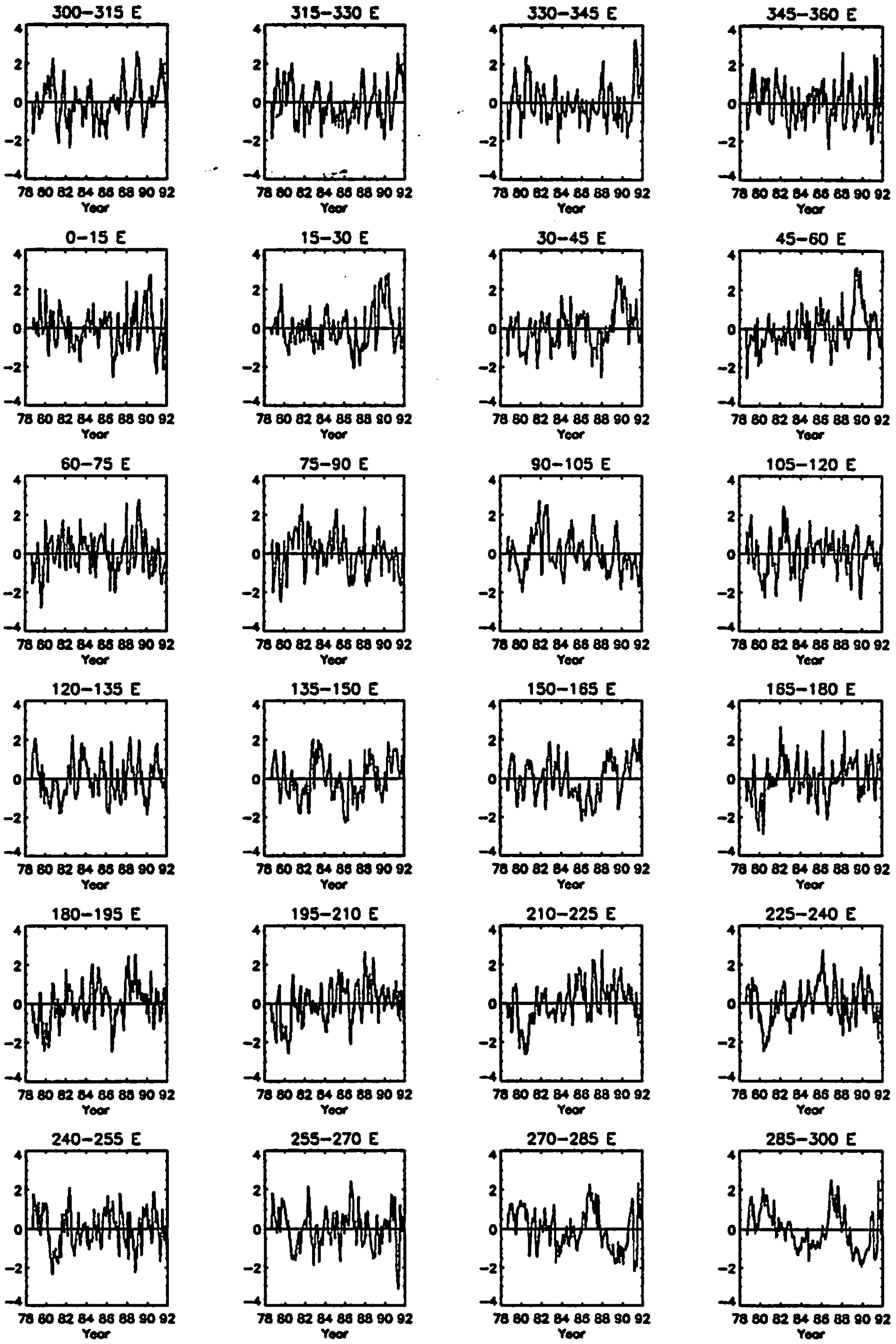

Figure 4.14: Standard deviates of monthly anomalies for 15° longitudinal pie sections.

sections and which seems to propagate *westward* from 75° E to 0° E between June 1988 and January 1990. There is a broad negative anomaly peak which appears in the 165-270° E pie sections and which seems to propagate *eastward* from 165° E to 270° E between August 1979 and February 1981. These two examples appear to be the only instances when the same broad peak is detectable in more than 3 adjacent pie sections. There are several other instances where the same peak is detectable in 2-3 pie sections. In general, there is little evidence that persistent anomaly fronts of interannual variability of Southern Ocean sea ice coverage propagate along lines of longitude. However, the 15° monthly anomaly time series do reveal that anywhere from 2 to 4 adjacent pie sections show similar patterns in overall interannual variability and could be grouped accordingly: 1) 300-360°, 2) 0-75°, 3) 75-135°, 4) 135-165°, 5) 165-225°, 6) 225-270°, and 7) 270-300°. These groups of pie sections which show similar interannual patterns do not necessarily conform to the regions which have typically been used in Southern Ocean regional studies. Only the 5th group roughly conforms to what is traditionally called the Ross region. The 6th group roughly conforms to the Amundsen region and the 7th group is the Bellingshausen region, as defined in this study. The other groups are unique from what has traditionally been called the Weddell, Indian and West Pacific regions. Another interesting feature in Figure 4.14 is that the pie sections which correspond to the Bellingshausen region (270-285° E and 285-300° E) are the only sections which exhibit a strong interannual pattern (ie., approximately 3 years of above mean monthly ice coverage followed by 3 years of below mean monthly ice coverage, as was noted in Section 4.3.1).

Chapter 5

Discussion

5.1 Interannual Spatial Patterns

The Southern Ocean as a whole exhibits little interannual variability. The highest year on the 13.25-year record, 1980, deviates only 1.9% from the mean maximum, and the lowest year on record, 1986, deviates 4.7%. In contrast, among six Southern Ocean regions (Weddell, Indian, West Pacific, Ross, Amundsen and Bellingshausen) deviations from mean maximum ice coverage can be as high as 39% above and 29% below the mean maximum. Thus, there is significant regional interannual variability, which appears to be a re-distribution of near constant ice coverage for the whole Southern Ocean. An attempt will be made to determine what, if any, patterns or trends may exist in this year to year re-distribution of Southern Ocean sea ice coverage.

Results have established that among the six Southern Ocean regions, all show unique interannual variability in ice coverage. No two regions have the same anomalous years of extreme maximum or minimum ice coverage. The monthly anomalies are distinctly different for each region, and cross-spectral analysis confirmed that little coherence exists between the six adjacent regions. Of the six Southern Ocean regions, the Weddell region has proportionately more ice coverage than the other five regions (as defined in Section 3.1.2) and contains 38% of the mean maximum ice coverage for the whole Southern Ocean (but accounts for only 21% of the physical area defining the Southern Ocean). However, the higher interannual variability in the Weddell region is not reflected in the time series for the whole Southern Ocean and therefore must be balanced by the interannual variability in the other regions. For example, Parkinson (1992) [2] in a study of monthly ice extents calculated from ESMR and SMMR data found high Ross ice extents versus low Weddell ice extents in ESMR years and then the reverse during SMMR years. There is also some evidence of this asymmetry in both the seasonal and monthly anomaly time series for the Weddell and Ross regions. The seasonal time series (page 38) show that for four out of five above mean ice coverage years in the Weddell region, the Ross experienced below mean ice coverage (1980, 1981, 1987 and 1991). For four out of five above ice coverage years in the Ross region, the Weddell experienced below mean ice coverage (1983, 1984, 1985 and 1989). In addition, the monthly anomaly time series (page 50) show that from approximately 1982 to 1987 the Weddell region had a majority of below mean anomolous months, whereas the Ross region had a majority of above mean anomolous months. These examples of a possible asymmetry between Weddell and Ross ice coverage may indicate that there is an asymmetry in synoptic scale atmospheric and/or oceanic circulation patterns. For example, Streten and Pike (1980) [27] claimed that observed asymmetries in the ice edge were coupled with a longitudinal pattern of atmospheric pressure minimums and maximums located along the Antarctic trough, where more northerly ice extents were associated with frequent low pressure systems, and more southerly ice extents were associated with frequent high pressure systems. However, this asymmetry in ice coverage is not strong or consistent enough to show a significant coherence in cross spectral analysis between the Weddell and Ross regions. This may be due to the fact that the asymmetry is stongest only during extreme high or low ice years and/or that the relationship is aperiodic.

There are other examples of asymmetry in ice coverage for other regional areas. Very different regional ice coverages contributed to the two highest ice coverage years for the whole Southern Ocean, 1980 (1.540 x 10^7 km^2) and 1985(1.536 x 10^7 km^2) and to the lowest ice coverage year, 1986 (1.439 x 10^7 km^2). Year 1980 was the highest ice coverage year for the Weddell region and the second highest ice coverage year for the Bellingshausen but all other regions experienced mean to below mean ice coverage. Year 1985 was the highest ice coverage year for the Ross region and the second highest ice coverage year for the Amundsen but again all other regions experienced mean to below mean ice coverage. Year 1986 was the one of the lowest ice coverage years for all regions except the Amundsen and Bellingshausen, for which 1986 was distinctly an above average ice coverage year. In these three examples, two adjacent regions had ice coverages which were either anomolously high or low while the other 4 regions experienced the opposite. While it is inconclusive what atmospheric or oceanic forcing mechanisms are contributing to variability in regional ice coverage, there seems to be a definite asymmetry in Southern Ocean ice distribution in years of extreme high or low ice coverage.

Another interesting pattern emerged in the analysis of the Amundsen and Bellingshausen seasonal and monthly anomaly time series. When comparing maximum ice coverages for the 13.25-year time series, inflection points or local maximums and minimums in maximum ice coverage were distinctly different for each region. Cross-correlation and cross spectral analysis between the Amundsen and Bellingshausen monthly anomalies indicated that ice coverage in the Bellingshausen lagged ice coverage in the Amundsen by 9-12 months, or approximately one year. Because maximum ice coverage in the Amundsen and Bellingshuasen regions occurs in September-October and in July-August, respectively, this explains the possible 9-11 month lags between the Amundsen and Bellingshausen maximum ice coverages. This approximate yearly lag could be due to prevailing low pressure systems in winter which in one year may be more frequent in the Amundsen region and in the other year more frequent in the Bellingshausen region. Frequent low pressure systems in the Amundsen region could result in advection of the Amundsen ice edge zonally (eastward) which would increase ice coverage in the Bellingshausen region while decreasing ice coverage in the Amundsen region. Frequent low pressure systems in the Bellingshausen region could result in low latitude warm air advection into the Bellingshausen region, preventing ice growth, while high latitude cold air advection into the Amundsen would promote ice growth. Similar patterns between the Amundsen and Bellingshausen ice extents and low pressure systems were observed by Cavalieri and Parkinson (1981) [26] and by Parkinson and Cavalieri (1982) [23].

Low frequency coherence between the Weddell and Indian monthly anomalies may also be due to atmospheric circulation patterns influencing adjacent regional ice coverages. The phase angle of the cross spectrum indicated that Indian ice coverage lags Weddell ice coverage by 6-7 months. Upon re-examination of the respective seasonal time series, it appears that below (or above) mean *summer* ice coverage in the Weddell region is followed by above (or below) mean *winter* ice coverage in the Indian region. This suggests an anticorrelation between Weddell and Indian monthly anomalies which is 6-7 months out of phase (Weddell leading). This pattern exists for 10 out of the 13 complete years, and in the other three years (1986, 1988 and 1990) there is, however, a tendency towards this pattern (ie, if both Weddell summer and Indian winter ice coverages are below mean, one would be increasing and the other decreasing with respect to the previous year). A possible driving force which may explain this pattern is the semi-permanent low located at about 20° E which influences both the Weddell and Indian ice coverages. When this low is well defined, cold air advection from the continent over the western Weddell region will promote ice growth, while at the same time, warm air advection from lower latitudes over the western Indian region will inhibit ice growth. When the low is not well defined, the western Weddell may experience less ice growth in winter and/or more ice melt in summer, and the Indian region may experience more ice growth in winter and/or less ice melt in summer. Typically this semi-permanent low intensifies in winter and weakens in summer, as well as shows interannual variability in overall intensity [1, 25]. Thus, the *interannual* variability of the semi-permanent low may be the driving force contributing to the 6-7 month lag between anticorrelated monthly anomalies in the Weddell and Indian regions.

The 13.25-year record is not nearly long enough to resolve any possible long term trends in ice coverage, and spectral analysis shows that the variability in monthly anomalies exhibits pure persistence. However, the time series of the Bellingshausen and LTER monthly anomalies (Figure 4.7, page 50) exhibit a tendency towards approximately three years of above mean monthly ice coverage followed by approximately three years of below mean monthly ice coverage, a pattern which repeats twice in the course of the 13.25-year record. This results in a 6-7 year difference between extreme high ice years (1980 and 1986-7) and a 6 year difference between extreme low ice years (1983 and 1989). This interannual pattern in ice coverage variability is not statistically significant (simply because the data record is not long enough to test it) and is meant only to be descriptive of the October 1978 to December 1991 data record. It is interesting to note, however, that none of the other regional or 15° monthly anomaly time series show as strong an interannual pattern.

There is little evidence that persistent anomaly fronts of interannual variability in Southern Ocean sea ice coverage propagate along lines of longitude as revealed by the 15° monthly anomaly time series. However, the 15° monthly anomaly time series did reveal that anywhere from 2 to 4 adjacent pie sections show similar patterns in interannual variability, and these groups which show similar interannual patterns do not necessarily conform to the regions which have typically been used in Southern Ocean regional studies. Therefore, it seems that homogeneity with respect to variability in ice coverage may better define a region and reveal possible patterns in interannual ice coverage. The areas which show similar patterns in interannual variability (as in the Bellingshausen region) indicate that the region is responding uniformally to the forcing mechanisms which are contributing to interannual variability. Thus, to better understand regional air-sea-ice dynamics, it is recommended that future studies should define regions by determining the areal extent of homogeneity in ice coverage variability instead of assigning arbitrary geographic boundaries.

5.2 Seasonal Spatial Patterns

The asymmetry in the Southern Ocean annual cycle which involves a long period of ice advance followed by a short period of ice retreat has been well documented in the literature [71, 1, 20]. This asymmetry is also revealed in the regional mean annual cycles, with the exception of the Bellingshausen and LTER mean annual cycles. The Weddell, Indian, West Pacific, Ross and Amundsen mean annual cycles all show a 7-month period of ice advance followed by a 5-month period of ice retreat, with December having the highest overall monthly rate. In contrast, the Bellingshausen and LTER mean annual cycles show a 5-month period of ice advance followed by a 7-month period of ice retreat, with June having the highest overall monthly rate. It appears that the oceanic and atmospheric forcings which are controlling the regional mean annual cycles are similar for all the regions except for the Bellingshausen. Hibler and Ackley (1983) concluded from numerical simulations of the Weddell pack ice that ice advance is mostly driven by thermodynamics and that ice retreat is mostly driven by advective processes (which open up leads within the pack ice allowing radiative heating of open water which in turn melts the pack ice). It may be that these processes are reversed for the Bellingshausen region. For example, if more ice is advected into the Bellingshausen region than is grown *in situ*, and if more ice is melted *in situ* than is advected out of the region, then this could explain the short period of ice advance followed by the long period of ice retreat. In order to confirm or discount the above explanation of the Bellingshausen and the LTER annual cycles, image data which allows ice tracking (ie., visible or SAR image data) needs to be analyzed for the Bellingshausen region. This will help determine the percentage of ice that is advected into or out of the region during periods of ice advance and retreat.

Parkinson (1992) [2] in a study of the interannual variability of Southern Ocean sea ice distributions observed that December was the month of highest interannual variability in ice extent. This agrees with the Southern Ocean mean annual cycle (Figure 4.3, page 42) which shows December as having the highest standard deviation (ie., interannual variability), but the months of April and May have high standard deviations as well. The regional mean annual cycles show that the highest interannual variability is typically in mid-winter to early spring (June to November). Part of the discrepancy between Parkinson's findings and these are due to the two different ice parameters used. Parkinson used ice *extent* whereas this study uses ice *coverage*, the difference being that the former measures the area within a given ice concentration threshold (30% for the Parkinson study), while the latter measures the actual ice coverage. Parkinson studied the interannual variability in spatial distribution of sea ice to establish a baseline from which future changes in sea ice extent can be monitored, in particular to better detect trends due to possible global climatic changes. Given that the interannual variability Parkinson observed is not in total agreement with the interannual variability observed here, it is important to consider the sea ice parameter being monitored and question whether it is the best one from which future trends can be detected. Variability in ice extent may be more of an indicator of variability in advective processes and less of an indicator of variability in thermodynamics, if in fact ice advance is mostly driven by thermodynamics. Therefore, ice *coverage* would be a better sea ice parameter to monitor, in that variability in ice coverage for most regions (the known exception would be the Bellingshausen region) would reflect variability in thermodynamic processes.

Spectral analysis of 2-day time series of each season indicated that there may exist an approximate 5-6 day periodicity in anomalous ice coverage. The 5-6 day signal was strongest for the Southern Ocean and LTER summer autospectra, but detectable in the Bellingshausen winter and LTER fall autospectra as well. Examination of the Southern Ocean summer (January to March) 2-day time series shows a regular annual trend where ice coverage decreases from January to February, then increases from February to March each year. Superimposed on this regular trend is a slight increase, then decrease in ice coverage about every 6 days (or every three data points), which is further accentuated in the 2-day anomaly time series and which is the cause for the 5-6 day peak in the autospectrum. One explanation for this periodicity could be related to the passive microwave radiometer and how it retrieves data. Although the data set includes data from two different radiometers, the majority is SMMR data (66%). This 5-6 day periodicity could be a regularly repeated noise. Another explanation could be a climatic forcing which operates on a 5-6 day frequency and which is strongest in summer. Because the signal is present in the Southern Ocean summer 2-day time series, it rules out the possibility that periodic storms may be advecting ice into or out of a region every 5-6 days, which would be a possible explanation for a subregion of the Southern Ocean, in particular for the LTER region. Summer is also the period in the Southern Ocean when year to year variability is the lowest, or ice coverage is the most predictable. The ice coverage in summer consists mostly of multiyear ice, of which the majority is located in the western Weddell and in the Amundsen and Ross regions. A climatic forcing such as winds could be periodically compressing the multiyear ice edges, causing rafting and hence decreasing ice coverage, followed by a windless period which would relax the multiyear ice pack, increasing ice coverage, or winds could switch direction and advect the ice edge out from the pack, which would also increase ice coverage. If this were true, then such wind events would be happening every 5-6 days. Explanation of this 5-6 day periodicity must first await a more detailed study of the SMMR and possibly SSM/I radiometric characteristics. If that possibility is ruled out, then further analysis is needed of the regions where multiyear ice is present, using higher resolution ice data and regional climatologies.

5.3 LTER Temporal and Spatial Patterns

Results from cross spectral analyses show that the region west of the Antarctic Peninsula to about 97° W is fairly homogeneous with respect to interannual variability in ice coverage. Thus, interannual variability in LTER ice coverage can be characterized by interannual variability in Bellingshausen ice coverage. On the other hand, there is no coherence between the west and east sides of the Antarctic Peninsula. In fact, the ice regimes of the two sides of the Peninsula are completely different. The east side of the Peninsula is characterized by permanent ice fields, the Larson and Ronne-Filchner Ice Shelves, and interannual variability is restricted to the seasonal ice zone to the northeast of it. In contrast, the entire west side of the Peninsula is characterized by a seasonal ice zone which has considerable interannual variability. Different atmospheric forcings can help explain the differences in ice regimes to either side of the Peninsula. The semi-permanent low pressure system, which is located in the Weddell Sea, helps maintain the permanent ice fields to the east of the Peninsula by advecting cold air from the interior of the continent over the western Weddell Sea in a clockwise rotation [1, 72]. No such persistent low occurs in the Bellingshausen, rather longitudinal variability in location and frequency of lows to the west of the Peninsula is high [25]. Depending on where these lows are positioned helps determine whether the Bellingshausen experiences a high or low ice year. A low positioned over the Bellingshausen region will promote low latitude warm air advection into the region west of the Peninsula, inhibiting ice growth, but a low positioned over the Amundsen region could advect ice zonally into the Bellingshausen region. Both scenarios have been observed by Parkinson and Cavalieri (1982) [23] and Carleton (1981) [25].

Thus, the high interannual variability in ice coverage for the LTER study area can in part be explained by the high interannual variability in the location and frequency of low pressure systems. Winter cyclogenesis in the Southern Ocean is located close to the Oceanic Antarctic Front (OAF), a zone of steep latitudinal temperature gradients which borders the poleward side of the Circumpolar Current and is located near 50° S in all regions except in the South Pacific regions (ie., the Bellingshausen, Amundsen and Ross regions), where it is located near 60° S. As cyclones mature, they migrate southeastward, and the maximum *poleward* extent of cyclone activity occurs in September (60-75° S) [25]. However, in the Bellingshausen and Amundsen regions the influence of the OAF on cyclogenesis is augmented by the close proximity of maximum winter sea ice coverage which reaches a mean latitude of 65° S [25]. No where else in the Southern Ocean is the OAF located within 5° of maximum ice extent, except for a narrow region just off east Victoria Land (a point of land west of the Ross Sea). In these regions where the OAF is in close proximity of maximum ice extent, a seasonal baroclinic zone develops near the ice margin which favors *in situ* cyclogenesis. These cyclones are often joined by cyclones migrating from lower latitudes in the South Pacific [25], resulting in a region of high interannual variability in both location and frequency of cyclones. Carleton (1981) [25] found that regions located north of the Ross Sea and in the Bellingshausen Sea showed the greatest interannual variability in cyclone frequencies for 1973-1977 winters. This may help explain why the interannual variability in Bellingshausen and LTER ice coverages is so distinctly different from interannual variability in the Amundsen. It may also explain why Bellingshausen and Amundsen regional ice coverages may be asymmetrical with respect to the other regional ice coverages, as illustrated in year 1986. It was mentioned previously that year 1986 was the lowest ice year on the 13.25-year record for the Southern Ocean and for all the regions except for the Amundsen and Bellingshausen regions. Since Amundsen and Bellingshausen regions are regions which support *in situ* cyclogenesis, these local cyclones may have contributed to the high ice coverages in the Amundsen and Bellingshausen regions in 1986.

In contrast to the high interannual variability in LTER ice coverage, the *spatial* distribution of ice coverage in the LTER study area during ice advance and ice retreat is fairly predictable. Ice typically advances from the southeast corner of the LTER study area towards the northeast corner, progressing both equatorward and outward from the Peninsula, typically retreating in the same fashion. Although the advance and retreat patterns are fairly consistent from year to year, the magnitude of ice coverage, the timing of advance and retreat and the duration of near minimum and maximum ice coverage is highly variable. In high ice years (1980, 1981, 1987 and 1991) the entire grid is covered with 50% and greater ice concentrations. (1986 was also a high ice year, but a coastal polynya north of Anvers Island prevented *total* ice coverage of the LTER study area.) In extreme low ice years (1983 and 1989), the 50% ice concentration contour only reaches 200 km south of Anvers Island and extends diagonally southwest across the study area (from 400.000 to 200.200 in LTER grid coordinates). In addition, the timing of minimum ice coverage can be either in March or April, but near minimum ice coverage can last for just one month to 5 months. The timing of maximum ice coverage can be in July, August, September or October and can remain near maximum for just one to 4 months. The high interannual variability in magnitudes, timing of ice advance and retreat and duration of near maximum and minimum ice coverages may have significant implications on the survival rate, distribution and/or migration patterns of marine communities which may either need ice or avoid ice in winter and during certain times in their life histories. It is also important to note that the marine communities in the southeast portion of the grid experience fairly consistent year to year ice coverage, whereas marine communities in the northeast portion of the grid experience the most dramatic year to year flucuations.

5.4 LTER Ice-Ecosystem Dynamics

As mentioned previously, a key hypothesis of the Antarctic Marine LTER proposes that interannual and annual variability in sea ice coverage is the major determinant in spatial and temporal changes in Antarctic marine communities. Many studies support this hypothesis. For example, studies have observed phytoplankton blooms in the vicinity of the retreating ice edge in spring [37, 73, 74, 75, 76, 77] and also along stationary ice edges in summer and winter [78, 79, 80], and it is believed that ice-edge blooms contribute significantly to total productivity of the Southern Ocean [81, 82]. In addition, the contribution from sea ice algal and bacterial production on total productivity appears to be significant as well [83, 84, 85, 86, 87]. Krill, a primary consumer, comprise over 50% of the total zooplankton biomass in the Southern Ocean epipelagic layer and therefore represent half the biomass for consumption by larger carnivores [88, 89]. Krill have been observed to be concentrated along the ice edge in spring and under the ice in winter, presumably grazing on ice edge blooms and sea ice algae [90, 91, 85]. Secondary consumers such as Adélie penguins not only depend on krill for food [92] but are dependent on pack ice for winter survival, which in turn effects recruitment and population growth [93, 94, 95]. The above observations indicate that interannual variability in sea ice coverage does impact the interannual variability in primary production, primary consumers and secondary consumers, thus impacting the entire Antarctic food web.

Given that the interannual variability in LTER ice coverage is known from October 1978 to December 1991, interannual variability in ice edge production can be estimated using an approach similar to Smith and Nelson (1986) [82] and Smith *et al.* (1988) [81]. This approach assumes that productivity in the region of the receding ice edge is enhanced due to meltwater induced stratification of the water column. The stratification traps the phytoplankton in a light-rich environment where it is assumed that nutrients are non-limiting. Prediction of ice edge productivity therefore assumes that production is enhanced throughout the length of the receding ice edge, thus the area uncovered by the receding ice edge each month is the areal extent of ice edge enhanced production. Smith and Nelson (1986) [82] and Smith *et al.* (1988) [81] used observed ice edge productivity rates taken in the Weddell and Ross Seas to estimate ice edge productivity for those regions. To estimate ice edge productivity in the LTER region, observed rates in the Bransfield region taken from the literature will be used. Studies in the Bransfield Strait region indicate that primary production rates in December can be from 0.91 g C m^{-2} d^{-1} [96] to 2.24 g C m^{-2} d^{-1} [97]. For the present, an estimate of production associated with the spring pack ice retreat for the LTER study area will be an average of the above production rates (ie., 1.6 g C m^{-2} d^{-1}). Thus, production associated with the *spring ice retreat* will be estimated as follows:

area uncovered each month x 1.6 g C m^{-2} d^{-1} x number of days in that month

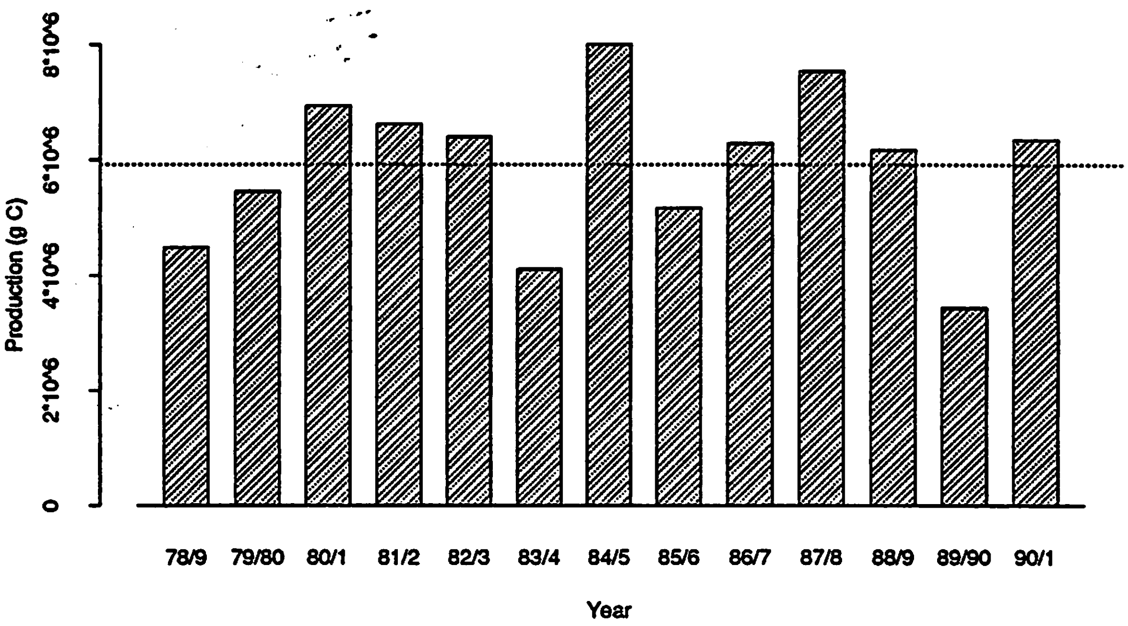

Figure 5.1: Estimated LTER production associated with the annual retreat of the pack ice, given a mean primary production rate of 1.6 g C m^{-2} d^{-1} . The dashed line represents the 13-year mean.

Figure 5.1 shows the estimates of yearly LTER production associated with the annual retreat of the pack ice. If the contribution from production associated with the retreating ice edge is greater than from any other source in the LTER study area, then Figure 5.1 represents the relative interannual variability in production one would expect given the assumptions. However, it is unknown whether production associated with the retreating ice in the LTER study area is greater than production associated with the LTER coastal area which also might effect the entire LTER study area. Holm-Hansen and Mitchell (1991) attributed the high production rates they observed in the Bransfield and Gerlache Straits to coastal dynamics (upwelling, shelter from winds, glacier melt) and not to the retreating ice edge. However, the production rates they observed decreased significantly from 2.5 g C m^{-2} d^{-1} in December to 0.25 g C m^{-2} d^{-1} in March, so one could argue that the higher production rates in December were in fact due to the recent presence of the pack ice. It is interesting to compare the primary production rate estimates from Bodungen *et al.* (1986) [96] and from Holm-Hansen and Mitchell (1991). Bodungen *et al.* were in the Bransfield region in November to December of 1980, which was one of the highest ice years for the 13.25-year record. However, their mean primary production rate was 41% of the Holm-Hansen and Mitchell (1991) mean primary production rate, who were in the Bransfield region in December of 1986, an average ice year. Of the three stations Bodungen *et al.* occupied, two stations had much lower rates of primary production, 0.23 g C m^{-2} d^{-1} and 0.83 g C m^{-2} d^{-1} , versus 1.66 g C m^{-2} d^{-1} observed at the other station. It was suggested that heavy grazing accounted for low accumulation rates at the station having the lowest observed production rate (0.23 g C m^{-2} d^{-1}) and that bloom decline accounted for low accumulation rates at the station having the second lowest observed production rate (0.83 g C m^{-2} d^{-1}). There are many factors which could account for high or low primary production rates in the Bransfield region, which may or may not be the dominant factors controlling production in the rest of the LTER study area. Nonetheless, the mean coastal production rate observed in the Bransfield region (ie., 1.6 g C m^{-2} d^{-1}) is 65% greater than that observed for one of the densest ice-edge blooms described in the literature (0.96 g C m^{-2} d^{-1}) [76]. If it is assumed that the production rates observed in the Bransfield region are due to coastal dynamics only and if *ice-free* coastal production contributes more to total production in the LTER study area than production associated with the annual retreat of the pack ice, then this could suggest that production may be higher in low ice years than in high ice years or in years that have long ice-free summers (ie., 1984, 1985, 1990 and 1991). Perhaps the most ideal ice year with respect to production would be one that had mean ice coverage followed by a relatively long ice-free summer, such as 1990-91 (see Figure 4.4, page 46). However, it is unknown at this time what the relative contributions of ice edge versus coastal production is for the LTER study area, but continued measurements of primary production in this region over the long term will allow this question to be addressed in the future.

Interannual variability in krill and Adélie penguin abundances could be estimated in a fashion similar to how production was estimated above, if we assume that ice coverage is positively correlated with krill and Adélie penguin abundances. The implications of whether high or low ice years and/or long, ice-free summers are more beneficial to krill and Adélie penguin populations also remain a question. It has been observed that both krill and Adélie penguins overwinter under and on the ice, respectively and that this habitat may be crucial to their overwinter survival [90, 91, 85, 93, 94, 95]. With respect to krill, it is unclear whether they *need* the ice in winter, but if the pack ice is present then it offers a food source for the krill in the form of ice algae. However, if the pack ice were not present, would they be sustained just as well or better on coastal production during winter? Again, it is unknown at this time what the relative contributions of winter coastal production versus ice algae on krill overwinter survival is. In contrast, it has been theorized that Adélie penguins do *need* the pack ice in winter and that overwinter survival rates are positively correlated with ice coverge [93, 94, 95]. Once more, the most ideal ice year for Adélie penguins may be one like 1990-91, where there was mean ice coverage in the LTER study area in winter followed by ice-free waters from January to April.

An objective of the Antarctic Marine LTER project is to characterize a season or year in terms of sea ice, a characterization which will be meaningful to the marine ecology being studied. For example, an *ice index* needs to be defined which can best be correlated to primary production or krill and Adélie penguin overwinter survival rates or krill and Adélie penguin recruitment rates. However, until we understand what an *ideal* ice year is for these key species, it will be difficult to define meaningful ice indices. Nonetheless, in the development towards better understanding of ice-ecosystem dynamics, several basic ice indices can be defined and correlated with various ecological indices to begin testing these relationships. Some basic ice indices are the following:

1. *Maximum* ice coverage within the 75% ice concentration contour; the percent of the LTER grid included within this contour; the dates; the number of months

this contour was in the immediate vicinity of Palmer Station

2. Same as #2, but for the 50% ice concentration contour

3. *Minimum* ice coverage within the 15% ice concentration contour; the percent of the LTER grid *free* of ice (ie., < 15%); the dates

These indices have been calculated from the SMMR and SSM/I data and are listed in Appendix D. It must be noted that whatever ice index is defined, it will be limited by the data from which it is calculated. For example, the indices calculated from SMMR and SSM/I data are limited to a 25 km spatial resolution, and in this particular instance, to a monthly temporal resolution (2-day ice *concentration* maps had not yet been calculated at the time of this writing). These spatial and temporal scales may or may not be relevant to the ice-ecosystem relationship being studied. Once again, ongoing investigation by the LTER project will help elucidate these ice-ecosystem spatial and temporal scales so that relevant ice indices can be defined.

Most studies of Southern Ocean ice-ecosystem relationships cited in the literature were located in regions that were *not* predominantly coastal, as is the LTER study area, and that *had* consistent ice coverage during winter. The ice-ecosystem relationships defined by these studies may not apply to the LTER study area. It has been shown that the interannual and annual variability in ice coverage for the LTER study area and for the Bellingshausen as a whole is unique with respect to other Southern Ocean regions. Undoubtedly, the LTER study area offers a unique environment, both with respect to ice coverage and with respect to the influences ice may have on the marine communities which inhabit this region. It is not unreasonable to think that both the ice-ecosystem and ice-ocean-air dyanamics in the LTER study area are similarly unique with respect to these dynamics in other Southern Ocean regions.

5.5 Future Directions

There are several approaches one could take to better understand the forcing mechanisms controlling the variability of the LTER sea ice. The following data should be analyzed for the western Antarctic Peninsula, including the Amundsen region due to interregional coupling with respect to atmospheric and oceanic circulation:

- atmospheric pressure fields
- geostrophic wind fields
- surface air temperatures
- sea surface temperatures
- ocean circulation patterns

Ocean circulation patterns are currently being studied for the western Antarctic Peninsula and are a major component of the LTER project. A future objective of the LTER project is to develop an ice model for the western Antarctic Peninsula region, and the above data sets will be needed for input parameters. However, from the current characterization of the spatial and temporal variability in Southern Ocean sea ice, it is likely that the western Antarctic Peninsula region is unique in how air-ocean-ice is coupled. Further characterization of the possible interrelationships is needed, hence the above data should be analyzed with respect to sea ice variability, to aid in the building of an appropriate ice model. In addition to analyzing atmospheric and oceanic fields, higher resolution ice data is needed to determine the following:

- the error involved in SMMR and SSM/I estimated sea ice concentrations for the LTER region, a region which is characterized by both a large coastal and marginal ice zone area
- characterization of sea ice variability in the Palmer Station vicinity to complement the near-shore sampling efforts

- characterization of sea ice variability throughout the LTER study region on spatial scales which are pertinent to ice-ecosystem interactions
- mapping of the ice edge, especially during ice advance and retreat
- estimate how much ice is advected into and out of the LTER study area versus how much is grown and melted *in situ*

The first item is necessary in order access the accuracy of SMMR and SSM/I estimated ice concentrations for a region which is characterized by features which have never been tested in any Southern Ocean validation programs. The second and third items are most relevant to the ecological objectives of the LTER project, and the last two items are critical to understanding the forcing mechanisms controlling variability of sea ice in the LTER region. Higher resolution data can be achieved with visible and thermal infrared AVHRR and OLS data which has a 0.6 to 1 km resolution and allows for the detection of new, young and thin ice, as well as make it possible to track ice movements. However, developing a time series with visible image data is difficult and time-consuming because of image contamination by clouds and low sun angle problems, but even an incomplete time series would provide much needed information. Maslanik *et al.* (1989) [98] outline the processes involved in merging AVHRR digitized data with SMMR imagery and discuss the advantages and applications of combining the two types of imagery. Another potential source for higher resolution image data is ERS-1 SAR data which has 25 m resolution and is uncontaminated by polar darkness and clouds. SAR data would in particular be beneficial for the near-shore sampling efforts in the Palmer Station vicinity.

Chapter 6

Conclusions

The Southern Ocean as a whole exhibits little interannual variability in ice coverage, and yet there is significant regional interannual variability which appears to be a re-distribution of near constant total ice coverage for the whole Southern Ocean. The six Southern Ocean regions (Weddell, Indian, West Pacific, Ross, Amundsen and Bellingshausen) all show unique interannual variability. No two regions have the same anomalous years of extreme maximum or minimum ice coverage, and cross spectral analysis of monthly anomalies confirmed that little to no coherence exists between adjacent regions. Spectral analysis of monthly anomalies confirmed that the interannual variability in all regional ice coverages shows pure persistence, but spectral anaylsis of the 2-day anomalies shows evidence of a 5-6 day periodicity. This 5-6 day peak is strongest for the summer Southern Ocean and LTER autospectra but is also evident in the winter Bellingshausen and fall autospectra. Further research is needed to determine whether this periodicity could be attributed to instrumental noise or climatic forcing.

Several patterns emerged from the analysis of interannual spatial variability in ice coverage. In extreme high or low ice coverage years for the whole Southern Ocean, there is a definite asymmetry in regional ice coverages, where two adjacent regions experience high or low ice coverages while the other four regions experience the opposite. In addition, cross spectral analysis revealed that Bellingshausen monthly anomalies lag Amundsen monthly anomalies by approximately one year, and that Weddell monthly anomalies lead Indian monthly anomalies by approximately a half year. Cross spectral analysis also showed that the region west of the Antarctic Peninsula to about 97° W is significantly coherent, confirming that the Bellingshausen region is homogeneous with respect to variability in ice coverage. This was further confirmed by the 15° longitudinal monthly anomaly plots which, in addition, revealed other areas which showed homogeneity with respect to variability in ice coverage. These other areas did not necessarily conform to the regions traditionally used in Southern Ocean regional studies. It is recommended that in future regional studies, which seek to resolve possible interannual patterns in ice coverage and associated air-sea-ice dynamics, regions should be defined by determining the areal extent of homogeneity in ice coverage, instead of arbitrarily defining them based on geographic delineations. Finally, evidence of a strong interannual pattern in ice variability was revealed only in one region, the Bellingshasuen region, where approximately three years of above average ice coverage are followed by approximately three years of below average ice coverage, a characteristic which repeats twice in the 13.25-year time series.

A few seasonal spatial patterns emerged from the analysis of regional annual cycles. All regional annual cycles revealed a temporal asymmetry in the annual advance and retreat of ice coverage. The Weddell, Indian, West Pacific, Ross and Amundsen show a 7-month period of ice advance followed by a 5-month period of ice retreat, with December having the highest overall monthly rates. In contrast, the Bellingshausen and LTER regions show the opposite temporal asymmetry, with a 5-month period of ice advance followed by a 7-month period of ice retreat, with June having the highest overall monthly rate. The implications of the former asymmetry may be that thermodynamics are mostly driving the long period of ice advance whereas advective dynamics are mostly driving the short period of ice retreat. This would be the opposite case in the Bellingshausen and LTER regions, where possibly advective dynamics are mostly driving the short period of ice advance (ie., ice advected zonally from the Amundsen region) and thermodyanmics driving the long period of ice retreat. In addition, in comparing the year to year variability in the regional annual cycles with a previous study which uses ice *extent*, it appears that ice *coverage* is the better ice parameter to monitor for regional long term trends. Variability in ice coverage reflects variability in thermodynamic processes more so than variability in ice extent, which reflects variability in dynamic processes such as wind-driven advection more so than variability in thermodynamic processes.

Analysis of spatial and temporal patterns of LTER ice coverage shows that although the spatial distribution of ice advance and ice retreat within the LTER study area is consistent year to year, the magnitude of ice coverage, the timing of advance and retreat and the duration of near minimum and maximum ice coverage is highly variable. Much of the interannual variability in the LTER ice coverage may be explained by the fact that the Bellingshausen and Amundsen regions experience the highest frequency of cyclones which not only vary in number year to year, but vary longitudinally between the two regions. However, the high interannual variability in LTER ice coverage is not consistent throughout the study area. The southeast portion of the study area experiences fairly consistent yearly ice coverage, whereas the northeast portion experiences dramatic flucuations. Thus, the interannual variability in LTER ice coverage may therefore have significant implications on the survival rate, distribution and/or migration patterns of marine communities. It is the objective of the Antarctic Marine LTER project, which provides long term monitoring of ice-ecosystem dynamics, to determine the implications interannual variability in LTER ice coverage may have on the marine communities inhabiting the study area. This thorough characterization of spatial and temporal variability in LTER ice coverage in the context of spatial and temporal variability in Southern Ocean ice coverage will help guide research on both ice-ocean-air and ice-ecosystem dynamics.

Appendix A

Acronyms

AES-YORK	Canadian Atmospheric Environmental Service at York
AIC	Akaike's Information Criterion
AR	Autoregressive
AVHRR	Advanced Very High Resolution Radiometer
DEC	Digital Equipment Corporation
DMSP	Defense Meteorological Satellite Program (USA)
ERS-1	European Remote Sensing Satellite - 1
ESA	European Space Agency
ESMR	Electrically Scanning Microwave Radiometer
FNOC	Fleet Numerical Oceanographic Center
FY	First year sea ice
GR	Gradient ratio
GSFC	Goddard Space Flight Center
IDL	Interactive Data Language
LTER	Long Term Ecological Research (NSF)
MSS	Multi-Spectral Scanner (Landsat)
MY	Multiyear sea ice
NASA	National Aeronautics and Space Administration (USA)

Nimbus 5, 6 and 7	NASA Meteorogical Research and Development Satellites 5, 6 and 7
NOAA	National Oceanic and Atmospheric Administration (USA)
NORSEX	Norwegian Remote Sensing Experiment
NSF	National Science Foundation
NSIDC	National Snow and Ice Data Center, University of Colorado, Boulder, Colorado 80309-0449
OAF	Oceanic Antarctic Front
OLS	Operational Linescan System (DMSP)
OW	Open water
PR	Polarization ratio
SAR	Synthetic Aperature Radar
SIR-B	Shuttle Imaging Radar - B (USA)
SMMR	Scanning Multi-Channel Microwave Radiometer
Splus	Statistical Sciences, Inc., software
SSM/I	Special Sensor Microwave/Imager (DMSP)
TIROS-N	Television Infrared Observation Satellite - N (USA)
U-Mass	University of Massachusetts
UTM	Universal Transverse Mercator
USAF	United States Air Force

Appendix B

NASA Team Algorithm

The NASA Team algorithm uses a polarization ratio (PR) and a spectral gradient ratio (GR) to calculate total, FY and MY sea ice concentrations:

$$PR = \frac{T_B[18V] - T_B[18H]}{T_B[18V] + T_B[18H]} \tag{B.1}$$

$$GR = \frac{T_B[37V] - T_B[18V]}{T_B[37V] + T_B[18V]} \tag{B.2}$$

Assuming that the three surface types sum to unity within a footprint, the radiative transfer equation can be written as:

$$T_B = T_{B,OW}(1 - C_{FY} - C_{MY}) + T_{B,FY}(C_{FY}) + T_{B,MY}(C_{MY}) \tag{B.3}$$

where

T_B is the brigthness temperature measured at the satellite,

$T_{B,OW}$, $T_{B,FY}$ and $T_{B,MY}$ are the algorithm tie points,

C_{FY} and C_{MY} are the fractional ice concentrations of FY and MY

Equation B.3 can be substituted into Equations B.1 and B.2 for each of the three channels (ie., 18 H, 18 V and 37 V) and solved simultaneously for C_{FY} and C_{MY}:

$$C_{FY} = \frac{a_0 + a_1 PR + a_2 GR + a_3 (PR)(GR)}{D} \tag{B.4}$$

$$\begin{aligned} C_{MY} &= \frac{b_0 + b_1 PR + b_2 GR + b_3 (PR)(GR)}{D} && \text{(B.5)} \\ C_{total} &= C_{FY} + C_{MY} && \text{(B.6)} \end{aligned}$$

where

$$\begin{aligned}
D &= c_0 + c_1 PR + c_2 GR + c_3 (PR)(GR) \\
a_0 &= A_0 B_4 - A_4 B_0 \\
a_1 &= A_1 B_4 - A_5 B_0 \\
a_2 &= A_0 B_5 - A_4 B_1 \\
a_3 &= A_1 B_5 - A_5 B_1 \\
b_0 &= A_0 B_2 - A_2 B_0 \\
b_1 &= A_1 B_2 - A_3 B_0 \\
b_2 &= A_0 B_3 - A_2 B_1 \\
b_3 &= A_1 B_3 - A_3 B_1 \\
c_0 &= A_2 B_4 - A_4 B_2 \\
c_0 &= A_3 B_4 - A_5 B_2 \\
c_0 &= A_2 B_5 - A_4 B_3 \\
c_0 &= A_3 B_5 - A_5 B_3 \\
A_0 &= -T_{B,OW}[18V] + T_{B,OW}[18H] \\
A_1 &= T_{B,OW}[18V] + T_{B,OW}[18H] \\
A_2 &= T_{B,MY}[18V] - T_{B,MY}[18H] - T_{B,OW}[18V] + T_{B,OW}[18H] \\
A_3 &= -T_{B,MY}[18V] - T_{B,MY}[18H] + T_{B,OW}[18V] + T_{B,OW}[18H] \\
A_4 &= T_{B,FY}[18V] - T_{B,FY}[18H] - T_{B,OW}[18V] + T_{B,OW}[18H] \\
A_5 &= -T_{B,FY}[18V] - T_{B,FY}[18H] + T_{B,OW}[18V] + T_{B,OW}[18H] \\
B_0 &= -T_{B,OW}[37V] + T_{B,OW}[18V] \\
B_1 &= T_{B,OW}[37V] + T_{B,OW}[18V]
\end{aligned}$$

$$\begin{aligned}
B_2 &= T_{B,MY}[37V] - T_{B,MY}[18V] - T_{B,OW}[37V] + T_{B,OW}[18V] \\
B_3 &= -T_{B,MY}[37V] - T_{B,MY}[18V] + T_{B,OW}[37V] + T_{B,OW}[18V] \\
B_4 &= T_{B,FY}[37V] - T_{B,FY}[18V] - T_{B,OW}[37V] + T_{B,OW}[18V] \\
B_5 &= -T_{B,FY}[37V] - T_{B,FY}[18V] + T_{B,OW}[37V] + T_{B,OW}[18V]
\end{aligned}$$

The A_i and B_i coefficients are determined using the empirically derived T_B's for each of the three surface types at each of the three channels. Table B.1 (page 90) lists the T_B's used for calculating ice concentrations from SMMR and SSM/I data, respectively. The three surface types empirically determined for the algorithm tie points used in calculating ice concentrations in the Southern Ocean are open water and type A and B sea ice. Type A and B sea ice are analogous to FY and MY and are substituted accordingly into Equation B.3. Because MY in the Southern Ocean is not as well define radiometrically from FY as it is in the Arctic, MY fractions are not determined, only *total* ice concentrations. Type A and B tie points represent the range in radiometric signatures of ice cover in the Southern Ocean which would include both FY and MY types. Therefore, Equations B.4 and B.5 are determined using type A and B tie points in place of FY and MY tie points, and then total ice concentrations are determined using Equation B.6.

Table B.1: SMMR and SSM/I algorithm tie points for the Southern Ocean

Channel	Open Water	Type A Sea Ice	Type B Sea Ice
SMMR Tie Points[a]			
18 GHz, H	098.5	232.2	205.2
18 GHz, V	168.7	247.1	237.0
37 GHz, V	199.4	245.5	210.0
SSM/I Tie Points[b]			
19.4 GHz, H	100.3	237.8	193.7
19.4 GHz, V	176.6	249.8	221.6
37 GHz, V	200.5	243.3	190.3

---

[a] from Gloersen *et al.* (1992) [3]

[b] from Cavalieri *et al.* (1991) [56]

Appendix C

LTER Sampling Grid

The Antarctic Marine LTER is based at Palmer Station, Anvers Island, midway down the western side of the Antarctic Peninsula ($64°46'S, 64°03'W$). The study area is roughly parallel to the Peninsula and is 900 km in length and 200 km from near- to off-shore. Figure C.1 (page 93) shows a Universal Transverse Mercator (UTM) projection of the study area. Transects which traverse the width of the study area are spaced 100 km along the Peninsula. Sampling stations along the transects are spaced 20 km apart (marked by the dots along the transects in Figure C.1) and range from shallow, near-shore stations (less than 200 m) to deep off-shore stations (greater than 5000 m). The study area is visited one to two times a year aboard ice-strengthened research vessels. Measurements and samples are taken of the following:

- hydrographic and optical characteristics of the water column
- phytoplankton biomass, photosynthetic potential and community composition
- distribution, abundance and physiological condition of selected secondary producers
- Adélie penguins and South Polar skua surveys

In addition, throughout the austral Spring and Summer a near shore sampling area in the immediate vicinity of Palmer Station (within two nautical miles of the Station) is sampled weekly from zodiacs. Similar parameters are measured and sampled with the addition of population dynamics and ecology of Adélie penguins and South Polar Skuas that nest on nearby islands.

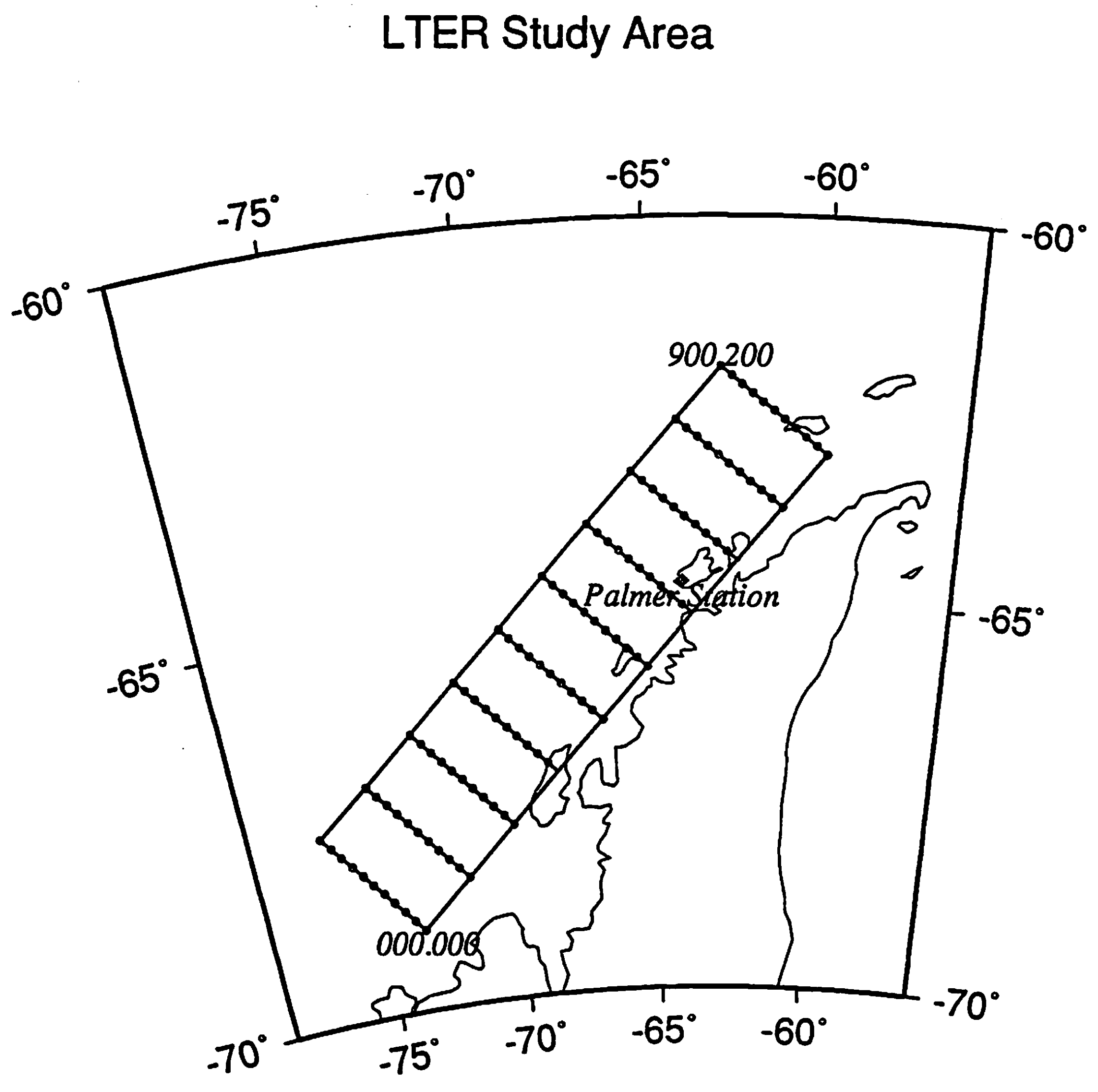

Figure C.1: Universal Transverse Mercator projection of the LTER study area. The box outlines the entire study area. See text for explanation of sampling grid.

Appendix D

LTER Ice Indices

The following three ice indices were calculated from the SMMR and SSM/I data and are listed in Tables D.1, D.2 and D.3:

1. *Maximum* ice coverage within the 75% ice concentration contour; the percent of the LTER grid included within this contour; the dates; the number of months this contour was in the immediate vicinity of Palmer Station
2. Same as #2, but for the 50% ice concentration contour
3. *Minimum* ice coverage within the 15% ice concentration contour; the percent of the LTER grid *free* of ice (ie., < 15%); the dates

Maximum ice coverage by the 75% or 50% ice concentration contour includes the region of the LTER grid within (or to the south of) the concentration contour at *maximum* ice coverage for the year in question. Ice concentrations of 75% correspond to close pack ice and ice concentrations of 50% correspond to mixtures of open drift ice or mixtures of close pack ice and open water. Minimum ice coverage by the 15% ice concentration contour includes the region of the LTER grid within (or to the south of) the concentration contour at *minimum* ice coverage for the year in question. The 15% ice concentration contour corresponds to the ice edge. Often at minimum

Table D.1: Maximum ice coverage within the 75% ice concentration contour

Year	Maximum Ice Coverage (LTER grid coordinates)	% of LTER Grid Covered	Date	Date within Palmer Vicinity
1979	600.200-600.000	67	Sep	Sep-Nov
1980	900.200-550.000	71	July	Jul-Nov
1981	650.200-550.000	67	Aug	Jul-Nov
1982	600.200-300.050	45	Aug	Aug
1983	000.200-300.000	17	Aug-Oct	–
1984	600.200-300.050	45	Aug	Aug
1985	100.200-400.050	32	Aug	–
1986	650.200-600.000	69	Oct	Aug-Oct
1987	900.150-600.000	88	Jul	Jul-Dec
1988	550.200-300.050	43	Sep	–
1989	000.150-200.000	8	Sep	–
1990	550.200-300.050	43	Oct-Nov	–
1991	600.200-600.000	67	Sep	Aug-Sep

ice coverage, ice will remain in the southern portion of the grid as well as along the coast (ice which presumably exists since the data were filtered to remove land contamination effects). The ice concentration contour given in Table D.3 therefore refers to the ice in the southern portion of the grid. However, in the calculation of the '% of LTER Grid Free' parameter, the contribution from coastal ice is included for all years except 1985 and 1989-91. For these four years, no sea ice remained within the LTER grid during minimum ice coverage. The parameter, 'Date within Palmer Vicinity' is defined as the months that the ice concentration contour was at least to the 600.100 location or to the south of Anvers Island. If this field has a '–', then the ice concentration contour never reached the Palmer vicinity.

Table D.2: Maximum ice coverage within the 50% ice concentration contour

Year	Maximum Ice Coverage (LTER grid coordinates)	% of LTER Grid Covered	Date	Date within Palmer Vicinity
1979	750.200-900.050	94	Aug	Jul-Dec
1980	entire grid	100	Jul-Oct	Jul-Nov
1981	entire grid	100	Aug	Jun-Dec
1982	900.150-650.050	84	Aug-Sep	Jul-Oct
1983	300.200-600.050	54	Sep-Oct	Oct
1984	900.100-650.050	71	Aug	Jul-Sep
1985	650.200-600.000	69	Aug	Aug
1986	entire grid[a]	97	Aug	Jul-Nov
1987	entire grid	100	Jul	Jul-Dec
1988	750.150-650.050	76	Sep	Aug-Sep
1989	200.200-400.000	33	Sep	–
1990	800.200-650.050	77	Sep	Sep-Nov
1991	entire grid	100	Aug	Aug-Nov

---

[a] except for a 75 x 75 km open ocean polynya centered on 800.100

Table D.3: Minimum ice coverage within the 15% ice concentration contour

Year	Minimum Ice Coverage (LTER grid coordinates)	% of LTER Grid Free	Date
1979	100.200-200.000	71	Mar-Apr
1980	000.200-300.000	72	Feb-Mar
1981	000.150-200.000	79	Mar
1982	000.100-200.000	82	Mar-Apr
1983	000.100-100.000	85	Feb-May
1984	coastal ice only	87	Mar-Apr
1985	–	100	Mar-Apr
1986	000.100-200.000	82	Feb-Apr
1987	000.150-200.000	79	Mar
1988	000.050-200.000	85	Mar-Apr
1989	–	100	Jan-May
1990	–	100	Dec-May
1991	–	100	Jan-May

Bibliography

[1] H. J. Zwally, J. C. Comiso, C. L. Parkinson, W. J. Campbell, F. D. Carsey, and P. Gloersen, "Antarctic sea ice, 1973-1976: Satellite passive-microwave observations," Tech. Rep. NASA SP-459, National Aeronautics and Space Administration, Washington, DC, 1983.

[2] C. L. Parkinson, "Interannual variability of monthly southern ocean sea ice distribution," *Journal of Geophysical Research*, vol. 97, no. C4, pp. 5349–5363, 1992.

[3] P. Gloersen, W. J. Campbell, D. J. Cavalieri, J. C. Comiso, C. L. Parkinson, and H. J. Zwally, "Arctic and Antarctic sea ice, 1978-1987: Satellite passive-microwave observations and analysis," Tech. Rep. NASA SP-511, National Aeronautics and Space Administration, Washington, DC, 1992.

[4] R. G. Barry, J. Maslanik, K. Steffan, R. L. Weaver, V. Troisi, D. J. Cavalieri, and S. Martin, "Advances in sea-ice research based on remotely sensed passive microwave data," *Oceanography*, vol. 6, no. 1, pp. 4–12, 1993.

[5] F. D. Carsey, "Remote sensing of ice and snow: review and status," *International Journal of Remote Sensing*, vol. 13, no. 1, pp. 5–11, 1992.

[6] F. D. Carsey, ed., *Microwave Remote Sensing of Sea Ice*. Geophysical Monograph 68, American Geophysical Union, 1992.

[7] M. L. V. Woert, R. H. Whritner, D. E. Waliser, D. H. Bromwich, and J. C. Comiso, "ARC: A source of multisensor satellite data for polar science," *EOS Transactions American Geophysical Union*, vol. 73, pp. 65–76, February 11 1992.

[8] J. C. Comiso, "Satellite remote sensing of the polar oceans," *Journal of Marine Systems*, vol. 2, pp. 395–434, 1991.

[9] R. Massom, *Satellite Remote Sensing of Polar Regions.* Polar Research Series edited by B. Stonehouse, 2000 Corporate Blvd., N.W., Boca Raton, Florida 33431: Lewis Publishers, 1991.

[10] J. A. Maslanik and R. G. Barry, "Remote sensing in antarctica and the southern ocean: applications and developments," *Antarctic Science*, vol. 2, pp. 105–121, 1990.

[11] R. A. Shuchman and R. G. Onstott, "Remote sensing of the polar oceans," in *Polar Oceanography* (W. O. Smith, Jr., ed.), vol. A, ch. 3, pp. 123–166, San Diego: Academic Press, Inc., 1990.

[12] R. J. Stouffer, S. Manabe, and K. Bryan, "Interhemispheric asymmetry in climate response to a gradual increase in atmospheric CO_2," *Nature*, vol. 342, pp. 660–662, 1989.

[13] H. J. Zwally, J. C. Comiso, and J. E. Walsh, "Variability of Antarctic sea ice," in *International Conference on the Role of the Polar Regions in Global Change: Proceedings of a Conference held June 11-15, 1990 at the University of Alaska Fairbanks* (G. Weller, C. L. Wilson, and B. A. B. Severin, eds.), vol. I, Geophysical Institute University of Alaska Fairbanks and Center for Global Change and Arctic System Research, 1991.

[14] P. Gloersen and W. J. Campbell, "Recent variations in arctic and antarctic sea-ice covers," *Nature*, vol. 352, pp. 33–36, 4 July 1991.

[15] T. H. Jacka and W. F. Budd, "Detection of temperature and sea ice extent changes in the Antarctic and Southern Ocean," in *International Conference on the Role of the Polar Regions in Global Change: Proceedings of a Conference held June 11-15, 1990 at the University of Alaska Fairbanks* (G. Weller, C. L. Wilson, and B. A. B. Severin, eds.), vol. I, Geophysical Institute University of Alaska Fairbanks and Center for Global Change and Arctic System Research, 1991.

[16] S. C. B. Raper, T. M. L. Wigley, P. R. Mayes, P. D. Jones, and M. J. Salinger, "Variations in surface air temperatures. part3: The Antarctic, 1957-82," *Monthly Weather Review*, vol. 112, pp. 1341–1353, 1984.

[17] F. D. Carsey, R. G. Barry, and W. F. Weeks, "Introduction," in *Microwave Remote Sensing of Sea Ice* (F. D. Carsey, ed.), Geophysical Monograph 68, ch. 1, American Geophysical Union, 1992.

[18] C. L. Parkinson, "On the development and cause of the Weddell Polynya in a sea ice simulation," *Journal of Physical Oceanography*, vol. 13, pp. 501–511, 1983.

[19] W. D. Hibler, III and S. F. Ackley, "Numerical simulation of the Weddell Sea pack ice," *Journal of Geophysical Research*, vol. 88, no. C5, pp. 2873–2887, 1983.

[20] A. L. Gordon, "Seasonality of Southern Ocean sea ice," *Journal of Geophysical Research*, vol. 86, no. C5, pp. 4193–4197, 1981.

[21] A. L. Gordon and H. W. Taylor, "Seasonal change of Antarctic sea ice cover," *Science*, vol. 187, pp. 346–347, 1975.

[22] A. M. Carleton and D. A. Duane, "Intermediate-scale sea ice - atmosphere interactions over high Southern latitudes in winter," *GeoJournal*, vol. 18.1, pp. 87–101, 1989.

[23] C. L. Parkinson and D. J. Cavalieri, "Interannual sea-ice variations and sea-ice/atmosphere interactions in the Southern Ocean, 1973-1975," *Annals of Glaciology*, vol. 3, pp. 249–254, 1982.

[24] W. F. Budd, "The role of Antarctica in southern hemisphere weather and climate," *Australian Meteorological Magazine*, vol. 30, pp. 265–272, 1982.

[25] A. M. Carleton, "Ice-ocean-atmosphere interactions at high southern latitudes in winter from satellite observation," *Australian Meteorological Magazine*, vol. 29, pp. 183–195, 1981.

[26] D. J. Cavalieri and C. L. Parkinson, "Large-scale variations in observed Antarctic sea ice extent and associated atmospheric circulation," *Monthly Weather Review*, vol. 109, pp. 2323–2336, November 1981.

[27] N. A. Streten and D. J. Pike, "Characteristics of the broadscale Antarctic sea ice extent and the associated atmospheric circulation 1972-1977," *Archiv für Meteorologie, Geophysik und Bioklimatologie*, vol. A29, pp. 279–299, 1980.

[28] J. W. Weatherly, J. E. Walsh, and H. J. Zwally, "Antarctic sea ice variations and seasonal air temperature relationships," *Journal of Geophysical Research*, vol. 96, no. C8, pp. 15,119–15,130, 1991.

[29] C. L. Parkinson and R. A. Bindschadler, "Response of Antarctic sea ice to uniform atmospheric temperature increases," in *Climate Processes and Climate Sensitivity* (J. E. Hansen and T. Takahashi, eds.), Geophysical Monograph 29 (Maurice Ewing Volume 5), pp. 254–264, American Geophysical Union, 1984.

[30] P. Lemke, E. W. Trinkl, and K. Hasselmann, "Stochastic dynamic analysis of polar sea ice variability," *Journal of Physical Oceanography*, vol. 10, no. 12, pp. 2100–2120, 1980.

[31] D. J. Karoly, "Southern hemisphere circulation features associated with El Niño-Southern Osciallation events," *Journal of Climate*, vol. 2, pp. 1239–1252, 1989.

[32] M. L. Savage, C. R. Stearns, and G. A. Weidner, "The Southern Oscillation signal in Antarctica," in *Second Conference on Polar Meteorology and Oceanography, March 29-31, 1988*, (Madison, Wisconson), pp. 141–144, American Meteorology Society, Boston, Mass., 1988.

[33] L. S. Chiu, "Antartic sea ice variations 1973-1980," in *Variations in the Global Water Budget* (A. Street-Perrott, M. Beran, and R. Ratcliffe, eds.), pp. 301–311, Dordrecht: D. Reidel Publishing Company, 1983.

[34] A. M. Carleton, "Sea ice-atmosphere signal of the Southern Oscillation in the Weddelll Sea, Antarctica," *Journal of Climate*, vol. 1, pp. 379–388, April 1988.

[35] A. M. Carleton, "Antarctic sea-ice relationships with indices of the atmospheric circulation of the Southern Hemisphere," *Climate Dynamics*, vol. 3, pp. 207–220, 1989.

[36] G. Peng and M. Domros, "Connections of the West Pacific subtropical high and some hydroclimatic regimes in China with Antarctic ice-snow indices," *Meteorology and Atmospheric Physics*, vol. 37, pp. 61–71, 1987.

[37] J. C. Comiso, C. R. McClain, C. W. Sullivan, J. P. Ryan, and C. L. Leonard, "Coastal Zone Color Scanner pigment concentrations in the southern ocean and relationships to geophysical surface features," *Journal of Geophysical Research*, vol. 98, no. C2, pp. 2419–2451, 1993.

[38] P. Gloersen and D. J. Cavalieri, "Reduction of weather effects in the calculation of sea ice concentrations from microwave radiances," *Journal of Geophysical Research*, vol. 91, no. C3, pp. 3913–3919, 1986.

[39] D. J. Cavalieri, P. Gloersen, and W. J. Campbell, "Determination of sea ice parameters with the NIMBUS 7 SMMR," *Journal of Geophysical Research*, vol. 89, no. D4, pp. 5355–5369, 1984.

[40] J. C. Comiso, "Sea ice effective microwave emissivities from satellite passive microwave and infrared observations," *Journal of Geophysical Research*, vol. 88, no. C12, pp. 7686–7704, 1983.

[41] J. C. Comiso, S. F. Ackley, and A. L. Gordon, "Antarctic sea ice microwave signatures and their correlation with *in situ* ice observations," *Journal of Geophysical Research*, vol. 89, no. C1, pp. 662–672, 1984.

[42] National Snow and Ice Data Center, Cooperative Institute for Research in Environmental Sciences, University of Colorado, Boulder, Colorado, 80309-0449, *DMSP SSM/I brightness temperature and sea ice concentration grids for the polar regions on cd-rom - user's guide*, January 1992. Special Report 1.

[43] J. C. Comiso, T. C. Grenfell, D. L. Bell, M. A. Lange, and S. F. Ackley, "Passive microwave *in situ* observations of winter Weddell Sea ice," *Journal of Geophysical Research*, vol. 94, no. C8, pp. 10,891–10,905, 1989.

[44] K. Liou, *An introduction to atmospheric radiation*, pp. 275–280. San Diego: Academic Press, Inc., 1980.

[45] K. Steffan, J. Key, D. J. Cavalieri, J. C. Comiso, P. Gloersen, K. S. Germain, and I. Rubinstein, "The estimation of geophysical parameters using passive microwave algorithms," in *Microwave Remote Sensing of Sea Ice* (F. D. Carsey, ed.), Geophysical Monograph 68, ch. 10, American Geophysical Union, 1992.

[46] F. D. Carsey and H. J. Zwally, "Remote sensing as a research tool," in *The Geophysics of Sea Ice* (N. Untersteiner, ed.), pp. 1021–1098, New York: Plenum Publishing Corporation, 1986.

[47] E. L. Andreas and S. F. Ackley, "On the differences in ablation seasons of Arctic and Antarctic sea ice," *Journal of Atmospheric Sciences*, vol. 39, pp. 440–447, 1982.

[48] A. J. Gow, S. F. Ackley, W. F. Weeks, and J. W. Govoni, "Physical and structural characteristics of Antarctic sea ice," *Annals of Glaciology*, vol. 3, pp. 113–117, 1982.

[49] M. A. Lange, S. F. Ackley, P. Wadhams, G. S. Dieckmann, and H. Eicken, "Development of sea ice in the Weddell Sea," *Annals of Glaciology*, vol. 12, pp. 92–96, 1989.

[50] W. B. Tucker, III, A. J. Gow, and W. F. Weeks, "Physical properties of summer sea ice in the Fram Strait," *Journal of Geophysical Research*, vol. 92, no. C7, pp. 6787–6803, 1987.

[51] J. C. Comiso, T. C. Grenfell, M. Lange, A. W. Lohanick, R. K. Moore, and P. Wadhams, "Microwave remote sensing of the Southern Ocean ice cover," in *Microwave Remote Sensing of Sea Ice* (F. D. Carsey, ed.), Geophysical Monograph 68, ch. 12, American Geophysical Union, 1992.

[52] G. F. N. Cox and W. F. Weeks, "Salinity variations in sea ice," *Journal of Glaciology*, vol. 13, pp. 109–120, 1974.

[53] C. T. Swift and D. J. Cavalieri, "Passive microwave remote sensing for sea ice research," *EOS Transactions American Geophysical Union*, vol. 66, pp. 1210–1212, December 3 1985.

[54] A. K. Fung and F. T. Ulaby, "Matter-energy interaction in the microwave region," in *Manual of Remote Sensing* (R. N. Colwell, ed.), vol. 1, pp. 144–161, 210 Little Falls Street, Falls Church, Virginia 22046: American Society of Photogrammetry, 1983.

[55] D. J. Cavalieri, "The validation of geophysical products using multisensor data," in *Microwave Remote Sensing of Sea Ice* (F. D. Carsey, ed.), Geophysical Monograph 68, ch. 11, American Geophysical Union, 1992.

[56] D. J. Cavalieri, J. P. Crawford, M. R. Drinkwater, D. T. Eppler, L. D. Farmer, R. R. Jentz, and C. C. Wackerman, "Aircraft active and passive microwave validation of sea ice concentration from the Defense Meteorological Satellite Program Special Sensor Microwave Imager," *Journal of Geophysical Research*, vol. 96, no. C12, pp. 21,989–22,008, 1991.

[57] K. Steffan and A. Schweiger, "NASA Team algorithm for sea ice concentration retrieval from Defense Meteorological Satellite Program Special Sensor Microwave Imager: comparisons with Landsat satellite imagery," *Journal of Geophysical Research*, vol. 96, no. C12, pp. 21,971–21,987, 1991.

[58] J. Hollinger, "DMSP Special Sensor Microwave/Imager calibration/validation, final report volume 2," tech. rep., Naval Research Laboratory, Washington, DC, 1991.

[59] D. R. Thomas, "Arctic sea ice signatures for passive microwave algorithms," *Journal of Geophysical Research*, vol. 98, no. C6, pp. 10,037–10,052, 1993.

[60] J. A. Maslanik, "Effects of weather on the retrieval of sea ice concentration and ice type from passive microwave data," *International Journal of Remote Sensing*, vol. 13, no. 1, pp. 37–54, 1992.

[61] D. T. Eppler, L. D. Farmer, A. W. Lohanick, M. R. Anderson, D. J. Cavalieri, J. C. Comiso, P. Gloersen, C. Garrity, T. C. Grenfell, M. Hallikainen, J. A. Maslanik, C. Mätzler, R. A. Melloh, I. Rubinstein, and C. T. Swift, "Passive microwave signatures of sea ice," in *Microwave Remote Sensing of Sea Ice* (F. D. Carsey, ed.), Geophysical Monograph 68, ch. 4, American Geophysical Union, 1992.

[62] D. A. Rothrock, D. R. Thomas, and A. S. Thorndike, "Principle component analysis of satellite passive microwave data over sea ice," *Journal of Geophysical Research*, vol. 93, no. C3, pp. 2321–2332, 1988.

[63] J. C. Comiso, "Characteristics of Arctic winter sea ice from satellite multispectral microwave observations," *Journal of Geophysical Research*, vol. 91, no. C1, pp. 975–994, 1986.

[64] S. Martin, B. Holt, D. J. Cavalieri, and V. Squire, "Shuttle Imaging Radar B (SIR-B) Weddell sea ice observations: a comparison of SIR-B and Scanning Multichannel Microwave Radiometer ice concentrations," *Journal of Geophysical Research*, vol. 92, no. C7, pp. 7173–7179, 1987.

[65] Research Systems, Inc., 777 29th Street, Suite 302, Boulder, Colorado 80303, *IDL User's Guide*, September 1992. version 3.0.

[66] C. Chatfield, *The Analysis of Time Series: An Introduction.* New York: Chapman and Hall Ltd, third edition ed., 1984.

[67] Statistical Sciences, Inc., 1700 Westlake Avenue North, Suite 500, Seattle, Washington 98109, *S-PLUS User's Manual*, September 1991. version 3.0.

[68] P. Bloomfield, *Fourier Analysis of Time Series: An Introduction.* New York: John Wiley & Sons, 1976.

[69] P. Whittle, *Prediction and Regulation by Linear Least-Square Methods.* Minneapolis: University of Minnesota Press, second ed., 1983.

[70] G. E. P. Box and G. M. Jenkins, *Time Series Analysis: Forecasting and Control.* San Fransisco: Holden-Day, 1976.

[71] R. A. Gow and R. G. Onstott, "Sea ice in the polar regions," in *Polar Oceanography* (W. O. Smith, Jr., ed.), ch. 2, San Diego: Academic Press, Inc., 1990. Part A.

[72] S. F. Ackley, "Mass balance aspects of Weddell Sea pack ice," *Journal of Glaciology*, vol. 24, no. 90, pp. 391–405, 1979.

[73] W. O. Smith, Jr. and D. M. Nelson, "Phytoplankton growth and new production in the Weddell Sea marginal ice zone in the austral spring and autumn," *Limnology and Oceanography*, vol. 35, no. 4, pp. 809–821, 1990.

[74] C. W. Sullivan, C. R. McClain, J. C. Comiso, and W. O. Smith, Jr., "Phytoplankton standing crops within an Antarctic ice edge assessed by satellite remote sensing," *Journal of Geophysical Research*, vol. 93, no. C10, pp. 12,487–12,498, 1988.

[75] D. M. Nelson, W. O. Smith, Jr., L. I. Gordon, and B. A. Huber, "Spring distributions of density, nutrients, and phytoplankton biomass in the ice edge zone of the Weddell-Scotia Sea," *Journal of Geophysical Research*, vol. 92, no. C70, pp. 7181–7190, 1987.

[76] D. L. Wilson, W. O. Smith, Jr., and D. M. Nelson, "Phytoplankton bloom dynamics of the western Ross Sea ice edge - I. Primary productivity and species-specific production," *Deep-Sea Research*, vol. 33, no. 10, pp. 1375–1387, 1986.

[77] W. O. Smith, Jr. and D. M. Nelson, "Phytoplankton bloom produced by a receding ice edge in the Ross Sea: spatial coherence with the density field," *Science*, vol. 227, pp. 163–167, 1985.

[78] Dieckmann, "High phytoplankton biomass at the advancing ice edge in the northern Weddell Sea during winter," *EOS Transactions American Geophysical Union*, vol. 68, p. 1765, December 15 1987.

[79] D. M. Nelson, W. O. Smith, Jr., R. D. Muench, L. I. Gordon, C. W. Sullivan, and D. M. Husby, "Particulate matter and nutrient distributions in the ice-edge zone of the Weddell Sea: relationship to hydrography during late summer," *Deep-Sea Research*, vol. 36, no. 2, pp. 191–209, 1989.

[80] J. C. Comiso, N. G. Maynard, W. O. Smith, Jr., and C. W. Sullivan, "Satellite ocean color studies of Antarctic ice edges in Summer and Autumn," *Journal of Geophysical Research*, vol. 95, no. C6, pp. 9481–9496, 1990.

[81] W. O. Smith, Jr., N. K. Keene, and J. C. Comiso, "Interannual variability in estimated primary production of the Antarctic marginal ice zone," in *Antarctic Ocean and Resources Variability* (D. Sahrhage, ed.), pp. 131–139, Berlin: Springer-Verlag, 1988.

[82] W. O. Smith, Jr. and D. M. Nelson, "Importance of ice edge phytoplankton production in the Southern Ocean," *BioScience*, vol. 36, no. 4, pp. 251–257, 1986.

[83] D. L. Garrison, "Antarctic sea ice biota," *American Zoology*, vol. 31, pp. 17–33, 1991.

[84] S. T. Kottmeier, S. M. Grossi, and C. W. Sullivan, "Sea ice microbial communities. viii. bacterial production in annual sea ice of McMurdo Sound, Antarctic," *Marine Ecology Progress Series*, vol. 35, pp. 175–186, 1987.

[85] S. T. Kottmeier and C. W. Sullivan, "Late winter primary production and bacterial production in sea ice and seawater west of the Antarctic Peninsula," *Marine Ecology Progress Series*, vol. 36, pp. 287–298, 1987.

[86] J. B. SooHoo, A. C. Palmisano, S. T. Kottmeier, M. P. Lizotte, S. L. SooHoo, and C. W. Sullivan, "Spectral light absorption and quantum yield of photosynthesis in sea ice microalgae and a bloom of *phaeocystis pouchetii* from McMurdo Sound, Antarctica," *Marine Ecology Progress Series*, vol. 39, pp. 175–189, 1987.

[87] S. M. Grossi, S. T. Kottmeier, R. L. Moe, G. T. Taylor, and C. W. Sullivan, "Sea ice microbial communities. vi. growth and primary production in bottom ice

under graded snow cover," *Marine Ecology Progress Series*, vol. 35, pp. 153–164, 1987.

[88] T. L. Hopkins, "Food web of an Antarctic midwater ecosystem," *Marine Biology*, vol. 89, pp. 197–212, 1985.

[89] R. M. Laws, "The ecology of the Southern Ocean," *American Scientist*, vol. 73, pp. 26–40, January-February 1985.

[90] V. Smetacek, R. Scharek, and E. M. Nöthig, "Seasonal and regional variation in the pelagial and its relationship to the life history cycle of krill," in *Ecological Change and the Conservation of Antarctic ecosystems* (K. R. Kerry and G. Hempel, eds.), pp. 103–114, Berlin: Springer-Verlag, 1990.

[91] D. L. Garrison and K. R. Buck, "The biota of Antarctic pack ice in the Weddell Sea and Antarctic Peninsula regions," *Polar Biology*, vol. 10, pp. 211–219, 1989.

[92] W. Z. Trivelpiece, S. G. Trivelpiece, and N. J. Volkman, "Ecological segregation of Adélie, Gentoo, and and Chinstrap penguins at King George Island, Antarctica," *Ecology*, vol. 68, no. 2, pp. 351–361, 1987.

[93] W. R. Fraser, W. Z. Trivelpiece, D. G. Ainley, and S. G. Trivelpiece, "Increases in Antarctic penguin populations: reduced competition with whales or a loss of sea ice due to environmental warming?," *Polar Biology*, vol. 11, pp. 525–531, 1992.

[94] D. G. Ainley, W. R. Fraser, and K. L. Daly, "Effects of pack ice on the composition of micronektonic communities in the Weddell Sea," in *Antarctic Ocean and Resources Variability* (D. Sahrhage, ed.), pp. 140–146, Berlin: Springer-Verlag, 1988.

[95] D. G. Ainley, R. E. LeResche, and W. J. L. Sladen, *Breeding Biology of the Adélie Penguin.* Berkeley: University of California Press, 1983.

[96] B. Bodungen, V. S. Smetacek, M. M. Tilzer, and B. Zeitzschel, "Primary production and sedimentation during spring in the Antarctic Peninsula region," *Deep-Sea Research*, vol. 33, no. 2, pp. 177–194, 1986.

[97] O. Holm-Hansen and B. G. Mitchell, "Spatial and temporal distribution of phytoplankton and primary production in the western Bransfield Strait region," *Deep-Sea Research*, vol. 38, no. 8/9, pp. 961–980, 1991.

[98] J. A. Maslanik, J. R. Key, and R. G. Barry, "Merging AVHRR and SMMR data for remote sensing of ice and cloud in polar regions," *International Journal of Remote Sensing*, vol. 10, no. 10, pp. 1691–1696, 1989.